INVESTIGATION OF THE BACTERIAL UPTAKE OF FLUORESCENTLY LABELED PEPTIDES AND MOTILITY STUDIES USING LAB-ON-A-CHIP TECHNOLOGY

by

Merve Yüce

B.S., Bioengineering, Yildiz Technical University, 2015

B.S., Chemical Engineering, Yildiz Technical University, 2016 (Double Major Program)

Submitted to the Institute for Graduate Studies in
Science and Engineering in partial fulfillment of
the requirements for the degree of
Master of Science

Graduate Program in Chemical Engineering

Boğaziçi University

2019

ACKNOWLEDGEMENTS

I would like to express my gratitude to everyone in my life for their kind helps and supports during these busy and challenging years. I cannot mention everybody individually, but there are special people who supported me most of the times and I would like to emphasize them particularly.

First and foremost, I would like to express my sincere thanks to my thesis supervisor, Prof. Kutlu Ülgen for her continuous support of my research, for her patience, motivation and her friendly guidance. I would like to thank my thesis co-supervisor Assoc. Prof. Elif Özkırımlı Ölmez for her motivation and understanding helped me throughout my studies and improved my work.

I am deeply grateful to Prof. Berna Sarıyar Akbulut for her continuous encouragement, motivation and guidance throughout my thesis studies. I would like to express my great appreciation the jury member Assist. Prof. Damla Eroğlu Pala for spending time on my thesis and her valuable recommendations. I would also thank Assoc. Prof. A. Kerem Uğuz for his encouragement and motivation especially taking advanced fluid dynamics course and being a role model for me. I know that the door of his office was always open whenever I had a question or need his guidance.

I would like to thank my precious family members, my mother Hatice Yüce, my father, Mehmet Yüce, and my brother, Hamit Yüce for their love, endless patience and encouragement through all my life. It couldnot be possible to finish this thesis without them. I would like to express my special thanks to my close friends Ayça Fırtın, Fethiye Kıyga and Kevser İhvan who are being there for me since my childhood.

Throughout our lives, we meet a lot people but there have been some exclusive friends whom I would like to express my deep gratitude. I am very lucky to know and work with Begüm Alaybeyoğlu. I am particularly grateful for her assistance while

teaching most of the experiments to me at the beginning of thesis studies patiently. Although she is far from me these years, she continuously encourages and motivates me.

I would like to express my deep thanks to Elif Gençtürk, for her support and friendship. I am very grateful to Elif Esvap, Begüm Yağcı, Özlem Özbek and Müge Kasım. They are not only great lab partners but also journey fellows. The memories of our never ending energy while touring around in France and Switzerland and also talkings at Louvre Museum will always remain. I want to thank people of Ulgen Research Group and Ozkırımlı Lab, especially Selma Başıbüyük and Şafak Kılıç for their support to get through deep thesis anxiety and friendship.

I would like to express my deep thanks to Özge Selçuk for her support, patience and friendship during these years. She made the difficult times easier on both of us. I would like to express my special thanks to Seymen İlke Kaykanat for always being there for me. I am grateful for her support, kindness, motivation and friendship during these years. I would like to thank Uğurcan Tozar for his friendship and coffee support especially at the weekends. They have never left me alone during the difficult times of this research. I would also thank my friends Pelin Yılmaz and Ezgi Öztürk for their friendship and kindness. Taking advanced courses would not be easy without them.

I would like to express my deep thanks to "Sabahlar Olmasın" group members. First, I would like to express my deep thanks to Atakan Yüksel for his support, patience and friendship in this period. Although I have known him just for a year and we have made each other upset mostly for no reason, he is one of my exclusive friends whom I trust completely and believe in his sincerity. I would like to express my special thanks to Ekin Yurdakul for her support to get through the difficult times and for her emotional support and entertainment she provided. She is the most naive and great-hearted person I have ever met and I feel very lucky to know her. I have to thank them for the sleepness nights we were working together when we had lots of fun especially in EE. I would also thank Mustafa Sertbaş for his helps in matlab codes and friendship. I

would like to express my special thanks to Hamdi Erkut for his friendship and making boring times bearable. During this year, we spent most of the time together and we had lots of fun and also pain. I am grateful to "Sabahlar Olmasın" group members for being with me in this period and share great memories that will remain in my mind forever.

Also, I would like to thank all my friends for their motivation during the time we spent in graduate education. In particular, Olcay Türkmen for his helps and support in Comsol simulations, Pınar Eribol, Feyza Kevser Öner, Deniz Köse, Gülten Çelebi, Sema Çömez and Onur Can Boy for their kind friendships.

I would like to acknowledge the guidance and support of all of my professors and supporting personnel of chemical engineering department.

ABSTRACT

INVESTIGATION OF THE BACTERIAL UPTAKE OF FLUORESCENTLY LABELED PEPTIDES AND MOTILITY STUDIES USING LAB-ON-A-CHIP TECHNOLOGY

Bacterial resistance in pathogens is a worldwide challenge associated with high mortality. The aim was to use microfluidic technology for two different applications in the fight with bacterial resistance. In the first part of the thesis the bacterial uptake of cell penetrating peptides (CPPs) was investigated with the motivation of following the internalization of peptide-based antibacterial drugs. In the second part, the changes in bacterial motility of *B*acillus strains were investigated upon treatment with amiloride, with the motivation of live monitoring of drug effects. The outer membrane slows down the entry of available antibiotics into the periplasm. In this regard, CCPs are considered as promising alternatives to conventional antibiotics. Oligopeptide permease (Opp) is a transport system, which has an important role in peptide uptake. By following fluorescence intensity of pVEC and chimeric P4 and P2 peptides, the constructed microfluidic system, confirmed by confocal microscopy, has shown that peptides were able to pass through the inner membrane in wild type cells, while they are accumulated on the periplasm in mutant cells. This result suggested that Opp system can be used as a target to control delivery of antimicrobial peptides into the cytoplasm. Bacterial virulence is in part controlled by the flagellar structures on cellular membranes. The microfluidic system has confirmed that the swimming rate of neutrophilic *B*acillus cells slightly decreased, while the alkaliphilic *B*acillus cells were totally immotile with amiloride treatment. Reaction and rhombic chambers (zeonor) enabled continuous live cell imaging of the bacterial cells and to study the effects of the peptides/drugs in terms of growth, peptide uptake and flagellar motility.

ÖZET

FlORESANLI PEPTİTLERİN HÜCREYE ALINMA MEKANİZMASI VE MOTİLİTE ÇALIŞMALARININ ÇİP TEKNOLOJİSİ KULLANILARAK İNCELENMESİ

Bakteriyel patojenlerin direnci, yüksek mortalite ile ilişkili dünya çapında bir sorundur. Bu çalışmanın amacı bakteri direnciyle mücadelede mikroakışkan teknolojisini iki farklı uygulamada kullanmaktır. Tezin ilk aşamasında hücreye nüfuz eden peptitlerin hücreye alınması incelenmiştir. Tezin ikinci aşamasında amiloride ile inkübe edilen basil hücrelerinin motilitesindeki değişimler incelenmiştir. Bakterilerin dış membranı mevcut antibiyotiklerin periplazmaya girişini yavaşlatmaktadır. Hücreye nüfuz eden peptitler geleneksel antibiyotiklere umut verici alternatiflerdir. Oligopeptit permeaz sistemi, peptit alımında önemli bir rolü olan protein taşıma sistemidir. Hücreye nüfuz eden pVEC peptidi ile kimerik P4 ve P2 peptitlerin floresan yoğunlukları mikroakışkan sistemiyle incelendiğinde ve konfokal mikroskobuyla doğrulandığında, peptitlerin yabanıl tip hücrelerde iç zardan geçtiği ancak mutant hücrelerde periplazmada biriktiği görüldü. Bu sonuçlar Opp sisteminin antimikrobiyal peptitlerin sitoplazmaya geçişini kontrol etmek için bir hedef olarak kullanılabileceği gözlemlendi. Bakterilerin virülans etkisi, hücresel zarı üzerindeki kamçı yapıları ile kısmen kontrol edilir. Bu çalışmada kullanılan mikroakışkan sistem ile amiloride varlığında nötrofilik basil hücrelerinin motilitesi hafifçe düşerken, alkalifilik basil hücrelerinin motilitesinin tamamen engellendiği görülmüştür. Reaksiyon ve rombik hazneler (zeonor), hücrelerin sürekli görüntülemesini ve peptit/ilaçların bakteri hücreleri üzerindeki etkilerini büyüme, peptit alımı ve kamçısal hareketlilik açısından incelememizi sağlamıştır.

TABLE OF CONTENTS

LIST OF FIGURES

LIST OF TABLES

LIST OF SYMBOLS

D	Diffusion coefficient
F	Body force
L	Characteristic length
U	Characteristic velocity
μ	Fluid viscosity
ρ	Fluid density
σ^{F}	Alternative sigma factor

LIST OF ACRONYMS/ABBREVIATIONS

AMPs	Antimicrobial Peptides
AST	Antibiotic susceptibility testing
BLIP	Beta-lactamase Inhibitor Protein
CPPs	Cell-penetrating peptides
CFUs	Colony forming units
CTCF	Corrected total cell fluorescence
DMSO	Dimethyl sulfoxide
FITC	Fluorescein isothiocyanate
GFP	Green fluorescent protein
GM	Growth medium
FITC	Fluorescein isothiocyanate
LB	Luria Bertani
LPS	Lipopolysaccharide
MD	Molecular Dynamics
MIC	Minimal Inhibitory Concentration
NB	Nutrient broth
OM	Outer membrane
Opp	Oligopeptide permease system
PBS	Phosphate buffered saline
PBPs	Penicillin-binding Proteins
PDMS	Polydimethylsiloxiane
PFA	Paraformaldehyde
PI	Propidium Iodide
PTDs	Protein Transduction Domains
SEM	Scanning Electron Microscopy
TLFM	Time-lapse fluorescence microscopy

1. INTRODUCTION

Bacterial cells are prokaryotes, lacking sterols on cellular membrane, and so they are incapable of endocytosis and exocytosis processes. Based on their simple structure, a large surface to volume ratio is seen in prokaryotes, meaning that nutrients can reach any part of the cells' interior from the pores through diffusion easily and rapidly. The internalization of molecules is restricted by the membrane pore size of the bacterium [4, 5]. Recently, it has been discovered that a restricted group of bacteria belonging to the Planctomycetes and Verrucomicrobia possess an endocytosis-like molecular mechanism, which is energy dependent and mediated by receptors. Proteins are internalized by these cells and collected into paryphoplasm [6–8]. This compartmentalization and endocytosis-like molecular mechanism, observed in *G. obscuriglobus* has not been discovered in many gram-negative and gram-positive bacteria. Passive diffusion through pores on cellular membrane is one of the major mechanism for bacterial uptake of many drugs; however, low membrane permeability due to the pore size prevents drug and molecules to pass through cellular membrane [9].

An efficient strategy to penetrate the membrane barrier was identified by the observation of cell-penetrating peptides (CPPs), which, when added to extracellular medium, were able to pass through the membrane. They can cross the cell membrane by direct penetration mechanism (energy independent) or endocytosis-mediated translocation pathway. They have been successfully used for drug delivery into cells. CPPs mediate the transport of proteins oligonucleotides, polysaccharides, nanoparticles and chemotherapeutics, and they have mostly low toxicity [10, 11]. Oligopeptide permease (Opp) system is a protein-dependent ABC transport system, which mediates the transportation of peptides. Opp system is found to allow peptides, the amino acid residues of which varies between three and eighteen depending on bacterial strains, to pass through the membrane. OppA protein is essential part of the Opp system, which has a role in binding peptides.

OppB and OppC are the integral membrane proteins, which form translocation pores for the transition of peptides from the membrane. OppD and OppF proteins are membrane-bound cytoplasmic ATP binding proteins that provide energy for this process [12, 13].

In the present thesis, the uptakes of fluorescently labeled cell-penetrating peptide, pVEC (H-LLIILRRRIRKQAHAHSKK(HF488)-NH_2), chimeric P4 (H-LLIILRRGHY YK(HF488)-NH_2) and P2 (5(6)-Fluoresceine-NH-LLIILHAAGDYYAY-$CONH_2$) peptides were investigated in two different bacterial strains. The internalization of these peptides was analyzed on both wild type *E. coli* K12 and opp-deleted SS5013 cells in order to determine the role of opp system on the peptide uptake. The understanding of the antimicrobial peptide uptake mechanism in bacterial cells may help us develop novel drugs against bacteria.

The virulence effect of bacteria is controlled by their flagella structures on the cellular membrane [14, 15]. This structure also allows bacteria to move towards favorable environments, which generally means exploration of new hosts, habitats or niches. A flagellum consists of three parts: the basal structure, the hook and the filament. It has been pointed that besides the motility and chemotaxis, the bacterial flagella participates in many additional processes including adhesion, biofilm formation, virulence factor secretion, and modulation of the immune system of eukaryotic cells [2, 16]. Due to its complex regulation and assembly, the flagellum has been the subject of broad research in recent times. Ongoing research is still revealing various aspects of flagella, from assembly to function. Several studies have been performed to block the motility and hence the virulence effect of flagella. Swimming and swarming assays are the commonly used methods to measure the motility of bacterial cells. In this study, an analysis method for the flagellar motility was established by using a microfluidic platform. The effects of high Na^+ concentration and amiloride on the flagellar motility of laboratory strain *B. subtilis* 168, undomesticated *B. subtilis* 3610 (an undomesticated derivative of *B. subtilis* 168 strain), DS222 (*B. subtilis* 3610 with a deletion of MotAB gene), and DS223 (*B. subtilis* 3610 with a deletion of MotPS gene) cells were investigated in

this microfluidic platform (zeonor microchips- reaction chambers of 10 μL). Swimming rates of bacterial cells were calculated from the time-lapse images. Finally, an alternative method was developed for the estimation of flagellar motility. This method may provide that flagella can be used as a tool to control infectivity and pathogenicity of bacterial strains.

Bacterial motility and uptake experiments were conducted using commercially available microfluidic devices (reaction chamber chips). The advantages such as low reagent and power consumption, high throughputs, short reaction time, portability for in situ use, low cost, versatility in design, and potentials for parallel operation and for integration with other miniaturized devices render microfluidic chip-based systems practical for biological cell studies. These microchips have been shown to be highly reliable and versatile devices for bacterial cells, providing an easily controllable and contamination-free environment [17]. This technology provides temporal and spatial control of cellular microenvironments by mimicking the complex physiological functions of normal cellular interactions in a controllable and reproducible way [18]. In the second chapter of this thesis, an extensive literature survey was given on live-cell imaging of bacterial cells, antibiotic resistance and motility studies using microfluidic devices. In the third chapter, experimental materials and methods used in the stuies were given in detail. In the fourth chapter, experimental results were presented and discussed under two parts; bacterial mechanism, and flagellar motility. In the fifth chapter, conclusions of the studies and recommendations for future studies were given.

2. THEORETICAL BACKGROUND

2.1. Antibiotic Resistance and Outer Membrane Permeability

Antibiotic resistance in bacterial cells is a growing problem for public health, resulting in high mortality. The emergence and spread of antibiotic resistance is increasing every passing day and urgent solutions are required to struggle against antibiotic resistance [19,20]. Bacterial cells can gain resistance against antibiotics in mainly three ways. First, they produce beta-lactamases to degrade β-lactam ring and render antibiotic inactive. The second mechanism is the alteration of the structures of drug-binding sites in peptidoglycan layer. Bacterial cells can also release antibiotics from cellular membrane via efflux pumps [21].

The outer membrane (OM) of gram-negative bacteria provides a barrier which slows down antibiotics entry into periplasm and decreases the antimicrobial activity. Some hydrophilic drugs, such as β-lactams, pass the cellular membrane by means of the pore-forming porins, while hydrophobic drugs cross the lipopolysaccharide (LPS) in the outer membrane. Size restriction of hydrophilic antibiotics prevents their internalization through cellular membrane. On the other hand, peptidoglycan and teichoic acids provides a permeability barrier for gram-positive bacteria. Because of the alterations in the lipid or protein structure of the OM, the accessibility of drugs into the bacteria decreased and antibiotic susceptibility decreased as well [22, 23].

2.2. Cell-penetrating Peptides (CPPs)

The outer membrane of gram-negative bacterial cells make the internalization of molecules difficult into the bacteria. To overcome outer membrane impermeability problem, several strategies have been used but most of them have disadvantages such as low efficiency, poor specificity, poor bioavailability and extensive toxicity. Protein transduction domains (PTDs), mostly called as cell-penetrating peptides (CPPs)

include all the peptides with the ability to pass through cellular membranes [24]. CPPs carry a positive net charge due to arginine and lysine aminoacids in the sequence, and some of them are characterized by an amphipathic (chimeric) structure. They can cross the cell membrane by direct penetration mechanism (energy independent) or endocytosis-mediated translocation pathway. CPPs are not only be able to cross the membrane but also capable of carrying biomolecules such as oligonucleotides, polysaccharides, nanoparticles and chemotherapeutics inside the cell with low toxicity [10, 11, 25].

pVEC is a recently described, an 18-amino-acid-long CPP (LLIILRRRIRKQAHAHSK) derived from the murine vascular endothelial-cadherin protein. It consists of a hydrophobic N-terminus, an arginine-rich middle region and a hydrophilic C-terminus [26, 27]. Previous studies demosntrated that N terminus five residues (LLIIL) of pVEC has effective on the internalization of this peptide. The approach is to synthesize chimeric peptides by combining the LLIIL residues of pVEC with betalactamase inhibitory based sequences to facilitate their uptake. As a result, the addition of N terminus five residues of pVEC to inhibitory proteins provides a promising strategy to design chimeric peptides to combat antibiotic resistance besides facilitating the internalization of these peptides through membrane.

2.3. Oligopeptide permease system (Opps)

Oligopeptide permease (Opp) system is a peptide transport system locating in the periplasm (a protein-dependent ABC transporter), which has an important role in the internalization of peptides. Opp is composed of five components, substrate binding protein (OppA), two transmembrane proteins (OppB and OppC) which form the translocate channel, and two membrane-bound cytoplasmic ATP-binding proteins (OppD and OppF) which provide energy for peptide importing and it is found in many bacteria and archea species (Figure 2.1) [12, 13]. Opp system is found to allow peptides, the amino acid residues of which varies between three and eighteen depending on bacterial strains, pass through the membrane. Opp systems are mainly involved in

peptide uptake and environmental sensing, but they may play other roles such as adhesion to the host cell, control of cell envelope permeability, drug resistance and virulence [13, 28].

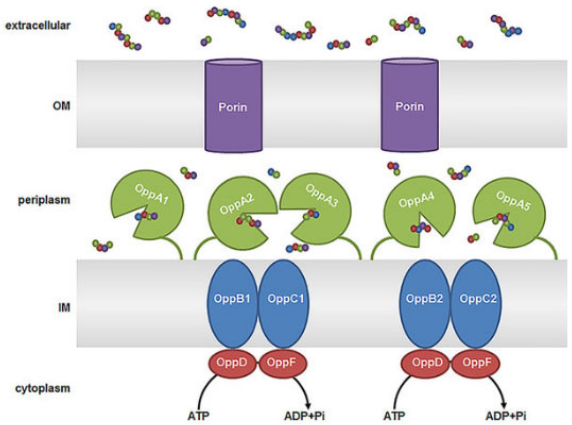

Figure 2.1. The oligopeptide permease system (Opps) [1]

2.4. Bacterial Flagellar Structure

Bacteria have flagella structures on the cellular membrane, whereby they acquire motility and also pathogenicity. Flagella enable bacterial cells to move towards favorable environments (chemotaxis) such as new hosts, habitats or niches. It has been pointed that besides the motility and chemotaxis, the bacterial flagella participate in many additional processes including adhesion, biofilm formation, translocation of virulence proteins into host cells, and stimulation of host immune system, so they are considered as important virulence factors [29].

Bacterial cells can colonize and move to various tissues, and then they may attack the host tissues and organs and proliferate there to bring about host infection. Expression of bacterial flagella is required for maximal bacterial adherence, colonization, and subsequent invasion (Figure 2.2). Studies have revealed that mutant bacteria lacking flagella were either impaired or completely disabled in colonization and also keeping their ability to cause disease. However, the underlying molecular mechanisms of how flagella impact host-microbe interactions remain largely unknown. Understanding of this mechanism may provide that flagella can be used as a tool to control infectivity and

pathogenicity of bacterial strains [14, 23, 29]. Bacterial flagellum can be investigated under three main structures, namely basal body, hook and helical filament.

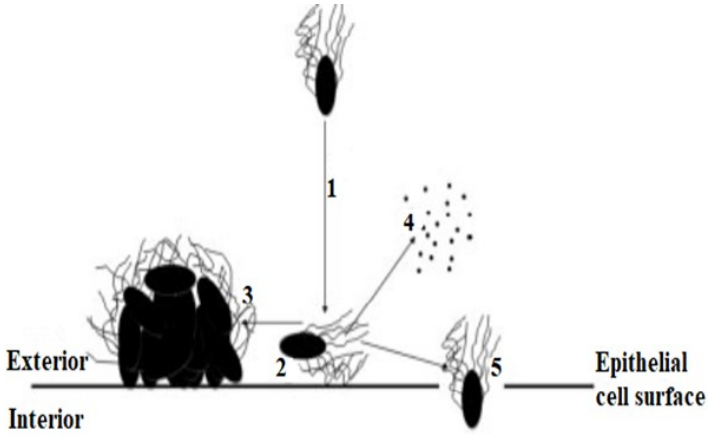

Figure 2.2. Contribution of the flagella to bacterial pathogenesis [2]

The basal body provides the power for rotation, and secretes the more distal components. The MotAB and MotPS stators located in basal body create an ion channel (H^+ or Na^+ ions)to rotate the flagellum. The rotation of the flagellar filament is powered through the proton/sodium motive force, not ATP [30, 31].

2.5. Microfluidic Technology

Microfluidic systems, also called "lab-on-a-chip" systems, integrate analytical processes such as sampling, sample pre-treatment, analytical separation, chemical reaction, analyte detection, and data analysis in a single microfluidic device. The advantages of their low reagent and power consumption, high throughput, short reaction time, portability for in situ use and low cost render these microdevices practical for biological cell studies. Microfluidic technologies enable temporal and spatial control of cellular microenvironments by mimicking the complex biological functions of normal cellular interactions [17,18,32]. Many drugs such as peptides, proteins and DNA-based therapeutics are susceptible to enzymatic degradation, and the long pathway of conventional drug delivery systems may make the drug ineffective. Recent advances in micro- and nanotechnologies provide a shorter and more targeted delivery pathway.

Miniaturization allows the integration of components of a drug delivery system into a single chip [33–35]. There are significant differences between individual cells, and therefore the development of single cell manipulation, screening and analysis methods have great significance for disease diagnosis and drug screening. Because microfluidic technology allows studying small sample volumes with high accuracy, it has great potential in manipulation of single cell fusion, transfection, dyeing, sorting, and sequencing [36]. Most in vitro cell-based biochemical experiments are performed in two-dimensional (2D) manner such that cells are cultured onto plastic surfaces and therefore poorly mimic the three dimensional (3D) cellular microenvironment. On the other hand, microfluidic chips allow cells to reside in a more physiologically relevant context and a controllable and reproducible way [37]. Table 2 summarizes the live cell imaging of bacterial cells performed with microfluidic systems.

Balaban *et al.* (2004) investigated the persistence of single cells of *E. coli* with the use of microfluidic devices. When a population of genetically identical bacterial cells is exposed to a sufficiently strong antibiotic treatment, most of the population is killed. Killing can be measured by monitoring the fraction of viable cells as a function of the exposure to the antibiotic treatment. By the time the antibiotic is removed, a small fraction of the cells still survives. These cells have not genetically acquired antibiotic resistance: They regrow a new population that is as sensitive to the antibiotic. This phenomenon, termed bacterial persistence, was first reported for staphylococcal infections treated with penicillin and has since been observed in many bacterial species. Previously isolated high persistence (hip) mutants of *E. coli* that have an increased proportion of persisters were used in the experiments. A microfluidic device was fabricated from polydimethylsiloxane (PDMS) and growth of individual bacteria under normal conditions was recorded. Bacterial cells were exposed to antibiotics and rare survivors were detected. Persister cells can be distinguished from normal cells by their reduced growth rate. For single-cell measurements, the hipA7 bacteria are first grown in a microfluidic device under the microscope on Luria-Bertani Lennox medium (LBL). By using time-lapse microscopy and measuring the length of newly formed linear microcolonies, growth rates of the progeny of individual cells were measured.

The average growth rate of *E. coli* in these devices was found to be the same as that for batch cultures. After several cell divisions, ampicillin was added to the medium, and the death of cells, accompanied by lysis, was easily observed. After the removal of ampicillin from the device, rare bacteria, which survived, started growing and dividing again. These were identified as the persister cells [38].

Table 2.1. Bacterial cell applications with microfluidic devices

Bacteria and medium	**Chip mat.**	**Chip Dimensions**	**Duration and Flow rates**	**Microscopy and camera**	**Parameters**	**Image Processing System**	**Single/ Mult.**
E. coli, LB medium [39]	PDMS	N/A	9 h	N/A	-Bacterial growth -Detecting persister cells	Time-lapse images	Single
E. coli [3]	PDMS	Channel depth of 6 μm, wide of 100 μm, length of 70-200 μm.	8 h, chamber flow of 0.1 μm/s and channel flow of 100 μm/s	Nikon Eclipse TE2000 microscope, 60x objective	-Bacterial growth	Phase-contrast images, 3-min. intervals	Single
E. coli, LB medium [40]	PDMS	Channel depth of 35 μm, channel wide of 100 μm, side-length of 300 μm.	8 h, cell loading (600 μL/h) for several minutes, fresh LB medium (600 μL/h) continuously	Inverted microscope with CCD camera	-Bacterial growth -Antibiotic testing	Phase-contrast images, 15-min. intervals	Mult.
E. coli, LB medium [41]	PDMS	Channel wide of 400 μm, depth of 15 μm, length of 500 μm	10 h, antibiotic solutions and cell loading	Inverted fluorescence microscope with CCD camera 10x objective	-Detection of GFP expression -Antimicrobial susceptibility	Time-lapse fluorescence images, 10-min. intervals	Mult.
E. coli, Mueller-Hinton Broth [42]	PDMS	50 μm long cell traps with 1.25x1.25 μmarea	30 minutes, pressure-driven flow	Nikon Ti-E inverted microscope, CMOS camera, 20x objective	-Antimicrobial susceptibility -Growth rate	Time-lapse microscopy images, 60 secs	Single

Groisman *et al.* (2005) developed a microfluidic chemostat to demonstrate the growth of bacterial and yeast colonies in shallow microscopic microchambers.

The microchemostat device was made of PDMS. The channels and chambers have a depth of 6 μm. The channels are 150 μm wide; the chambers have a width of 100 μm and lengths of 70–200 μm (Figure 2.3). A single *E. coli* JM109 cell was introduced into a chamber. Afterwards, it divided multiple times and formed a branched network of nonmotile cells that then disintegrated as the cells initiated random movement. Fluorescence, bright-field and phase-contrast micrographs were captured at 20x, 40x and 60x magnification with a Nikon Eclipse TE2000 epifluorescence microscope. The rate of colony growth was studied by taking a series of fluorescence images of the same chamber at 3 minute intervals [3].

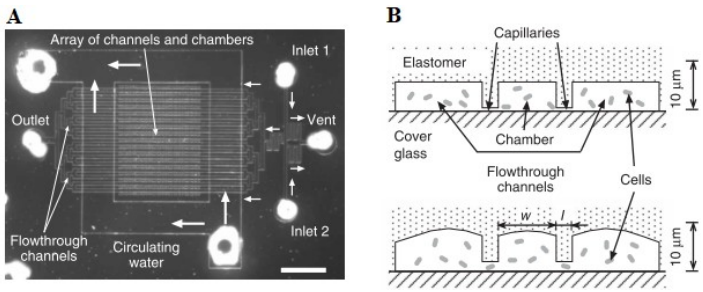

Figure 2.3. Design of microfluidic device to demonstrate the growth of bacterial and yeast colonie [3]

Sun *et al.* (2011) presented a high-throughput microfluidic system for long-term bacterial colony monitoring and on-chip bacterial inhibition test. The microfluidic system is composed of seven parallel channels, each containing 32 square-shaped microchambers. The channels and chambers have a depth of 35 μm. The channels are 100 μm wide, while the square-shaped microchambers have a side length of 300 μm. The channels and chambers are connected by capillaries with a width of 30 μm and a length of 180 μm. By inducing recombinant *E. coli* HB101 pGLO to synthesize green fluorescent protein (GFP) with 1-arabinose (1-Ara), the real-time analysis of GFP expression in different initial bacterial densities was performed. Tetracycline and erythromycin inhibition on bacterial cell growth was measured. Bacterial morphology changes during antibiotic treatment were observed. An inverted microscope with a CCD camera was used to acquire phase contrast and fluorescent images. Temporal changes to the synthesized GFP were used to characterize the growth of bacteria. The effect of the

initial densities of *E. coli* cell suspensions on the growth state of bacterial cells in a microenvironment, as well as bacterial cell growth states in different microchambers at the same initial loading cell density was analyzed by employing three initial loading cell densities (2×10^9, 1×10^9, and 2×10^8 CFU/mL). Although the initial cell densities were different, the cell growth curves were similar but the main difference was the long periods of latency. Different antibiotic solutions along with freshly supplemented LB growth medium and l-Ara were continuously provided at a flow velocity of 20 μL/h. Previous studies demonstrated that tetracycline and erythromycin act on the 30S and 50S ribosomal subunits of cells and inhibit protein synthesis. Concentrations of 3 μg/mL tetracycline facilitated the formation of long filamentous bacteria with the average length of more than 50 μm. On the other hand, erythromycin had no effect on the bacterial cell morphology. These findings provides an on-chip framework for bacteriological research in a high-throughput manner and the development of recombinant bacteria-based biosensors for the detection of specific substances [40].

Mohan *et al.* (2013) developed a microfluidic platform for rapid antibiotic susceptibility testing. Microfluidic platforms with improved sensitivity and fast analysis have been developed for antimicrobial susceptibility testing recently. However, many of these methods suffer from one or more limitations. They require complicated platform fabrication and/or operation procedures. These devices are also not portable due to the requirement for syringe pumps, pneumatic actuators, and other ancillary equipment. In this study, a microfluidic chip based on fluorescence detection of bacteria which express GFP was produced from PDMS using photolithography. GFP is used as a genetically encodable indicator of cell viability. This platform possesses several advantages compared to conventional methods such as analysis of antibiotic action in two to four hours, enhanced detection sensitivity, minimal consumption of cell samples and antibiotic reagents, and improved portability through the implementation of normally closed valves. This platform was used to quantify the effects of four antibiotics (ampicillin, cefalexin, chloramphenicol, tetracycline) and their combinations on *E. coli*. Antibiotic and cell solutions are placed on their respective inlet ports and introduced into the wells by actuating the filling valves using a vacuum pump. To compare

the microfluidic platform with macroscale methods for antibiotic screening, antibiotic susceptibility testing on *E. coli* using 96-well plates was also performed. On-chip measurements were performed by TLFM using an inverted fluorescence microscope. Images were acquired every 10 min over a period of 10 h using a 10x objective. Antibiotic efficiency was quantified in terms of the fraction of the initial cell population in a chamber that survives antibiotic treatment at the end of an experiment. All four antibiotics failed to inhibit cell growth when employed at low concentrations (0.5 μg/mL). At a 10-fold higher concentration (5 μg/mL), addition of ampicillin results in a substantial amount of cell death by lysis, while tetracycline and chloramphenicol inhibited cell division without causing significant lysis. At the highest concentration (500 mg/mL), significant cell death was observed. The combination of two antibiotics showed improved or decreased efficiency compared to each antibiotic applied individually. The combinations of three or more antibiotics are not necessarily better for eradicating pathogens compared to pairs of antibiotics. Overall, this microfluidic based biosensor technology has the potential to provide rapid and precise guidance in clinical therapies by identifying the antibiograms of pathogens [41].

Baltekin *et al.* (2017) designed a microfluidic chip to monitor individual bacterial cell growth rates using microscopy and to perform antibiotic susceptibility testing (AST) within 1-3 h. In this study, a microfluidic device involving two rows of cell traps was produced. In each row, there are 2,000 cell traps of dimension 1.25 $\times$ 1.25 $\times$ 50 μm that can be loaded with bacterial cells (red) from the front channel. A constriction at the end of each trap prevents cells from passing to the back channel, while allowing the media to flow around the cells. Bacteria were loaded into the microfluidic chip and growth medium (GM) without antibiotic was supplied to one row (reference population) and GM with antibiotic to the other (treatment population). With this setup, the differential growth rate between treatment and reference populations was detected. Using the fast antibiotic susceptibility test (fASTest), the antibiotic response time of *E. coli* (MG1655) to nine different antibiotics that are used for urinary tract infections (UTIs) was determined. Samples with more than 10^4 CFU/mL can be loaded in less than 10 min, and thus, no precultivation is needed for patient urine samples. It is

possible to determine if a urinary tract infection is caused by resistant bacteria within 30 min of loading a urine sample, even if the bacterial concentration in the urine is very low. The presented antibiotic susceptibility test is sufficiently fast to be used at the point of care [42].

Table 2.2. Bacterial motility studies in microfluidic devices

Bacteria and medium	**Chip mat.**	**Chip Dimensions**	**Duration and Flow rates**	**Microscopy and camera**	**Parameters**	**Image Processing System**	**Single/ Mult.**
E. coli HCB437, LB [43]	PDMS	Channel height of 5 μm, width of 10 μm	N/A	Fluorescence microscopy, 100x obejective	-Bacterial motility -Channel height	Time-lapse imaging	Single
E. coli RP437, LB [44]	PDMS	Channel wide of 0.3 μm, height of 300 nm and length of 50 μm.	Chemotaxis driven flow	Inverted fluorescence microscopy, CCD camera, 100x objective	-Bacterial growth, -Bacterial motility	Time-lapse imaging	Single
B. subtilis, LB [45]	PDMS	Channel depth of 1.06μm, width of 600 μm and length of 300 μm.	20 h, LB perfusion of 0.9 μm/s	Nikon Ti-E fluorescence microscope, 60x oil objective	-Bacterial growth -Division time	Time-lapse imaging	Single
B. subtilis 3610 [46]	PDMS	Channel volume of 6.4 μL, height of 160 μm	12 h	Inverted optical microscope, 10x objective	-Bacterial growth -Cell density	Time-lapse imaging, 30-min. intervals	Mult.
B. subtilis, Minimal Medium [47]	PDMS	Channel width of 1 μm	12 h, medium flow rate of 1.5 μL/min	Nikon Ti-E inverted microscope, 600x objective	-Tracing cell fate -Divison time	Time-lapse fluorescence imaging, 10-min intervals	Single

Flagella structure plays an important role in adhesion, invasion and biofilm formation of bacteria. Flagella provides motility for bacteria and enables them move towards host cells. Therefore, the identification and characterization of flagella are important for the development of therapies against infectious bacteria. Motility studies performed using microfluidic devices in the literature were summarized in Table 2.2.

Diluzio *et al.* (2005) developed a technique for observing isolated *E. coli* cells moving on an agar substrate and confined in shallow, oxidized PDMS microchannels. Individual *E. coli* cells swim in clockwise, circular trajectories near planar glass surfaces. Bacterial cells elongated and migrate cooperatively on a semi-solid agar. A new technique was presented to examine the movement of individual bacteria on nutrient agar by confining the cells in shallow microchannels constraining their motion to two dimensions. Using soft lithography, thin (150 μm thick), flexible, gas-permeable films of PDMS embossed with grooves were fabricated. The surface of the film was treated with an air plasma. The oxidized PDMS (ox-PDMS) film was placed on the agar a few millimetres from the edge of a swarm of *E. coli*. The film sealed conformally to the agar substrate and formed microchannels in which the bottom agar surface formed the floor of the channel, and the ox-PDMS film formed the sidewalls and ceiling. When the channel height was 10 μm, about equal number of cells swam to the right (closer to the microchannel floor) and to the left (closer to the microchannel ceiling), indicating no side preference. Swimming speed of 50 individual cells in channels with porous agar floors and in channels with solid ox-PDMS floors was measured. Cells moving on the right in channels with agar floors swam at an average speed of 31 ± 3 $\mu m/s$ and cells in channels with ox-PDMS floors swam at 27 ± 4 $\mu m/s$. The composite agar/ox-PDMS channels presented in this study can be extended to study the growth or movement of motile microorganisms in a confined but nutritive environment [43].

Mannik *et al.* (2009) investigated the growth and motility of Gram-negative Escherichia coli and Gram-positive Bacillus subtilis in microfabricated channels. Most bacteria in soil and bedrock live in pores of size 6 micrometer and smaller. It is largely unknown how bacteria grow, move, and penetrate pores of very small size. To understand this, *E. coli* and Bacillus subtilis bacteria were grown in very narrow constrictions and the lower limits for the constriction size that these bacteria were able to penetrate were determined. Vertical or horizontal channels were fabricated using Si microfabrication techniques. The channels and chambers on the chip were defined by using e-beam lithography. The channels and chambers were covered using PDMS glass coverslips of 150 μm thickness. *E. coli* and Bacillus subtilis carries GFP and an Olympus IX81

inverted fluorescence microscope with a 100X NA 1.3 oil immersion and a 60X dry objective was used for imaging these bacteria. Bacterial movement in channels is partially driven by chemotaxis toward the nutrient source which consists of growth media in the feeding channel. From left to right, the channels are fabricated progressively narrower in order to monitor how the population of bacteria is able to negotiate increasingly narrower channels and adapt to life in such a confined environment. The widths of the channels (W) reported in this study vary from 5 μm to 0.3 μm. The widths of the channels on these chips are comparable to or even smaller than the diameters (D) of the *E. coli* and *B. subtilis* bacteria, which are 0.76 μm and 0.86 μm respectively. *B. subtilis* bacteria can grow in channels as narrow as their diameter, whereas *E. coli* cells are able to penetrate channels with a width that is much smaller than their diameter. It was demonstrated that growth in channels narrower than the bacterial diameter can drastically change the shape of *E. coli* and lead to a morphological phenotype which has not been described previously [44].

Baker *et al.* (2017) created a microfluidic device with an integrated nanochannel array to trap individual bacteria and monitor growth and reproduction of lineages over multiple generations. This device immobilizes cells for high-resolution, time-lapse fluorescence imaging and tracking, has dynamic control of cell loading and nutrient flow, and can rapidly exchange media. Because of adhesion, cells accumulated in the microchannels and eventually blocked media flow through the device. Therefore, non-adherent strains were chosen to facilitate long-term growth and observation on the devices. Cell loading was performed on-chip in manual operation mode. Once the cells were trapped, media from the media reservoir was pumped at a rate of 0.9 μL/min to flush away excess cells and provide fresh media to the trapped cells. Images were acquired at 16 locations across the nanochannel array at 5 min intervals over 20 h. Over the duration of the experiment, individual cells are tracked, their growth and division rates are determined, and lineages spanning several generations are reconstructed. Rates of division and growth of the trapped bacteria as a function of time and position within the nanochannels were measured [45].

Massalha *et al.* (2017) describe a microfluidics-based approach enabling direct imaging of root-bacteria interactions in real time. The intimate interaction of *B. subtilis* with plant roots is accurately traced in high resolution to the root elongation zone. The microfluidic device termed as tracking root interactions system (TRIS), allows up to nine independent chambers of Arabidopsis seedlings that can be monitored in parallel. The principal assay monitors behavior of fluorescently labeled *B. subtilis* as it colonizes the root of Arabidopsis thaliana within the TRIS device. The total internal volume of the channels is 6.4 μL, and their height is 160 μm. Arabidopsis seeds are first germinated in agar-filled pipette tips, which are subsequently placed at the dedicated port of each channel, and the device is incubated for up to 5 d under appropriate conditions. After root elongation, the device is placed on a microscope stage, with polyethylene tubes connected to the inlet and outlet ports for liquid handling and inoculation with bacteria. Fluorescently labeled *B. subtilis* were injected into the TRIS microfluidic system using preloaded syringes. Using time-lapse microscopy, bacteria-root interactions of nine independent inoculations were monitored at 30 minute intervals over a period of 12 h. Bacterial cells continuing to accumulate throughout the imaging period. Bacterial density at the same position increased significantly by fivefold during the first 6 h postinoculation. After 6 h, bacterial density decreased above the root tip and bacterial accumulation appearing as large bacterial plugs (likely showing biofilm formation) on the root surface farther from the growing tip [46].

Russel *et al.* (2017) studied a microfluidics-based platform to investigate the activation of Spo0A (response regulator) and σ^{F} (a hallmark for entry into sporulation) in individual cells held under constant, sporulation-inducing conditions. In the absence of nutrient, cells of *B. subtilis* enter the pathway to form a spore, a multihour morphogenetic process in which a growing cell is converted into a dormant cell type. Sporulation is a switch from binary fission to asymmetric division in which the division septum is positioned near one pole of the cell. Formation of this asymmetrically positioned septum divides the developing cell (sporangium) into a small forespore compartment, which then become the spore, and a large mother cell, which nurtures the developing spore. In this study, a microfluidic platform was used to investigate sporu-

lation in a way to visualize the behavior of individual cells for long periods of time under uniform and constant conditions after a switch to sporulation-inducing medium. σ^{F}-directed gene expression was used as an early, diagnostic marker for cells having entered the pathway to form a spore. Synthesis of a fluorescent reporter produced under the control of σ^{F} was visualized in individual cells using a microfluidic platform. The platform was used to visualize and analyze σ^{F} activation in multiple cells after the switch to sporulation medium. The results showed heterogeneity in the time of σ^{F} activation, even though the cells were held under constant conditions after the switch. In addition, it was found that there is no stereotyped time, number of cell cycles, or cell-cycle length associated with σ^{F} activation [47].

3. MATERIALS AND METHODS

3.1. CFD Simulations by Comsol

The zeonor reaction chip and also tubings system (purchased from Microfluidic ChipShop GmbH, Germany) used in the experiments are modeled by Comsol Multiphysics 5.3 software and series of fluid dynamic simulations were performed to analyze the fluid flow and concentration distribution in tubings and the chamber. Microfluidics module is utilized with Creeping flow and Transport of diluted species physics. Creeping flow physics is employed for identifying the fluid flow and pressure drop inside the chamber and tubings, and transport of diluted species physics is employed for obtaining the concentration distribution within the microfluidic device. The flow rate at the inlet of the chip is approximately 0.37 mm/s. The Reynolds number, which is important for characterizing the flow is given by:

$$Re = \frac{\rho U L}{\mu} \tag{3.1}$$

where ρ is the fluid density (1000 kg/m^3), U is a characteristic velocity of the flow (0.37 mm/s), μ is the fluid viscosity (0.00089 Pa·s) and L is a characteristic dimension of the device (333.34 μm) which is calculated for a rectangular duct as follows:

$$L = \frac{4ab}{2(a+b)} = \frac{4 * 500 * 250}{2 * (500 + 250)} = 333.34\mu m \tag{3.2}$$

where a is the width of the chip inlet and b is the height of the chip inlet. The Reynolds number is calculated as follows:

$$Re = \frac{\rho U L}{\mu} = \frac{(1000\text{kg/m}^3)(0.00037\text{m/s})(333.34x10^{-6}\text{m})}{0.00089\text{Pa.s}} \tag{3.3}$$

Because the Reynolds number is less than 1, the inertial forces are very small compared to the viscous forces, being neglected when solving the Navier-Stokes equations and the Creeping Flow interface is used. The convective term in the Navier-Stokes equations can be dropped, leaving the incompressible Stokes equations:

$$-\nabla \cdot (\mu(\nabla u + (\nabla u)^T)) + \nabla p = F \tag{3.4}$$

$$\nabla \cdot \ u = 0 \tag{3.5}$$

Steady-state incompressible Navier-Stokes Equations (Equation 4) and the continuity equation (Equation 5) with the constant fluid density and the mass conservation assumptions given above are applied to run the simulations. In Equation 4, u is the velocity (m/s), p is the pressure (Pa), μ is the dynamic viscosity (Pa.s), ρ is the density (kg/m^3) and F is the body forces such as gravity. During the simulations, body forces are taken as zero.

In the device, the solute molecules interact only with water molecules, and Fick's law can be used to describe the diffusive transport. Mass transport equation used in the simulations is (Equation 6):

$$\nabla \cdot (-D\nabla c + cu) = 0 \tag{3.6}$$

where D represents the diffusion coefficient (m^2/s) and c is the concentration (mol/m^3). Several flow rates are applied through the inlets by using velocity component, and pressure was set to zero at the outlet. No-slip boundary conditions ($u = 0$) are used for the walls and convective flux ($-n \cdot \ (D\nabla c) = 0$) is set to the outlets. The tubing system is composed of three inlets. Bacterial cell solution is fed through the first inlet, medium is fed through the second inlet and the drug is fed through the third inlet. The medium contains tryptone concentration of 1 % by weight (10 g/L, 20 gmol/m^3)

was set into the second inlet. The density of tryptone solution is calculated according to the supplied tryptone concentration, and the density is found as 618.68 kg/m^3. The dynamic viscosity is 0.000894 Pa.s and diffusion constant of water is 2.34×10^{-9}m^2/s used to stimulate trypsin concentration. Two different cases are handled in the model; one of them is flow rate optimization for cell attachment to the chamber, the other one is the time-dependent concentration profile within the tubing system.

3.2. Bacterial Strains and Growth Conditions

The wild type *E. coli* K12 (ATCC 29425) was from our own laboratory stock. An isogenic derivative of *E. coli* K12 SS320 strain *E. coli* K12 SS5013 Δ (tdk-oppABCDF-tonB-trp) with a complete deletion of the opp operon, was kindly sent by James T. Park (Tufts University).The non-motile strain *E. coli* K12 HCB137 (= RP3098) that lacks flagella (Parkinson and Houts 1982), was generously provided by the laboratory of Howard Berg (Harvard University).

The wild type *B. subtilis* 168 and *B. marmarensis sp. nov.* was kindly supplied by Berna Sariyar Akbulut (Marmara University). An undomesticated derivative of *B. subtilis* 168 strain, *B. subtilis* 3610, DS222 (*B. subtilis* 3610 with a deletion of MotAB gene), and DS223 (*B. subtilis* 3610 with a deletion of MotPS gene) were kindly supplied by Daniel Kearns (Indiana University Bloomington).

E. coli K12 and *B. subtilis* cells were grown in Luria-Bertani (LB) broth (10 g/L tryptone, 5 g/L yeast extract, 10 g/L NaCl) and stored at -80°C in 50 % glycerol stocks. Growth curves were obtained during growth LB broth at 37°C and 180 rpm. After the preparation of LB media, all equipment including glassware, pipette tips, eppendorf tubes etc. were sterilized in the autoclave at 1 atm and 121°C for 15 minutes. After sterilization, the preculture was prepared by inoculating 15 mL sterile LB media with 130 μL of bacterial stock culture kept at -80°C and bacterial cells were allowed to grow overnight at 37°C and 180 rpm in a shaking incubator.

The growth of *B. marmarensis sp. nov.* was achieved in Nutrient Broth (NB) prepared in Na-sesquicarbonate buffer. To prepare 1 L NB growth media, NB broth powder was dissolved in 900 mL of sterilized distilled water and then autoclaved at 1 atm and 121°C for 15 minutes. 10X concentrated Na-sesquicarbonate buffer prepared from an equimolar mixture of 0.1 M Na_2CO_3 and 0.1 M Na_2HCO_3 was filter sterilized. The pH of the resulting NB media was 9.7, the optimum pH for the growth of *B. marmarensis*, 100 mL of this buffer was added to the 900 mL of sterilized NB broth.

3.3. Drugs and Other Solutions

Dimethyl sulfoxide (DMSO), amiloride hyrochloride and fluoresceinamine dye were from Sigma-Aldrich. Amiloride hydrochloride-labeled pVEC and P4 peptides were purchased from Anaspec Inc. Fluoresceine-labeled P2 was purchased from Thermo Fisher Scientific Inc. Propidium Iodide (PI) dye was purchased from Neofroxx Inc. Phosphate Buffered Saline (PBS) tablets were purchased from MP Biomedicals Inc. PBS solution was prepared by dissolving 1 tablet in 100 mL of sterile distilled water and autoclaved at 1 atm and 115°C for 10 minutes. The pH of this buffer is in the range of 7.3-7.5.

Fluoresceinamine dye was dissolved in sterile distilled water to a final concentration of 600 μM and stored at -20°C. Then, this solution was diluted to 100 μM for the uptake studies. PI dye solution was prepared by dissolving 1 mg of powder in 1 mL of PBS solution.

Amiloride was first dissolved in DMSO at a concentration of 100 mM and 1 mL of aliquots were prepared and stored at -20°C. Afterwards, aliquots were diluted to 1 mM final concentration (final DMSO concentration is 1 %) with sterile distilled water to be used in motility analyses.

Fluorescently labeled cell-penetrating peptide, pVEC (H-LLIILRRRIRKQAHAH-SKK (HF488)-NH_2) was first dissolved in the minimum possible volume of DMSO and then diluted to 5 mM final concentration (final DMSO concentration was 2 %) with sterile distilled water. 50 μL of peptide aliquots were prepared and stored at -20°C. For uptake studies, one aliquot was diluted with sterile distilled water to obtain final concentrations of 50 μM and 100 μM. Fluorescently labeled P4 peptide (H-LLIILRRGHYYK(HF488)-NH_2) was first dissolved in the minimum possible volume of DMSO and then diluted to a final concentration of 5 mM (final DMSO concentration was 4 %) with sterile demineralized water. 50 μl of peptide aliquots were prepared and stored at -20°C. For uptake studies, one aliquot was diluted with sterile distilled water to obtain final concentrations of 50 μM and 100 μM. Fluorescently labeled P2 peptide (5(6)-Fluoresceine-NH-LLIILHAAGDYYAY-$CONH_2$) was first dissolved in the minimum possible volume of DMSO and then diluted to a final concentration of 1 mM with sterile 50 mM K^+PO_4 buffer (pH 7.0) solution. The final peptide solution had 20 % (v/v) DMSO. 100 μL of peptide aliquots were prepared and stored at -20°C. For uptake studies, one aliquot was diluted with sterile distilled water to obtain a final concentration of 50 μM.

3.4. OD_{600} Measurement

To monitor cell growth, 1 mL of bacterial culture was taken every hour and the optical density at 600 nm was measured in a UV-vis spectroscopy. NB medium was used for both the blank and dilution of the B. marmarensis samples and LB medium was used for the blank and dilution of the other bacterial cells. The spectroscopic readings were kept within the reliable range of 0.2 to 0.8.

3.5. Determination of Colony Forming Units (CFUs)

LB and NB liquid media were supplemented with 15 g/L agar to prepare LB or NB plates, respectively. 10 fold serial bacterial dilutions were prepared by mixing 100 μL of the bacterial sample with 900 μL fresh LB medium until the desired dilution was

obtained. 1 ml of a diluted bacterial sample was plated to determine the CFUs. The plates were incubated at 37°C in an incubator. The number of CFUs were counted after incubation up to 24 hours.

3.6. Visualization of Cell Heterogeneity of *Bacillus* Species Under UV-light Microscopy

15 mL of sterile LB medium was inoculated with a single colony of *B. subtilis* 168 strain grown on the plate by using a loop, and cells were grown overnight (16 hours) at 37°C and 180 rpm in a shaking incubator. The next day, the preculture of *B. subtilis* 168 strain was used for inoculation into fresh LB medium. 15 mL of sterile LB medium was inoculated with 130 μL of preculture. Starting from the second hour of incubation, a bacterial sample of 2.5 μl was taken from the culture at predetermined times (in lag phase, log phase and early stationary phase) to observe cell heterogeneity. 2.5 μL of a sample was placed on a microscopy glass and covered with a coverslip. The slides were visualized under a Nikon inverted microscope. Bright field images were captured at 60X zoom and movies were recorded. A similar procedure was followed for *B. marmarensis* cells incubated in NB media. Bright field images were captured at 20X, 40X, 60X and 90X zoom and videos were recorded at 40X zoom.

3.7. Determination of Minimal Inhibitory Concentration (MIC)

To observe the effects of drugs on the bacterial growth, MIC values of these drugs were determined. Inoculum size, type of growth medium, incubation time and inoculum preparation method can all influence MIC values. Therefore, broth dilution has been standardized by Clinical and Laboratory Standards Institute (CLSI) for testing bacteria that grow aerobically [48]. Low bacterial inoculum dose (2x10^4 to 10^5 CFU/mL) is suggested in literature [49, 50]. However, in order to visualize bacterial viability and membrane damage induced by drugs using fluorescence microscopy and SEM and TEM imaging techniques, high inoculum cell density is required (10^8-10^{10} CFU/mL) [51]. Since the MIC values of drugs are highly dependent on the inoculum cell density,

determination of MIC was carried out at both high and standard inoculum doses. The measurement of CFUs were also carried out at both high and standard inoculum doses, while the visualization experiments were carried out only at high inoculum cell density. To be able to observe the effects of DMSO and fluorescently labeled peptide solutions on bacterial growth, MICs of this solutions were determined. Schematic diagram for the preparation of 96-well microplate was given in Figure 3.1. The general protocol used for MICs determination experiments at standard and high inoculation cell density, followed by the measurement of CFUs is as follows:

- Prepare drug solution by adding 200 μL of the highest concentration to be tested to the well on the far right of each row and add 100 μL water solution to the other wells.
- Perform 2-fold serial dilutions by first withdrawing 100 μL of the highest drug concentration and pipetting it to the next well on the left that has 100 μL water solution.
- Continue performing 2-fold serial dilutions by mixing thoroughly and withdrawing 100 μL of drug solution and adding it to the next well on the left until reaching to the first column. Discard 100 μL of the diluted drug solution in the last well on the far left.
- To carry out the experiment at standard inoculum dose (2x10^4 to 10^5 CFU/mL), dilute the culture at OD_{600} = 0.3 by 1:5000 for both wild type *E. coli* K12 and opp-deleted mutant cells.
- Add 100 μL of the diluted culture to the wells that have 100 μL of drug solution at 2-fold concentrations.
- To carry out the experiment at high inoculum dose (10^7 to 10^8 CFU/mL), add 100 μL of the culture at OD_{600} = 0.3 to the wells that have 100 μL of drug solution at 2-fold concentrations.
- For MIC determination at standard and high inoculum doses, incubate the microplate for 20 hours in a microplate reader, while taking OD_{600} measurements at every 5 minutes. MICs are determined as the lowest drug concentrations at which no visible growth is observed.

To make sure that the initial cell counts are in the desired range, CFU measurements were performed. CFU measurements of three samples at $OD_{600} = 0.2$ (Sample 1), 1:20 dilution (Sample 2) and 1:600 dilution (Sample 3) were performed. The protocol for CFU measurements is as follows:

- Withdraw 100 μL of the bacterial solution and transfer to an eppendorf containing 900 μL fresh LB medium
- Dilute the sample in 10-fold serial dilution until the desired dilution was obtained
- Plate in Agar-LB solid medium to count the number of colony forming units after incubation at 37°C for up to 24 hours.

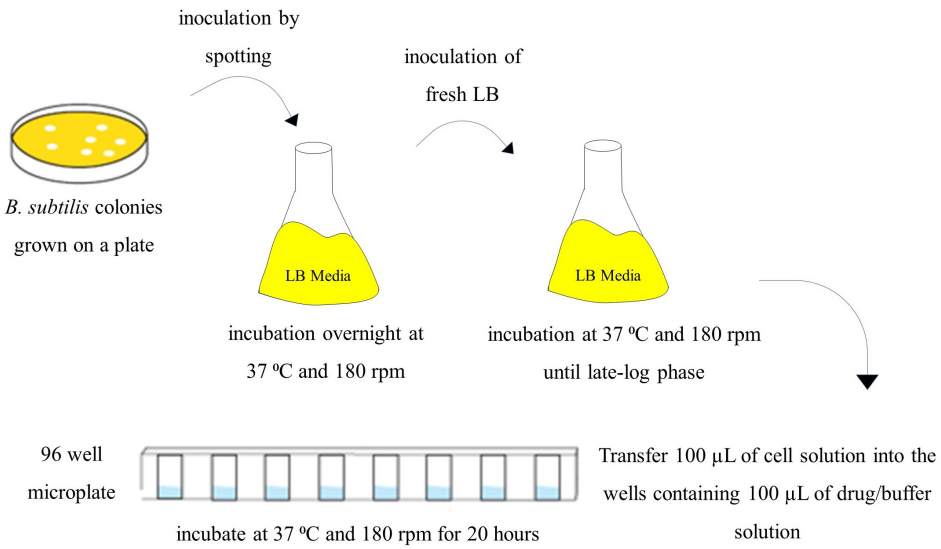

Figure 3.1. Schematic diagram for the preparation of 96-well microplate

3.8. Preparation of Swim-Swarm Plates for Bacillus Species

15 mL of sterile LB medium was inoculated with 130 μl of *B. subtilis* 168 cells from stock solution kept at -80°C and cells were grown overnight (16 hours) at 37°C and 180 rpm in a shaking incubator. The next day, the preculture of *B. subtilis* 168 strain was used for inoculation of fresh LB medium. 100 mL of LB medium was inoculated with 1 mL of preculture. It was incubated at 37°C and 180 rpm until mid-exponential phase (approximately $OD_{600} = 1.4$).

Plates containing less than 0.5 % agar allow cells to move through the porous medium and form a large zone of colonization, and therefore they are called as swim plates. On the other hand, plates containing greater than 0.5 % agar are called as swarm plates that reduce swimming through the agar because of small pore size and let bacterial movement only over the agar surface [52].

First experiment, the effect of different amiloride concentrations (1 mM, 2 mM and 3 mM) on both swimming and swarming motility was analyzed. To be able to observe the effect of amiloride on the motility, two different LB-agar solid media were prepared. The required amount of amiloride was weighed and added to the plates before the addition of agar medium. Using standard LB-agar solid medium procedure, 0.3 % agar plates (10 g NaCl, 5 g yeast extract, 10 g tryptone and 3 g agar per liter) for swimming analyses and 0.7 % agar plates (10 g NaCl, 5 g yeast extract, 10 g tryptone and 7 g agar per liter) for swarming analyses were prepared.

Next, four different LB-agar solid media were prepared to be able to observe the effect of Na^+ concentration on the bacterial motility. Using standard LB-agar solid medium procedure, 0.3 % agar plates (10 g NaCl, 5g yeast extract, 10 g tryptone and 3 g agar per liter) for swim plates and 0.7 % agar plates (10 g NaCl, 5g yeast extract, 10 g tryptone and 7 g agar per liter) for swarm plates were prepared. By increasing Na^+ concentration to 550 mM, 0.3 % agar plates (32 g NaCl, 5g yeast extract, 10 g tryptone and 3 g agar per liter) for swim plates and 0.7 % agar plates (32 g NaCl, 5g yeast extract, 10 g tryptone and 7 g agar per liter) for swarm plates were prepared. 250 mM of amiloride stock was prepared. Amiloride was dissolved in DMSO and added to the plates at a final concentration of 1 mM and 2 mM. Control plates were treated with the same DMSO concentrations for comparison.

Prepared LB-agar solid media were sterilized by autoclaving at 1 atm and 121 °C for 15 minutes. After the sterilization, LB-agar media were incubated at 70°C. Before the experiment started, LB-agar media were transferred to a water bath set at 54 °C.

Motility assays were prepared by spot inoculation method as described previously [53, 54]. After amiloride at the determined concentrations were added to the plates, 20 mL of LB-agar medium was added to the plates and dried for 30 minutes in a laminar flow hood. Then, agar plates were centrally inoculated with bacterial cells at OD = 1.4 by spotting the bacterial culture with a sterile toothpick. Afterwards, the plates were dried for another 10 minutes and incubated for 18 hours at 37 °C. After incubation for 18 h interval, the diameter of the colonies was measured.

For B. marmarensis cells, the motility assay was performed twice. In the first experiment, the effect of different amiloride concentrations (0.5 mM and 1 mM) on both swimming and swarming motility was analyzed. In the second experiment, the concentration range of amiloride was extended and the effect of different amiloride concentrations ranging from 0.2 mM to 1 mM on both swimming and swarming motility was analyzed.

3.9. Live-cell Imaging Using Microfluidics Systems

3.9.1. Microfluidic Devices for Monitoring of Bacterial Cells

Bacterial growth, motility experiments and fluorescent peptide uptake experiments were first carried out in hydrophilized zeonor reaction chamber chips of 10 μL volume with 500 μm chamber depth and 188 μm lid thickness. Microchips were purchased from Microfluidic ChipShop GmbH (Germany) (Figure 3.2). For the validation of bacterial uptake of fluorescently labeled peptide, the reaction chamber type of chips are not suitable. Trypsin enzyme will be used after fluorescent peptide perfusion into the chamber to understand whether peptide was internalized by bacterial cells or not. When the amount of fluorescent peptide increases in the chamber, the fluorescence background also increases and bacterial cells become invisible.

To be able to control the amount of fluorescent peptide perfusion into the chamber, the trypsin enzyme solution should be perfused from another inlet. For this reason,

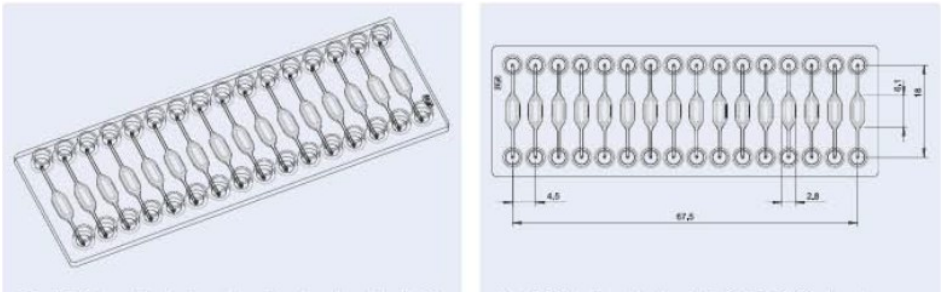

Figure 3.2. Schematic drawing of reaction chamber chips of 10 μL volume with 500 μm chamber depth and 188 μm lid thickness.

hydrophilized zeonor rhombic chamber chips eP2 of 6 μL volume with 200 μm chamber depth and 188 μm lid thickness were purchased from Microfluidic ChipShop GmbH (Germany) (Figure 3.3).

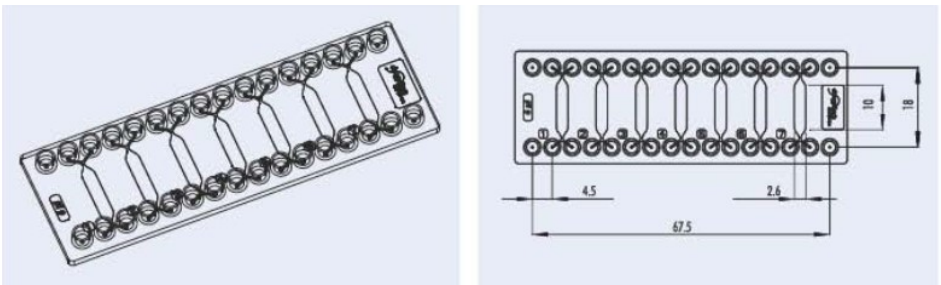

Figure 3.3. Schematic drawing of rhombic chamber chip of 6 μL volume with 200 μm chamber depth and 188 μm lid thickness.

3.9.2. Bacterial Growth in Zeonor Microchips-Reaction Chambers of 10 μL Volume

For bacterial growth, the microfluidic system was composed of two syringes (5 mL and 10 mL), one for diluted bacterial cell solution and the other one for fresh LB, connected by a Y-shaped capillary connector, purchased from Idex Health & Science (USA). Silicon tubing with an inner diameter of 0.5 mm and an outer diameter of 2.5 mm were used to connect the syringes to the zeonor microchip (Figure 3.4). The outlet of the silicone tubing was connected to the chip inlet using Opaque and Thermoplastic Elastomer (TPE) Male Mini Luer fluid connectors. Silicon tubing and Male Mini Luer connector were purchased from Microfluidic Chipshop GmbH (Germany). Before the

tubing was connected to the microchip, fresh LB media and bacterial cells were perfused separately to fill their tubings.

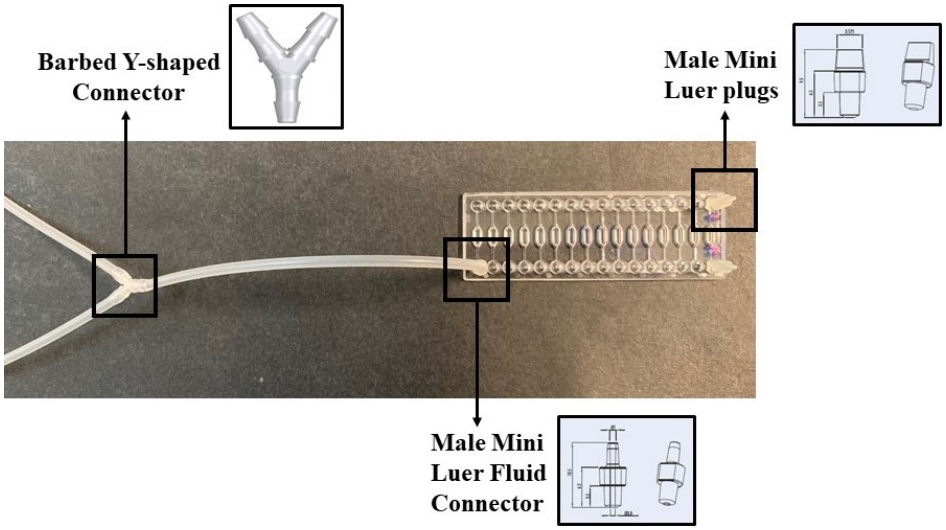

Figure 3.4. Silicon tubing, Barbed Y-shaped connectors, Male Mini Luer connector and Male Mini Luer plugs used in the experiments.

After filling the tubings and being sure that there is no bubble in the microfluidic system, Luer fluid connector (placed at the outer of the tubing) was connected to the inlet of the chip and the reaction chamber chip was placed under the inverted microscope (Figure 3.5). After the chamber was filled with LB medium, cell solution pump was switched on and then, the cells were delivered to the chamber at a rate of 0.2 μL/min for 30 minutes. Then, the cell solution was switched off, and fresh LB medium was perfused at a rate of 1 μL/min for 30 minutes in order to sweep the cells from the tubings to the chamber.

After the LB perfusion of 30 minutes, the perfusion rate was decreased to 0.5 μL/min. LB perfusion was continued at a rate of 0.5 μL/min for 45 minutes. Because the bacterial cells were swept from the chamber even at this rate, the perfusion rate was decreased to 0.3 μL/min and images were captured from the same spots every 15 minutes at 60X zoom using a 16.25 megapixel Nikon microscope camera (DS-Ri2). Cells were allowed to grow in the reaction chamber chip at room temperature as they were monitored.

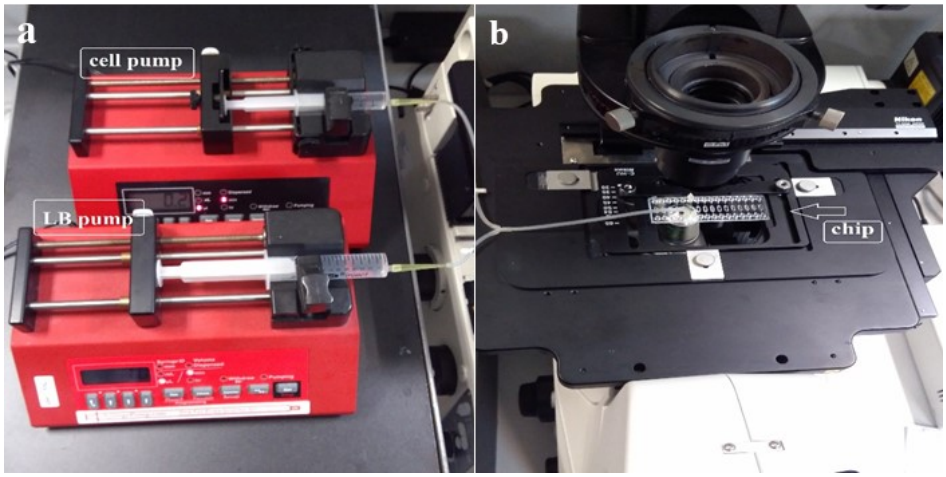

Figure 3.5. Experimental set-up to monitor bacterial growth. a) Two-pump system to enable controlled mixing of LB with cell suspension before entering the chip chambers; b) Visualization of the loaded chip using an inverted microscope.

3.9.3. Bacterial Motility in Microchips-Reaction Chambers of 10 μL Volume

For motility experiments in the absence of drug treatment, the experimental microfluidic system is composed of two syringes of different volumes, a syringe of 10 mL for sterile LB media perfusion, and the other syringe of 5 mL for the perfusion of diluted bacterial cell solution, connected by a Y-shaped capillary connector. Silicon tubing was used to connect the syringes to the zeonor microchip. The outlet of the silicone tubing was connected to the chip inlet via Mini Luer fluid connectors. For motility experiments in the presence of drug treatment, one more syringe of 1 ml for amiloride perfusion is included to the system and two Y-shaped capillary connectors are used to connect the syringes. Before the tubing was connected to the chip, fresh LB media and the cell solution were perfused separately to fill their tubings. After filling the tubings and being sure that there is no bubble in the system, Luer fluid connector (placed at the outer of the tubing) was connected to the inlet of the zeonor microchip, and the reaction chamber of the chip was placed under the inverted microscope.

After the chamber was filled with LB media, the pump of the cell solution was switched on and then, the cells were delivered to the chamber at a rate of 2 μL/min for

30 minutes. Then, the cell solution was switched off and fresh LB media was perfused at a rate of 0.8 μL/min for 1 hour in order to sweep the cells from the tubings to the chamber. After the LB perfusion of 1 hour, the perfusion rate was decreased to 0.5 μL/min for 30 minutes because bacterial cells were swept from the chamber at the perfusion rate of 0.8 μL/min. After LB pump was switched off, amiloride pump was switched on, and the drug amiloride was perfused at a rate of 0.5 μL/min for 2 hours. After amiloride perfusion, the pump of LB medium was switched on again and perfused at a rate of 0.5 μL/min for 30 minutes. Images were captured from the same spots every 15 minutes at 30X zoom using a 16.25 megapixel Nikon microscope camera (DS-Ri2). Cells were allowed to grow in the reaction chamber chip at room temperature as they were monitored.

3.9.4. Visualization of Fluoresceinamine Uptake by *E. coli* K12 Cells in Zeonor Microchips-Reaction Chambers of 10 μL Volume

After bacterial growth was observed in reaction chambers, these chambers were tested whether fluoresceineamine is internalized by bacterial cells spontaneously or not. The microfluidic system was composed of three syringes of different volumes, a syringe of 1 mL for fluoresceinamine perfusion, a syringe of 5 mL for washed bacterial cell solution and a syringe of 10 mL for sterile distilled water, connected by two Y-shaped capillary connectors. Silicon tubing connected the syringes to the microchip and the outlet of the silicone tubing was connected to the chip inlet using a Mini Luer Fluid connector.

To prevent the binding of the medium components to fluoresceinamine dye and mislead the uptake results, growth medium components were removed by washing steps. Once cells reached mid-logarithmic phase, 4 mL of sample was taken from the bacterial culture and transferred into the 1.5 mL of eppendorf tubes. 4 mL of sample was centrifuged at 10,000 rpm for 10 minutes, and then the supernatant was removed. Pellets were dissolved in sterile distilled water and these cell solutions were centrifuged at 10,000 rpm for 5 minutes. By centrifugation and washing steps, the undissolved

components of growth medium were removed from the bacterial culture. 4 mL of washed cell solution was transferred into a beaker containing 16 mL of sterile distilled water. Thus, washed cell solution was diluted 1:5 before perfusing into the chamber. Dilution was required since high density restrained cell monitoring and image capturing in the chamber.

Before the tubing was connected to the chip, sterile distilled water, fluoresceinamine dye (100 μM, in distilled water) and washed bacterial cells were perfused separately to fill their tubings. After filling the tubings and being sure that there is no bubble in the system, Luer fluid connector (placed at the outer of the tubing) was connected to the inlet of the chip and the reaction chamber chip was placed under the inverted microscope. After the chamber was filled with sterile distilled water, washed bacterial cell solution pump was switched on and then, the cells were delivered to the the chamber at a rate of 0.5 μL/min for 30 minutes. Then, cell solution was switched off and sterile distilled water was perfused at a rate of 1 μL/min for 1 hour in order to sweep the cells from the tubings to the chamber. After the sterile distilled water perfusion of 1 hour, the perfusion rate decreased to 0.5 μL/min. Sterile distilled water perfusion was continued at a rate of 0.5 μL/min for 30 minutes. Because bacterial cells swept from the chamber even at this rate, perfusion rate decreased to 0.2 μL/min and sterile distilled water was perfused at this rate for 25 minutes. Afterwards, fluorescein amine pump was switched on and perfused to the chamber at a rate of 0.2 μL/min. After time interval of 15 minutes, brightfield and fluorescence images were captured from the same spots every 15 minutes at 20X, 40X and 60X zoom using a 16.25 megapixel Nikon microscope camera (DS-Ri2). Fluorescence microscopy images were captured using the FITC filter. The chamber was monitored at room temperature continuously.

3.9.5. Visualization of Fluorescently Labeled Peptide Uptake by Bacterial Cells in Zeonor Microchips-Reaction Chambers of 10 μL Volume

For peptide uptake studies, the microfluidic system was composed of three syringes of different volumes, a syringe of 1 mL for peptide/dye perfusion, a syringe of 5

mL for washed bacterial cell solution and a syringe of 10 mL for sterile distilled water, connected by two Y-shaped capillary connectors. Silicon tubing with an inner diameter of 0.5 mm and an outer diameter of 2.5 mm connected the syringes to the microchip. The outlet of the silicone tubing was connected to the chip inlet using Mini Luer fluid connectors.

Growth medium components were removed by washing steps in order to prevent fluorescently labeled pVEC and P4 peptides from interacting with these components. Once the cells reached mid logarithmic phase, 4 mL of sample was taken from the bacterial culture and transferred into the 1.5 mL of eppendorfs. 4 mL of sample was centrifuged at 10,000 rpm for 10 minutes, and then its supernatant was removed. Pellets were dissolved in sterile distilled water and these cell solutions were centrifuged at 10,000 rpm for 5 minutes. By applying the centrifugation and washing steps, the undissolved growth medium components were removed from the bacterial culture. 4 mL of washed cell solution was transferred into a beaker containing 16 mL of sterile distilled water. Thus, washed cell solution was diluted 1:5 before perfusing into the chamber. This dilution was required since high density restrained cell monitoring and image capturing.

After the chamber was filled with sterile distilled water, washed bacterial cell solution pump was switched on and then, the cells were delivered to the chamber at a rate of 0.2 μL/min for 30 minutes. Then, the cell solution was switched off, and sterile distilled water was perfused at a rate of 1 μL/min for 1 hour in order to sweep the cells from the tubings to the chamber. After the sterile distilled water perfusion of 1 hour, the perfusion rate decreased to 0.5 μL/min. Sterile distilled water perfusion was continued at a rate of 0.5 μL/min for 30 minutes. Because bacterial cells swept from the chamber even at this rate, the perfusion rate was decreased to 0.2 μL/min and sterile distilled water was perfused at this rate for 30 minutes. Afterwards, fluorescently labeled pVEC solution (100 μM) was perfused to the chamber at a rate of 0.2 μL/min. After a 30 minutes time interval, brightfield and fluorescence images were captured from the same spots every 10 minutes at 40X zoom using a 16.25 megapixel Nikon

microscope camera (DS-Ri2). Fluorescence microscopy images were captured using the FITC filter. Nikon inverted microscope was used to visualize cells in the chamber continuously.

3.9.6. Visualization of Fluorescently-labeled Peptide Uptake by *E. coli* K12 Cells in Zeonor Microchips-Rhombic Chambers of 6 μL Volume

Experimental setup was composed of three syringes of different volumes, a syringe of 1 mL for peptide/dye perfusion, a syringe of 5 mL for washed bacterial cell solution and a syringe of 10 mL for sterile distilled water, connected by two Y-shaped capillary connectors. Silicon tubings connected the syringes to the microchip and the outlet of the silicone tubing was connected to the chip inlet using Mini Luer fluid connectors (Figure 3.6).

At the beginning, the drug solution was perfused from the second inlet using separate tubing. However, the fluorescence intensity increased in the chamber immediately after the connection of the tubing to the inlet. Even if sterile distilled water pump was switched on to sweep fluorescent peptide from the chamber before cell perfusion, fluorescent peptide residuals remained in the chamber and high fluorescence density was observed in the chamber. For this reason, same tubing system used in experiments with reaction chamber chips was used in this experiment and the second inlet was plugged with Male Mini Luer fluid plugs, purchased from Microfluidic Chipshop GmbH (Germany).

After the chamber was filled with sterile distilled water, washed bacterial cell solution pump was switched on and then, the cells were delivered to the chamber at a rate of 2 μL/min for 15 minutes. Then, the cell solution was switched off and sterile distilled water was perfused at a rate of 1 μL/min for 1 hour in order to sweep the cells from the tubings to the chamber. After that, the perfusion rate was decreased to 0.2 μL/min and sterile distilled water was perfused at this rate for 30 minutes. Afterwards, fluorescent peptide solution (50 μM) was perfused to the chamber at a rate of 0.5

μL/min. At the same time, the brightfield and fluorescence images were started to be captured from the same spots every 15 minutes at 40X zoom and 60X zoom using a 16.25 megapixel Nikon microscope camera (DS-Ri2). Fluorescence microscopy images were captured using the FITC filter. Nikon inverted microscope was used to visualize cells in the chamber continuously.

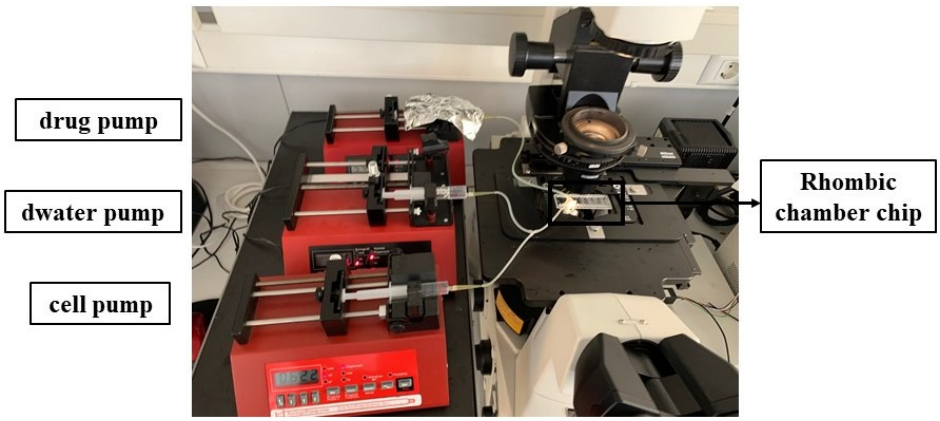

Figure 3.6. Experimental set-up for the visualization of bacterial uptake of fluorescent peptides. Three-pump system provides cell, distilled water and drug perfusion into the rhombic chamber, respectively.

3.9.7. Confirmation of Bacterial Uptake of Fluorescently-labeled Peptide in Zeonor Microchips-Rhombic Chambers of 6 μL Volume

Using zeonor microchips-rhombic chambers of 6 μL volume, the cell solution and fluorescent peptide perfusion was performed from separate inlets, the cell-peptide solution was perfused using one inlet and trypsin perfusion was conducted using the other inlet. The microfluidic system was composed of three syringes (1 mL and 10 mL), a syringe of 10 mL for washed bacterial cell solution and the other syringe of 1 mL for peptide/dye perfusion, connected by a Y-shaped capillary connector. A 1 mL syringe was used for trypsin perfusion into the chamber.

After OD_{600} of wild type *E. coli* K12 cells reached 0.25 (at the beginning of log phase), 2 eppendorfs were prepared and 1 mL of culture at OD_{600} of 0.25 was taken and placed into these eppendorfs. Bacterial cell samples were washed with sterile distilled

water in order to remove LB medium. In washing steps, eppendorfs were centrifuged at 6000 rpm for 10 minutes and supernatants were removed by pipetting. Afterwards, cell pellets were dissolved in 1 mL of sterile distilled water. 99 ml of sterile distilled water was added to a beaker and the cell solution in the eppendorf was transferred to this beaker and mixed thoroughly (1:100 dilution). Diluted cell solution was filled into a syringe of 10 mL.

Zeonor microchip-rhombic chamber of 6 μL was placed on the stage of inverted microscope. Before the capillary tubings were connected to the inlets of microchip, the pumps were operated and the solutions were perfused successively in order to fill the tubings with solutions and prevent bubble formation. First, the diluted cell solution was perfused at a rate of 1 μL/min to the chamber for 30 min and then, the flow rate was decreased to 0.2 μL/min and the cell solution was continued to perfuse into the chamber for 30 min. Afterwards, the cell solution pump was switched off, and the peptide solution pump was switched on at a rate of 0.2 μL/min. After 2 hours of perfusion of the fluorescent peptide, the peptide pump was switched off, and the trypsin pump was switched on at a rate of 0.2 μL/min for 1 hour. Microscopy images from the same spot in the chamber were captured every 15 minutes at 40X and 60X zoom. Fluorescence microscopy images were captured using the FITC filter.

3.9.8. Bacterial Motility in Microchips-Reaction Chambers of 10 μL Volume

For motility experiments in the absence of drug treatment, the experimental microfluidic system is composed of two syringes of different volumes, a syringe of 10 mL for sterile LB media perfusion, and the other syringe of 5 mL for the perfusion of diluted bacterial cell solution, connected by a Y-shaped capillary connector. Silicon tubing was used to connect the syringes to the zeonor microchip. The outlet of the silicone tubing was connected to the chip inlet via Mini Luer fluid connectors. For motility experiments in the presence of drug treatment, one more syringe of 1 ml for amiloride perfusion is included to the system and two Y-shaped capillary connectors are used to connect the syringes.

Before the tubing was connected to the chip, fresh LB media and the cell solution were perfused separately to fill their tubings. After filling the tubings and being sure that there is no bubble in the system, Luer fluid connector (placed at the outer of the tubing) was connected to the inlet of the zeonor microchip, and the reaction chamber of the chip was placed under the inverted microscope.

After the chamber was filled with LB media, the pump of the cell solution was switched on and then, the cells were delivered to the chamber at a rate of 2 μL/min for 30 minutes. Then, the cell solution was switched off and fresh LB media was perfused at a rate of 0.8 μL/min for 1 hour in order to sweep the cells from the tubings to the chamber. After the LB perfusion of 1 hour, the perfusion rate was decreased to 0.5 μL/min for 30 minutes because bacterial cells were swept from the chamber at the perfusion rate of 0.8 μL/min. After LB pump was switched off, amiloride pump was switched on, and the drug amiloride was perfused at a rate of 0.5 μL/min for 2 hours. After amiloride perfusion, the pump of LB medium was switched on again and perfused at a rate of 0.5 μL/min for 30 minutes. Images were captured from the same spots every 15 minutes at 30X zoom using a 16.25 megapixel Nikon microscope camera (DS-Ri2). Cells were allowed to grow in the reaction chamber chip at room temperature as they were monitored.

3.10. Confocal Analyses

Bacterial uptake of fluorescently labeled peptides by wild type *E. coli* K12 and opp-deleted mutant *E. coli* K12 SS5013 cells were performed in both reaction chambers of 10 μl and rhombic chambers of 6 μL. Fluorescence images were then processed to figure out fluoresence intensity inside the bacterial cells. Afterwards, trypsin treatment was conducted to reveal whether florescent peptides were internalized by bacterial cells or just stuck on the membrane of these cells. However, bacterial cells look like small dot-like stains on fluorescence images. Whether fluorescent peptides were internalized or not is unclear in these images. For this reason, bacterial cells were analyzed under confocal microscopy to observe the location of fluorescent peptides in bacterial cells.

3.10.1. Cell Fixation

After OD_{600} of wild type *E. coli* K12 cells reached 0.2-0.3 (at the beginning of log phase), 8 eppendorfs for *E. coli* K12 cells and 8 eppendorfs for mutant cells were prepared and 1 mL of bacterial culture at OD_{600} of 0.2-0.3 was taken and placed into these eppendorfs. Bacterial cell samples were centrifuged at 6000 rpm for 10 minutes. The supernatant parts were removed by pipetting and cell pellets were resuspended in 1 mL of sterile 1X PBS. Then, the bacterial solutions in 4 eppendorfs were transferred into an erlenmeyer flask of 50 mL. To get the final concentration of 50 μM of fluorescently labeled pVEC, 40 μL of the fluorescent peptide was taken from the stock solution and transferred to the erlenmeyer flask. One erlenmeyer flask was used for the incubation of *E. coli* K12 cells with fluorescently labeled P4 peptide, another one was used for the incubation of opp-deleted mutant *E. coli* K12 SS5013 cells with fluorescenly labeled pVEC and the last one was used for the incubation of mutant cells with fluorescently labeled P4 peptide. Then, bacterial cells in erlenmeyer flasks were incubated at 37°C and 180 rpm for 30 minutes and 60 minutes. After the 30 minute-incubation with fluorescent peptides, 1 mL of bacterial sample was taken and transferred to an eppendorf and centrifuged at 8000 rpm for 10 minutes. The supernatant was removed and cell pellet was resuspended in 500 μL of 1X PBS.

37 % paraformaldehyde (PFA) solution was diluted with 1X PBS to obtain 3.7 % concentration. Sterile coverslips were placed into sterile 24 well culture plate. The washed bacterial cell solution was added on the surface of the coverslips. The plate was centrifuged at 6000 rpm for 15 minutes. The media was removed by pipetting slowly and 200 μl of 3.7 % PFA was added on the coverslip and the plate was incubated for 15 minutes at room temperature. After the incubation, the plate was centrifuged at 6000 rpm for 15 minutes. PFA was removed and bacterial cells were washed with 500 μL of 1X PBS carefully. 5 μL of mounting media was added on a microscopy slide and coverslips were put on the slides. Bacterial cells were faced with the mounting media to improve the image and prevent the sample from drying. The edge of the coverslips was glued via transparent nail and visualized under confocal microscopy.

3.10.2. Confocal Microscopy Imaging

After the removal of LB medium, bacterial solutions were transferred into an eppendorf and final concentration of fluorescent peptides was adjusted to 50 μM. Bacterial cells were incubated with 50 μM of fluorescent peptides for 1 hour. After incubation, fluorescent peptides being not internalized were removed from bacterial cells by filtration with Ultra-15 Centrifugal Filter Devices (30,000 MWCO). Since fluorescenly labeled pVEC and P4 peptides precipitated with bacterial cells during centrifugation steps, bacterial cells could not have removed from fluorescent peptides and this filters were used.

After centrifugation, 1 mL of sterile distilled water was added on the filter to wash bacterial cells. 1 mL of this cell solution was taken and transferred to an eppendorf. Afterwards, 10 μL of PI dye was added on this solution and incubated for 5 minutes in the dark at room temperature. After 5 minutes of incubation, this solution was centrifuged to remove PI dye. The supernatant was removed and cell pellets were resuspended in 500 μL of PBS. 2.5 μL of cell solution was added on a microscopy glass and covered with a coverslip. Then, the edges of the coverslip was glued with a transparent nail. Bacterial cells were observed on an inverted Confocal Microscopy. Brightfield, Texas Red and FITC images were captured at 40X zoom.

3.11. Image Processing

3.11.1. Fluorescence Image Processing

The aim is to determine the fluorecence intensity around the bacterial cells as well as the ratio of fluorescent to nonflourescent bacterial cells in the chamber. A fluorescent image of the bacterial cells and the image processing steps were illustrated below. The image was in RGB format and the channels need to be splitted for the analysis of fluorescence image. *Image* $\rightarrow$ *Colour* $\rightarrow$ *Split Channels* command was used to split the channels.

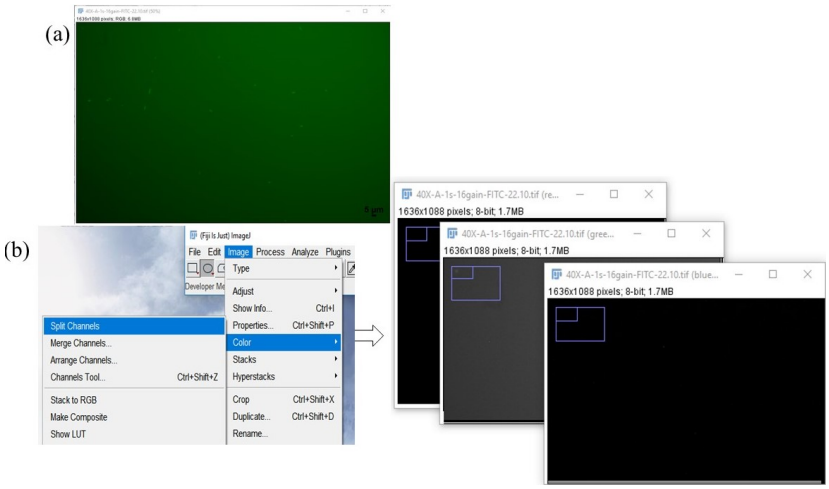

Figure 3.7. Image processing steps (a) the selected fluorescence image (b) applying split channels command.

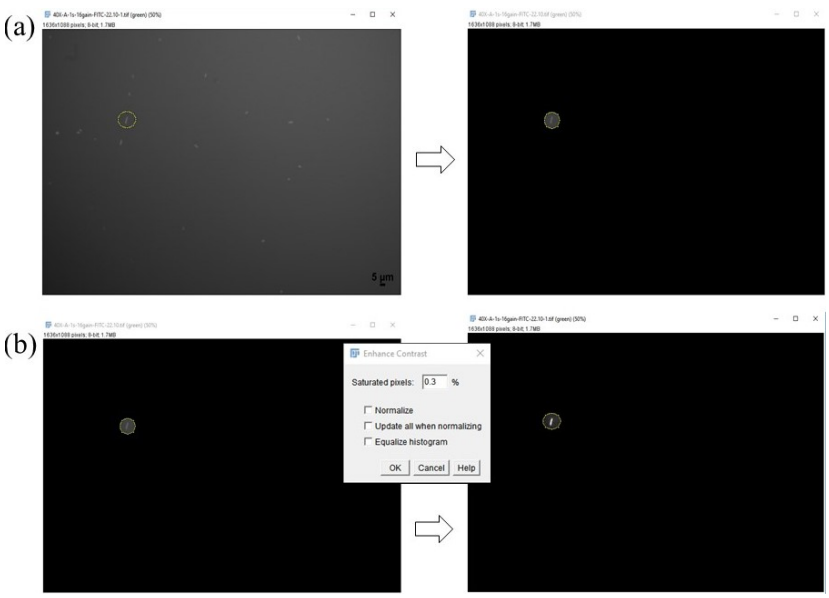

Figure 3.8. Image processing steps (a) applying clear outside (b) enhancement of the image contrast.

The RGB image (or stack) was split into three 8–bit grayscale images containing the red, green and blue components of the original, which are opened in separate windows (Figure 3.7). The interested region is drawn with Oval selection in toolbox and *Edit* → *Clear Outside* was used to erase the area outside the selected interested area to the background color. *Process* → *Enhance Contrast* increases contrast of the image or selection. Saturated pixels were adjusted to 0.3 % (Figure 3.8). *Auto Threshold* tool was used to set lower and upper threshold values, segmenting grayscale images into features of interest, automatically. *Image* → *Adjust* → *Auto Threshold*, Otsu was selected from Method and White objects on black background was chosen. *Process* → *Binary* → *Convert to Mask* was selected to display black objects on a white background (Figure 3.9).

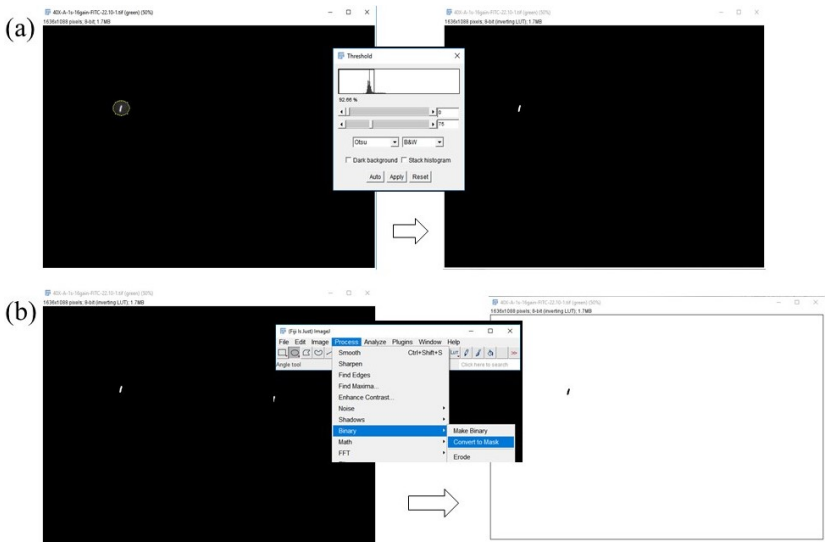

Figure 3.9. Image processing steps (a) applying auto threshold (b) converting into mask.

Analyses and measurements were performed using Analyze → Analyze particles tool. *Analyze* → *Set measurements* commands were used to specify the measurements such as area, integrated density (intensity), and perimeter. On the Analyze Particles box, Size (pixel^2) was arranged between 30-infinity and it was adjusted to show outline. Display results, clear results and add to manager choices were chosen (Figure 3.10). In the Results section, all properties of the cells were written individually and the specific cell from ROI manager was selected to see its features (Figure 3.10).

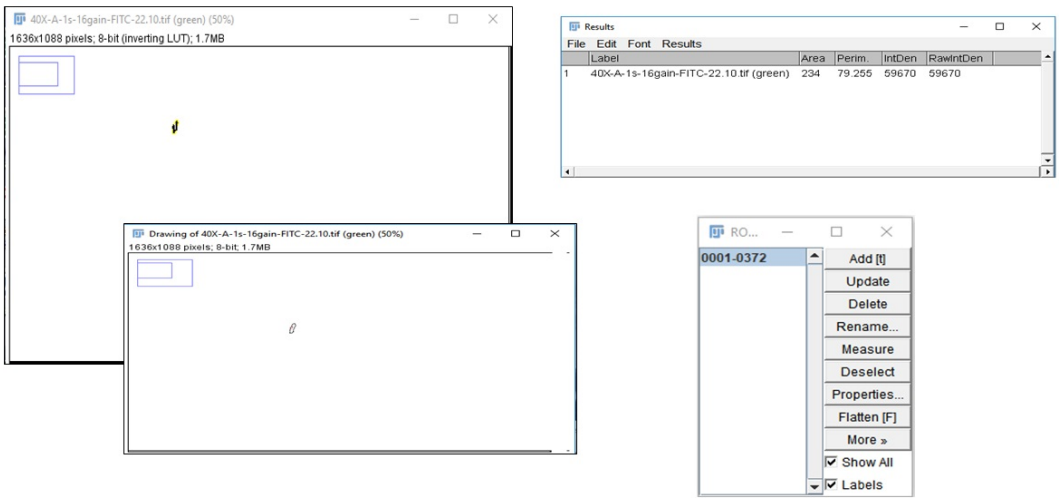

Figure 3.10. Analyses and measurents of bacterial cells.

The processing steps mentioned above were applied for each image. A macro code was written to speed up this process. The macro code for fluorescence images was given in Figure 3.11.

```
run("Enhance Contrast...", "saturated=0.2");
setAutoThreshold("Otsu dark");
//run("Threshold...");
setOption("BlackBackground",false);
run("Convert to Mask");
```

Figure 3.11. Macro for the analysis of fluorescence images.

To be able to measure the corrected total cell fluorescence (CTCF), the fluorescence density of background was subtracted from the measured integrated density of cells. Five different regions with the same area near the cell were selected, mean grey value was measured and average mean grey value of these regions was calculated. This step was repeated for all cells in the field of view that we want to measure. Then, CTCF was calculated as follows:

CTCF = Integrated Density - (Area of selected cell x Mean fluorescence of background readings)

3.11.2. Confocal Image Processing

The aim is to determine the location of fluorescent peptide inside the bacterial cells and fluorecence intensity of bacterial cells. A confocal image of the bacterial cells and the image processing steps were illustrated below. The image was in 8-bit and the channels need to be arranged for the analysis of confocal image. *Image* → *Color* → *Channels Tool* was used to arrange the channels. Color was chosen and there is a button labeled "More" at the bottom of the window that allows you to choose new channel colors from a list. Green was assigned to channel 1, green was assigned to channel 2, and grays was assigned to channel 3.

Image→ *Color* → *Split Channels* command was used to split the channels. The 8-bit confocal image was split into three 8–bit confocal images containing the green, red and gray components of the original, which are opened in separate windows.

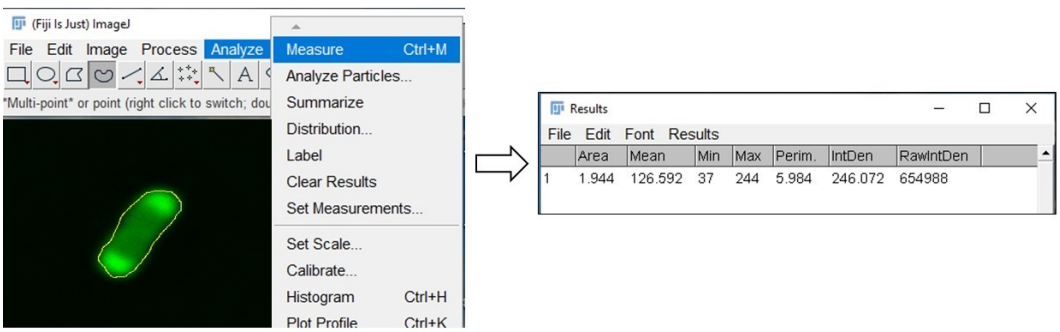

Figure 3.12. Confocal image processing steps. The region of interest is drawn with freehand selection and fluorescence intensity is measured using Analyze → Measure command.

Images were in 8-bit format and they need to be converted to RGB color. *Image* → *Color* → *Merge Channels* command was used to merge channels and make a composite. Composite was in 8-bit format and it was converted to RGB color as well. Those images can be put into a stack via *Image* → *Stacks* → *Images to Stack* command. Then, the stack is displayed along with the separate channels in a final figure. This can be done with *Image* → *Stacks* → *Make Montage* command.

Analyze → *Tools* → *Scale Bar* was selected to add scale bar into the montage image. When the size, color and placement of the scale bar were adjusted and clicked on "OK", it appears on the image. This image with scale bar is saved as Jpeg. To measure the fluorescence intensity of bacterial cells, a region of interest (ROI) around the bacterial cells with one of the drawing tools such as *polygon or freehand* → *Measure* command was used (Figure 3.12).

In addition, *Analyze* → *Plot Profile* command was used to create a plot of intensity values across features in the image. In the example given in Figure 3.13, the plot gives the intensity values along the straight line drawn across the width of the bacterial cell.

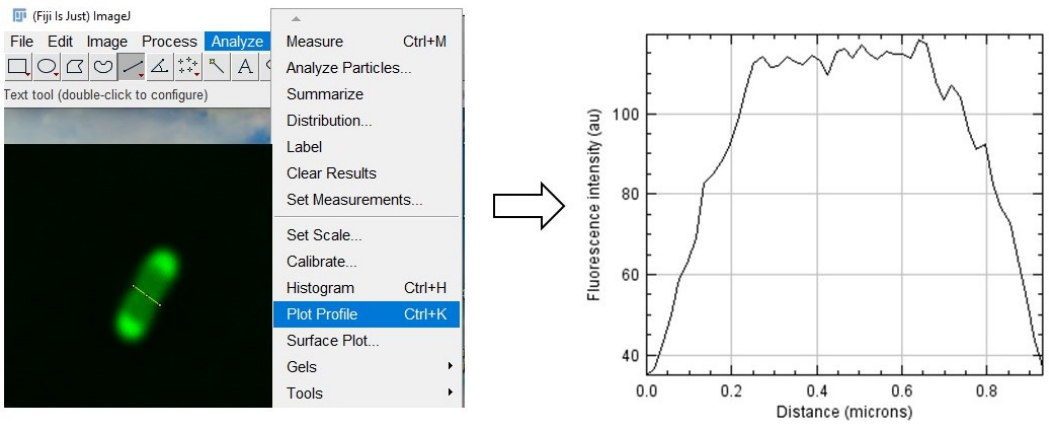

Figure 3.13. Confocal image processing steps. A straight line is drawn across the width of a bacterial cell and fluorescence intensity distribution of the interested region is measured using Analyze → Plot Profile command.

3.11.3. Determination of Bacterial Swimming Rate

Time-lapse images of bacterial cells captured every 15 minutes during the experiment were analyzed via Fiji-ImageJ software. Motile *B. subtilis* 168 cells were followed in time-lapse images taken at 1 second intervals for 8 seconds in the reaction chambers of 10 μl volume and 500 μm depth.

Due to its dimensions, this microchip provides bacterial cells with a wide environment in which cells move randomly. An example of the bacterial motility in a zeonor microchip-reaction chamber of 500 μm depth and 10 μl volume is shown in Figure 3.14.

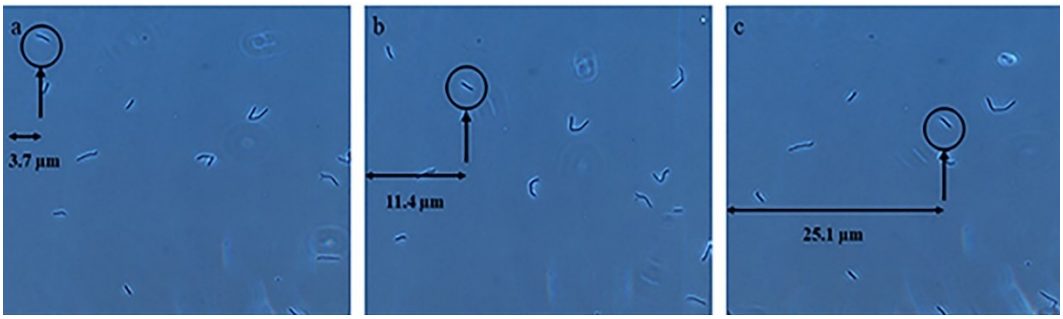

Figure 3.14. Bacterial motility in a reaction chamber. Time-lapse images captured at 3 s intervals show the swimming of *B. subtilis* 168 strain. A selected *B. subtilis* 168 bacterium is followed through a 10 μL volume reaction chamber.

Since we focused on a fixed area in the chamber during the image capturing process, we analyzed the cells, that move around this area, simply. As a result, we assumed that the bacterial movement is two-dimensional in our case. By ignoring the depth of the microchip, the positions of bacterial cells in x-direction and y-direction in time-lapse images were determined by ImageJ and collected in an excel file. A matlab code was written to calculate the distance, that the bacterial cells moved along the reaction chamber every second, and so the swimming rate of bacterial cells was determined using a microfluidic chip platform.

4. RESULTS AND DISCUSSION

Effects of drugs on bacterial cells were analyzed in two aspects; bacterial uptake mechanism of fuorescently labeled peptides and motility studies in microfluidic devices, respectively. Experimental results involves MIC results, swim-swarm assays, live-cell imaging using microdevices and confocal analyses. Before chip experiments, CFD simulations were performed to determine flow rates of cell, LB and drug perfusion into the chamber.

4.1. CFD Simulations

In CFD simulations, five models were tested to analyze the fluid flow and concnetration distribution in tubings and the chamber.Inlet flow rate values for cell, LB ad drug perfusion were taken from the reported microchip experiments previously. Fluid flow and concentration distribution profiles of five models tested were given below.

4.1.1. Determination of Optimum Inlet Flow Rates

The system is composed of three inlets (tubings) and the chip. In the tubing system, the first and the second tubings are connected by a Y-shaped capillary connector and another Y-shaped capillary connector is used to connect the third tubing to the other tubings. First, the outlet of the tubing system is connected to the chip inlet. When the tubing and the chip system is combined, the simulation does not work properly because of the geometry difference. Therefore, the tubing and the chip systems are simulated separately.

For tubing system, stationary study was used for both velocity and concentration distribution and the flow rate and concentration values taken from tubing outlet is set as the inlet parameter for the chip. Then, stationary study was used to obtain velocity profile and time-dependent study was used to obtain concentration distribution with

respect to time within the chip. The aim is to find optimum flow rate for cell attachment in the chamber efficiently. To achieve this aim, several inlet flow rates were tested and the flow profile inside the system was analyzed. Table 1 shows the summary of flow rates and profiles which were tested to identify the optimum velocity values for the inlets.

Table 4.1. Summary of inlet flow rates and velocities in the models.

Model	**Cell loading (μL/min)**	**Medium loading (μL/min)**	**Drug loading (μL/min)**	**Velocity (m/s)**	**Flow**
1	1	1	1	5.62x10^{-5}	Too slow
2	10	10	10	8.35x10^{-4}	Rapid
3	5	2	2	2.6x10^{-3}	Too rapid
4	2	1	1	1.38x10^{-4}	Optimum
5	1	0.5	0.5	5.55x10^{-5}	Too slow

In the first simulation study, same inlet flow rates of 1 μL/min were used in three inlets. Fluids perfused from the inlets merged in the Y shaped connectors. The diameter of the connectors is 1.5 mm which is the three times larger than the the tubing diameter. Velocity decreased within the connector due to increase in volume but velocity increased just in the exit of the connector where the flow at the two tubings combined and move on via one tubing. Cell solution concentration of 1.33x10^{-10} mol/m^3 is fed through the first inlet, medium concentration of 20 mol/m^3 is fed through the second inlet and drug concentration of 5 mol/m^3 is fed through the third inlet. Concentration profile shows distinct concentration changes within the connectors. To obtain the flow rate and concentration at the outlet of the tubing, velocity and concentration graphs were drawn. From the velocity and concentration graphs along horizontal axis given in Figure 4.1, the flowrate and concentration at the outlet of the tubings are found as 3.7x10^{-4} m/s and 1.25 mol/m^3, respectively.

These values are set as inlet parameter for the chip. Concentration distribution was obtained by time-dependent study. Maximum velocity value of 0.41 mm/s is seen

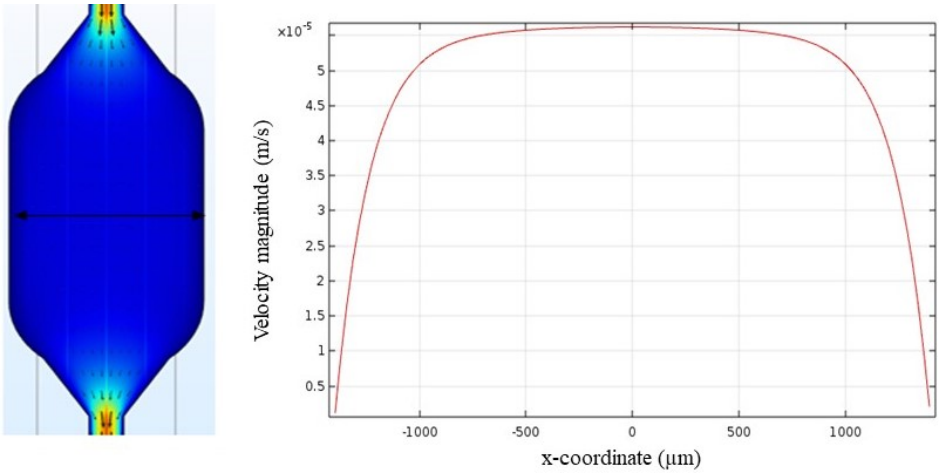

Figure 4.1. Velocity profile along horizontal axis at the center of the chip in model 1.

in the inlet and the outlet of the chip. Velocity decreased in the middle of the chamber. Maximum pressure of 0.23 Pa is in the inlet of the chip and decreased towards outlet of the chip. To obtain the flow rate and concentration at the center of the chip, velocity, pressure and concentration profiles were obtained. The velocity at the center of the chip is found as 5.62x10^{-5} m/s. Since the outlet of the device is open to the atmosphere, the pressure at the outlets is zero. The pressure difference between the inlets and outlets shows the progress of fluid flow within the chamber. Pressure drop was small at the center of the chamber due to the increase in volume.

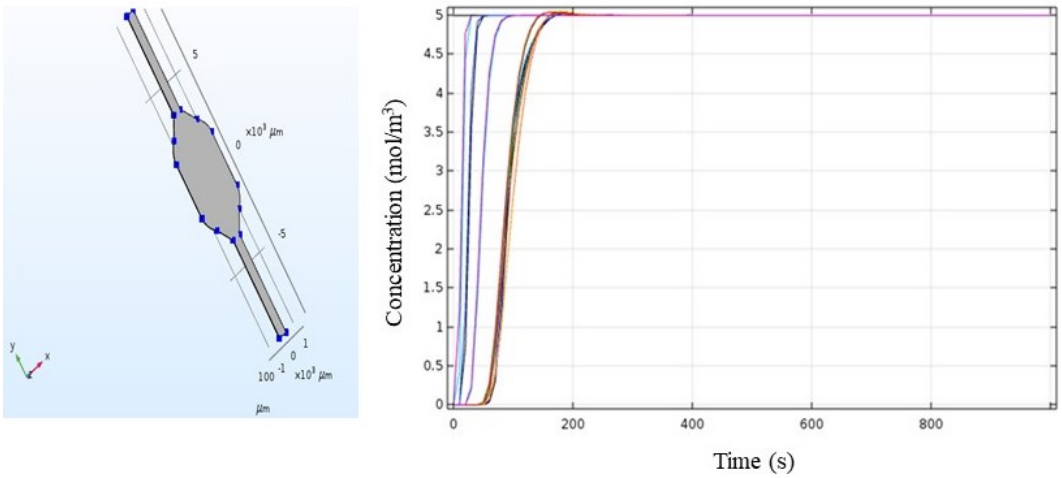

Figure 4.2. Concentration distribution at all points with respect to time in model 1.

Concentration profile in time-dependent study (Figure 4.2) indicates that the fluid

reaches to outlet in 320 seconds. The concentration profiles at the chamber entrances show that the time necessary to reach the concentration of 1.25 mol/m^3 is very short compared to other points along the chamber. Over time, the other points also reach to the desired concentration. Therefore, it can be said that proper diffusion is achieved in the chamber. Speed in the chamber indicates that the fluid flow is too slow. Therefore, flow rate at 1 μL/min is not efficient for cell and nutrient loading into the chamber.

In model 2, inlet flow rates were increased by 10 fold and same inlet velocities (10 μL/min) were used for all the inlets. To obtain the flow rate and concentration at the outlet of the tubing, velocity and concentration graphs were drawn. From the velocity and concentration graphs along horizontal axis the flowrate and the average concentration at the outlet of the tubings are found as 0.0055 m/s and 8.32855 mol/m^3, respectively. These values are set as inlet parameter for the chip.

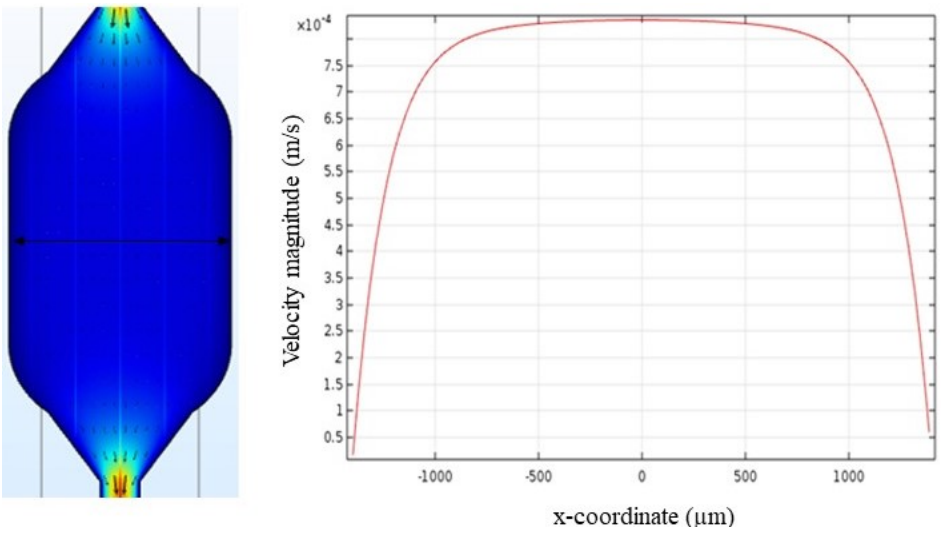

Figure 4.3. Velocity profile along horizontal axis at the center of the chip in model 2.

The steady-state velocity distribution within the chip is given in Figure 4.3. Maximum velocity value of 6.06 mm/s is seen in the inlet and the outlet of the chip. Velocity decreased in the middle of the chamber which can be seen from the blue color. Maximum pressure of 3.44 Pa is in the inlet of the chip and decreased towards outlet of the chip. To obtain the flow rate and concentration at the center of the chip, velocity and concentration graphs were drawn.

The velocity at the center of the chip is found as 8.35x10^{-4} m/s. Pressure profile indicates that pressure decreases along the chip but pressure drop was small at the center due to the increase in volume. Concentration profile given in Figure 4.4 indicates that the fluid reaches to outlet in 30 seconds which is a very short time to fill the chamber and may lead to sweep of the cells in the chamber. Velocity in the chamber indicates that the fluid flow is rapid. Therefore, flow rate at 10 μL/min is not efficient for cell and nutrient loading into the chamber.

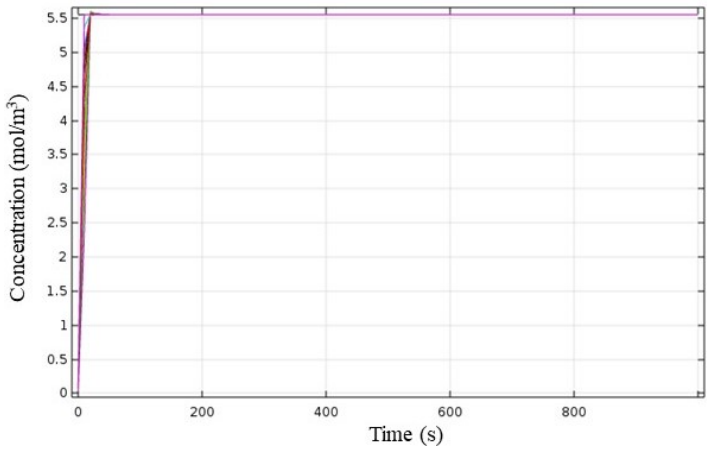

Figure 4.4. Concentration distribution at all points with respect to time in model 2.

In model 3, different inlet velocities were used. Flow rate of 5 μL/min is used for cell loading, flow rate of 2 μL/min is used for both medium and drug perfusion. In the first Y-shaped connector, distinct concentration change was seen but concentration distribution was uniform in the second connector. The flowrate and the average concentration at the outlet of the tubings are found as 0.0017 m/s and 5.5511 mol/m^3, respectively. These values are set as inlet parameter for the chip.

Maximum velocity value of 18.7 mm/s is seen in the inlet and the outlet of the chip. Velocity decreased in the middle of the chamber which can be seen from the blue color. Maximum pressure of 10.6 Pa is in the inlet of the chip and decreased towards outlet of the chip. To obtain the flow rate and concentration at the center of the chip, velocity and concentration graphs were drawn and given in Figure 4.5 and Figure 4.6. The velocity at the center of the chip is found as 0.0026 m/s. Pressure profile indicates that pressure decreases along the chip but pressure drop was small at the center.

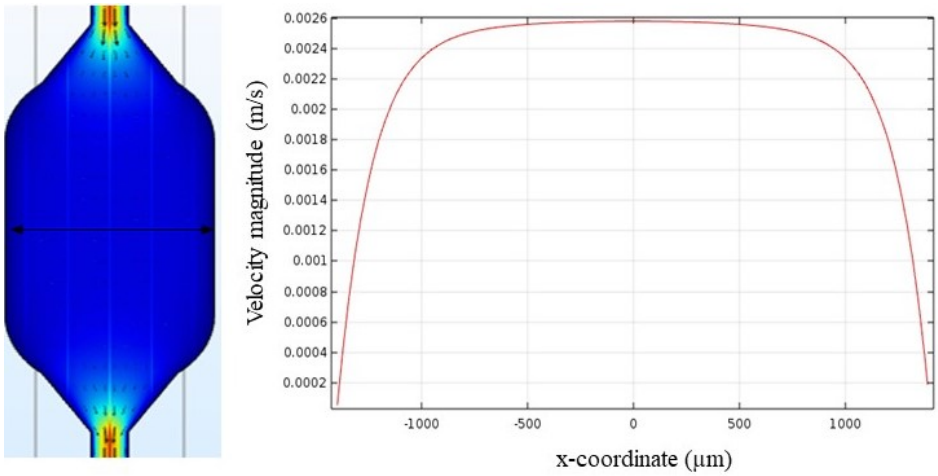

Figure 4.5. Velocity profile along horizontal axis at the center of the chip in model 3.

Concentration profile indicates that the fluid reaches to outlet in 10 seconds which is a pretty short time for cell and nutrient loading and lead cells to sweep from the chamber probably. Velocity in the chamber indicates that the fluid flow is too rapid. Therefore, flow rate at 5 μL/min for cell loding and 2 μL/min for medium and drug perfusion is not efficient.

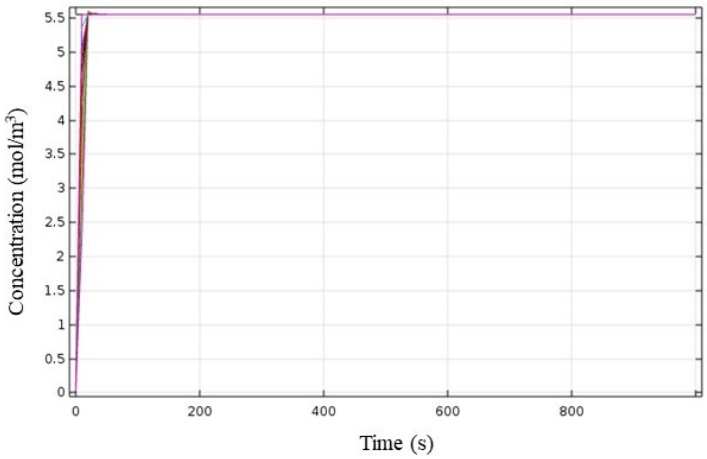

Figure 4.6. Concentration distribution at all points with respect to time in model 3.

In model 4, different inlet velocities were used. Flow rate of 2 μL/min is used for cell loading, flow rate of 1 μL/min is used for both medium and drug perfusion. In the first Y-shaped connector, distinct concentration change is seen. On the other hand, the second connector has a uniform concentration distribution, which is important for efficient nutrient feeding. The flowrate and the average concentration at the outlet of

the tubings are found as 9.15x10^{-4} m/s and 5 mol/m^3, respectively and these values are set as inlet parameter for the chip.

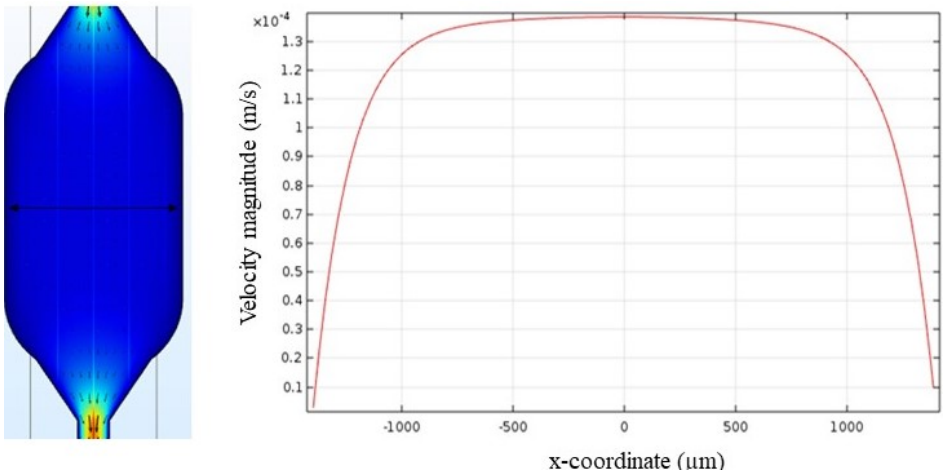

Figure 4.7. Velocity profile along horizontal axis at the center of the chip in model 4.

Maximum velocity value of 1 mm/s is seen in the inlet and the outlet of the chip. Velocity decreased in the middle of the chamber which can be seen from the blue color. Maximum pressure of 0.57 Pa is in the inlet of the chip and decreased towards outlet of the chip.

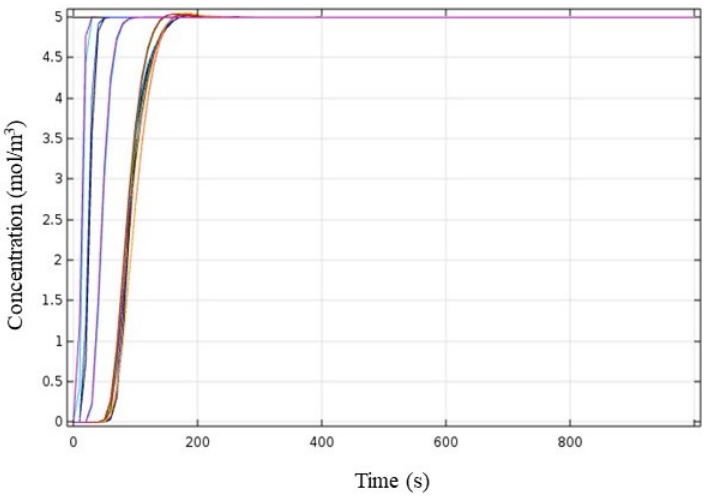

Figure 4.8. Concentration distribution at all points with respect to time in model 4.

The velocity at the center of the chip is found as 9.15x10^{-4} m/s (Figure 4.7). Pressure profile indicates that pressure decreases along the chip but pressure drop was small at the center due to the increase in volume. Concentration profile given in Figure

4.8 indicates that the fluid reaches to outlet in 150 seconds which is effective for nutrient loading. Velocity in the chamber indicates that the fluid flow is optimum for both cell and medium feeding. As a result, flow rate at 2 μL/min for cell loading and 1 μL/min for medium and drug loading into the chamber is efficient.

In model 5, different inlet velocities were used. Flow rate of 1 μL/min is used for cell loading, flow rate of 0.5 μL/min is used for both medium and drug perfusion. A distinct concentration change is seen in the first Y-shaped connector, whereas an almost uniform concentration distribution was observed in the second connector. From the velocity and concentration graphs along horizontal axis, the flowrate and the average concentration at the outlet of the tubings are found as 3.66x10^{-4} m/s and 6.25 mol/m^3, respectively, which are set as inlet parameter for the chip. Maximum velocity value of 0.4 mm/s is seen in the inlet and the outlet of the chip. Velocity decreased in the middle of the chamber. Maximum pressure of 0.23 Pa is in the inlet of the chip and decreased towards outlet of the chip.

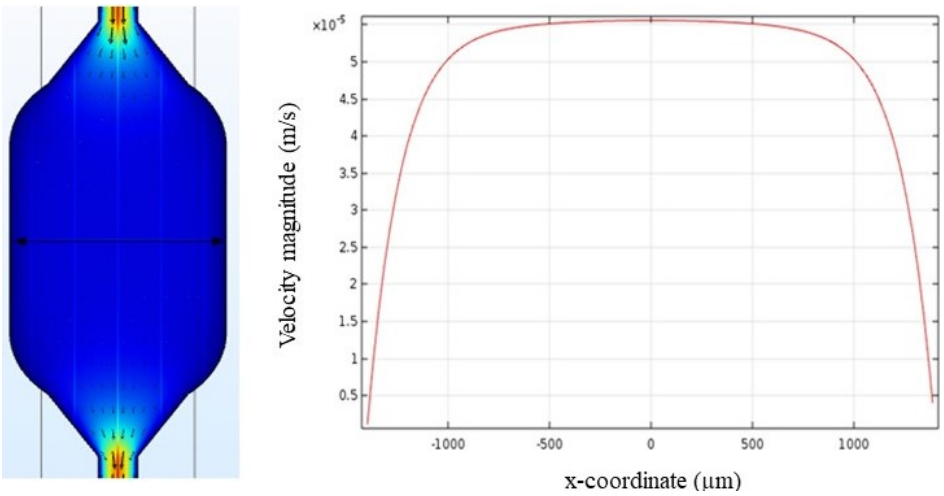

Figure 4.9. Velocity profile along horizontal axis at the center of the chip in model 5.

The velocity at the center of the chip is found as 5.55x10^{-5} m/s (Figure 4.9). Pressure profile indicates that pressure decreases along the chip but pressure drop was small at the center due to the increase in volume. Concentration profile given in Figure 4.10 indicates that the fluid reaches to outlet in 350 seconds. Velocity in the chamber indicates that the fluid flow is not sufficient for both cell and medium feeding. As

a result, flow rate at 3 μL/min for cell loading and 1 μL/min for medium and drug loading into the chamber is not efficient.

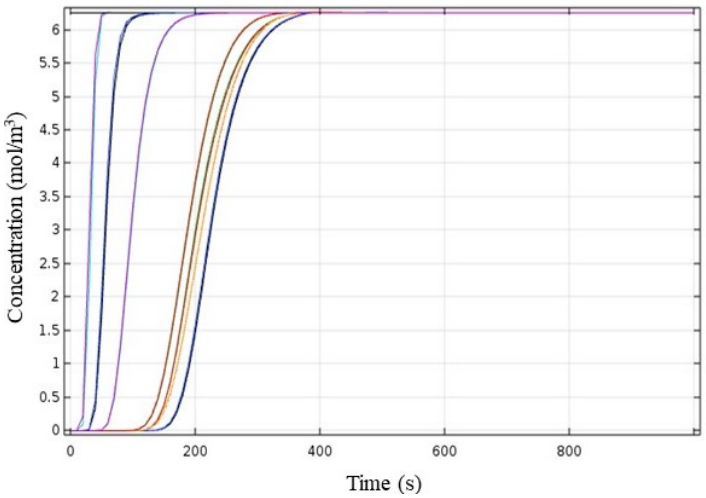

Figure 4.10. Concentration distribution at all points with respect to time in model 5.

4.1.2. Time-dependent concentration distribution within the tubing system

In model 4, time-dependent study was used to reveal concentration profile with respect to time within the tubing system and figure out the loading time of tubings. The steady-state velocity distribution and time-dependent concentration profile within the first connector is given in Figure 4.11.

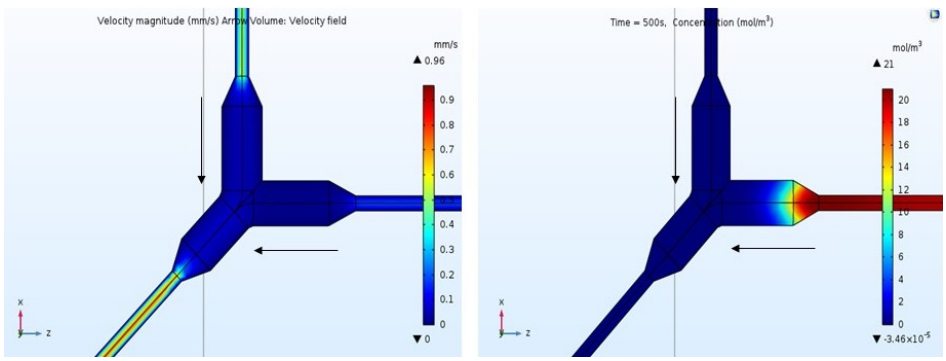

Figure 4.11. Steady-state velocity (left) and time dependent concentration (right) distributions within the first Y-shaped connector

The flow rate at the second inlet is 1 μL/min and length of the second tubing is 4 cm. Fluid reaches to Y-shaped connector in 500 seconds.

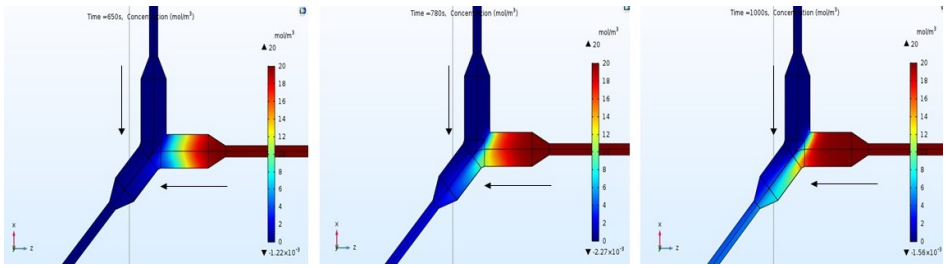

Figure 4.12. Concentration distribution within the first Y-shaped connector with respect to time

Over time, concentration in the connector increases (Figure 4.12). From steady state solution, concentration values along horizontal axis at the outlet of the first connector varies between 2.5 and 6.5 mol/m^3. These concentration values can be obtained form time-dependent solution in approximately 1300 seconds. The steady-state velocity distribution and time-dependent concentration profile within the second connector is given in Figure 4.13.

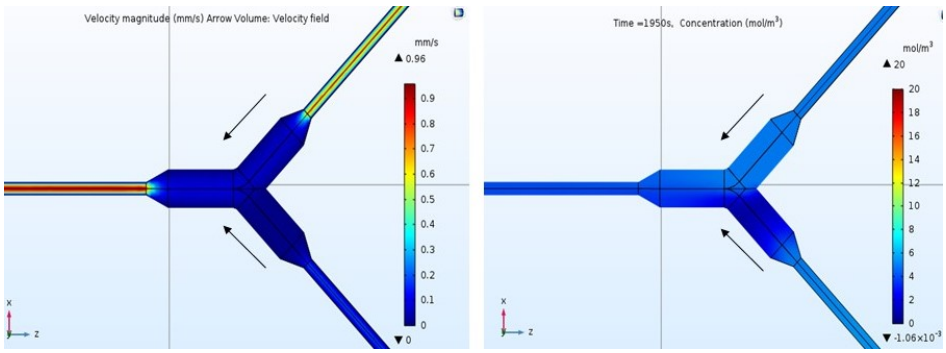

Figure 4.13. Steady-state velocity (left) and time dependent concentration (right) distributions within the second Y-shaped connector

The flow rate at the third inlet is 1 μL/min and length of the second tubing is 17 cm. Fluid reaches to Y-shaped connector in 1950 seconds. Over time, concentration in the connector increases (Figure 4.14). From steady state solution, concentration value of which along horizontal axis at the outlet of the second connector is found as 5 mol/m^3. These concentrations can be obtained form time-dependent solution in approximately 2450 seconds.

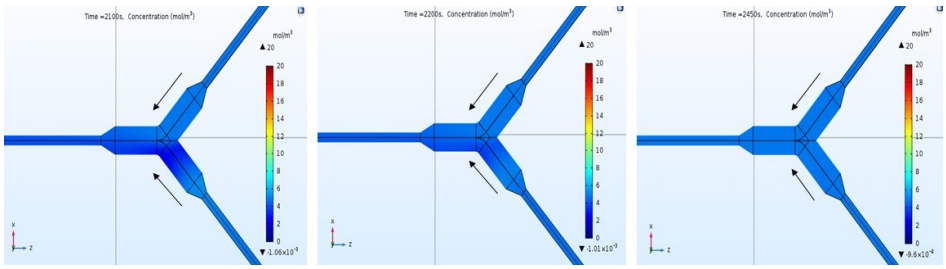

Figure 4.14. Concentration distribution within the second Y-shaped connector with respect to time

4.2. Effects of Drugs on Bacterial Growth

The experiments for the determination of minimal inhibitory concentrations (MICs) were carried out at both high and standard inoculum doses because MICs of drugs are highly dependent on the inoculum cell density. Then, the colony forming units (CFUs) were measured at both high and standard inoculum doses in order to check whether initial CFUs values are among the indicated range, while visualization experiments were carried out at high inoculum cell density of bacteria.

4.2.1. Effects of DMSO on Bacterial Growth

To be able to determine the effect of DMSO on wild-type *E. coli* K12 cells and opp-deleted mutant *E. coli* K12 SS5013 cells, cultures at standard ($2x10^4$-10^5) and high (10^8-10^9) inoculum cell density were treated with different DMSO concentrations in 0.39 - 50 % range. Control samples were treated with distilled water, for comparison.

After 20 hours of incubation of cultures treated with DMSO and control cultures, visible growth was observed in control cultures at both standard and high inoculation density of both wild-type *E. coli* K12 and opp-deleted mutant *E. coli* K12 SS5013 cells. At high inoculum density, visible growth was not observed in both cells treated with 25 % or higher concentration of DMSO. At standard inoculum cell density, visible growth was not observed in both cells treated with 12.5 % or higher concentration of DMSO.

Growth curves at high and standard inoculation densities were given in Figure 4.15.

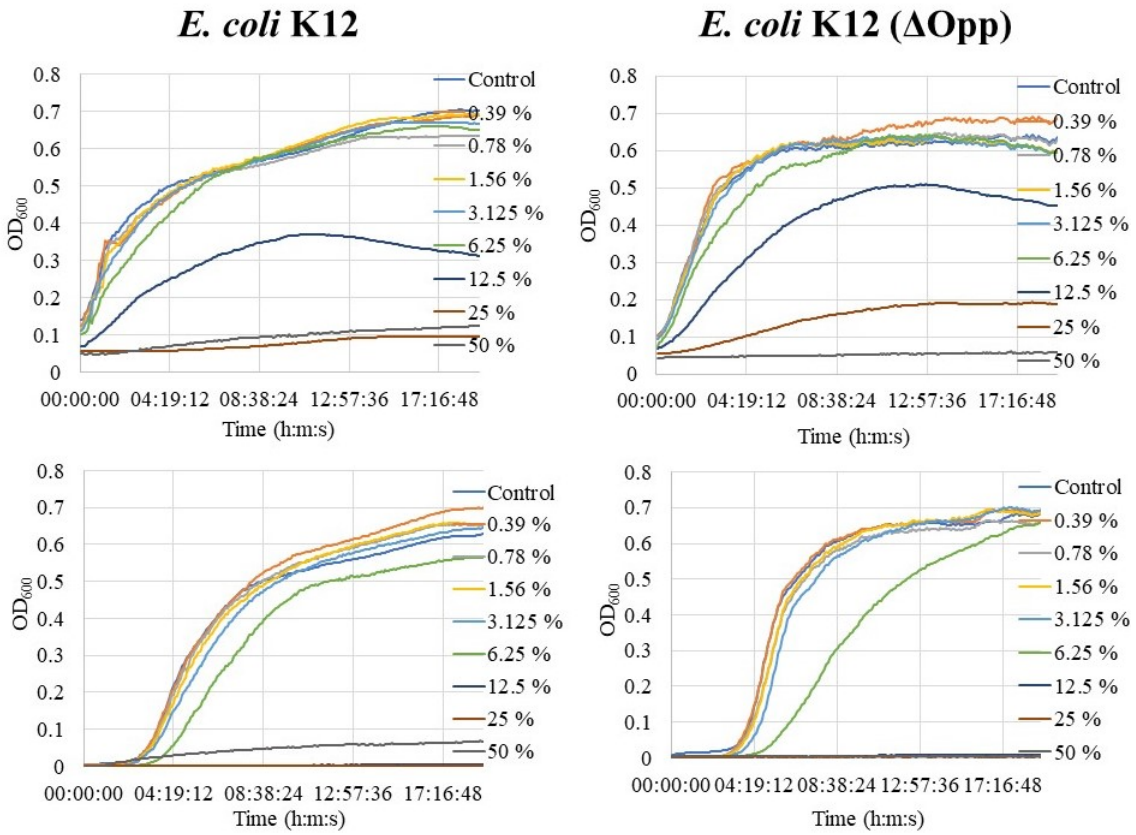

Figure 4.15. Growth curves of *E. coli* K12 (left) and mutant SS5013 (right) strains for 20 hours of incubation. Bacteria at standard inoculum (bottom) and high inoculum (top) dose were treated with different DMSO concentrations.

OD_{600} measurements and plate counts were given in Figure 4.16 From the CFUs results of Sample 2, it can be said that the dilution is suitable for the experiments which are carried out at standard inoculum cell density. Minimum inhibitory concentration for DMSO was determined as 25 % (v/v DMSO) at high inoculation density and 12.5 % (v/v DMSO) at standard inoculation density of both wild-type and mutant strains, respectively.

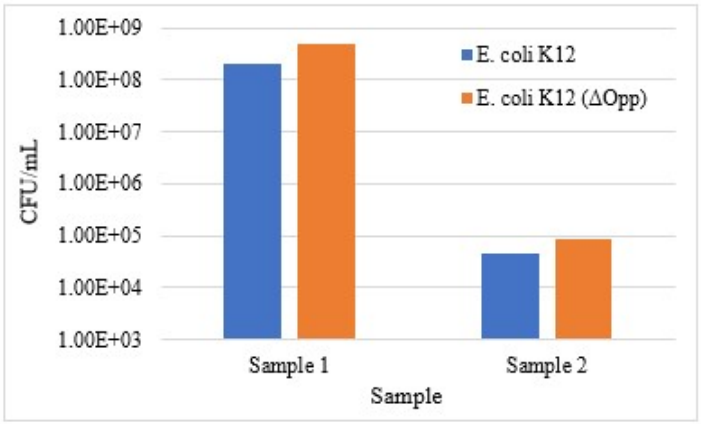

Figure 4.16. CFU counts of the sample at OD600 = 0.3 (Sample 1) and when Sample 1 is diluted 1:5000 (Sample 2).

4.2.2. Effects of Fluorescently Labeled pVEC on Bacterial Growth

To be able to determine the effect of fluorescently labeled pVEC on wild-type *E. coli* K12 and opp-deleted mutant *E. coli* K12 SS5013 cells, cultures at standard ($2x10^4$-10^5) and high (10^8-10^9) inoculum cell density were treated with different fluorescently labeled pVEC concentrations in 6.25 – 400 μM range. Since fluorescently labeled pVEC stock solution was prepared in DMSO-water mixture, control samples were treated with the same concentration of this mixture, for comparison.

After 20 hours of incubation of cultures treated with fluorescently labeled pVEC and control cultures, visible growth was observed in control cultures at both standard and high inoculum density of wild-type *E. coli* K12 cells. Visible growth can be observed in certain wells by naked eye after incubation of 20 hours. However, microplate image of wild-type *E. coli* K12 cells may be misleading because fluorescently labeled pVEC precipitated at the bottom of the wells, especially at the wells containing higher concentration of fluorescently labeled pVEC.

Therefore, growth curves were plotted from the analysis of data obtained from microplate reader. As a result, at high inoculum density, visible growth was not observed in *E. coli* K12 and opp-deleted mutant *E. coli* K12 SS5013 cultures treated with

200 μM or higher concentration of fluorescently labeled pVEC. At standard inoculum cell density, visible growth was not observed in *E. coli* K12 cultures treated with 100 μM or higher concentration of fluorescently labeled pVEC. On the other hand, visible growth was not observed in mutant SS5013 cultures treated with 50 μM or higher concentration of fluorescently labeled pVEC at standard inoculum cell density. Growth curves of both cells at high and standard inoculum density were given in Figure 4.17.

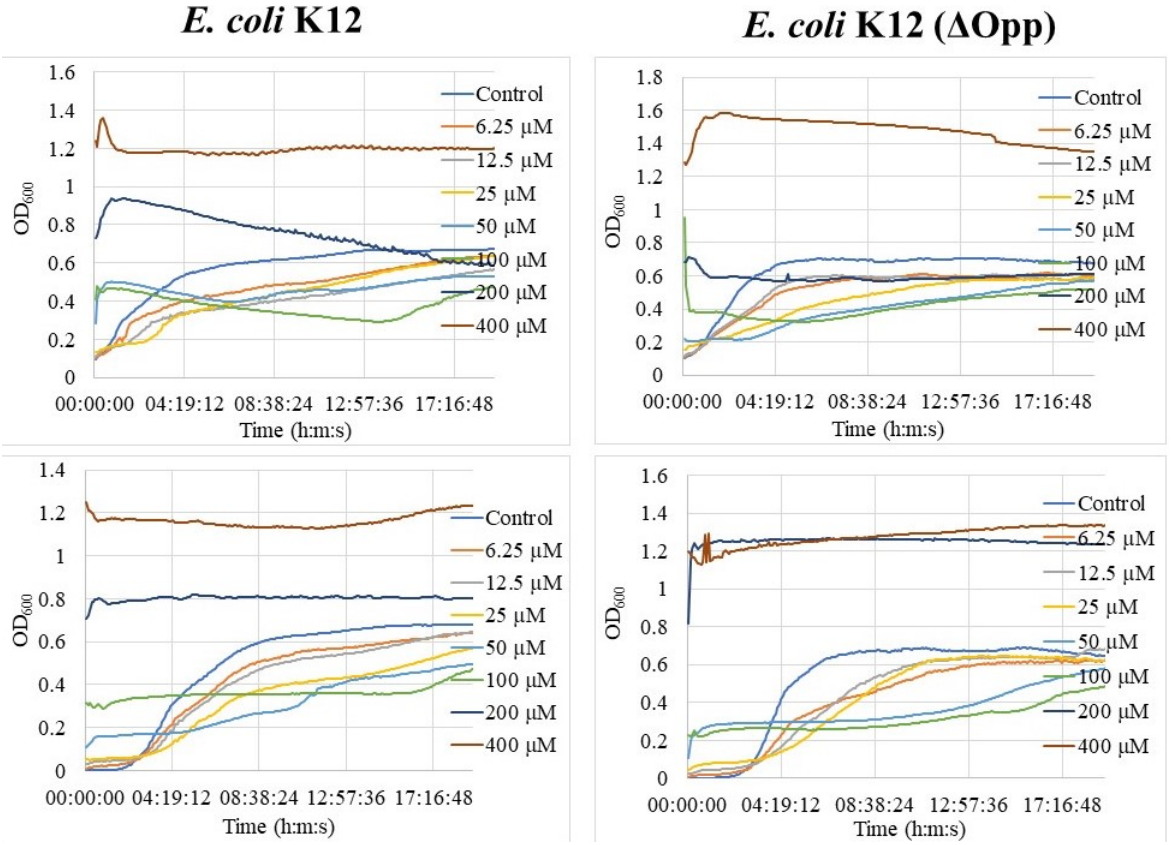

Figure 4.17. Growth curves of strains for 20 hours of incubation. Bacteria at standard inoculum (bottom) and high inoculum (top) dose were treated with different fluorescently labeled pVEC concentrations.

Growth curves of both cells contain some fluctuations particularly when fluorescently labeled pVEC concentraion increased. CFUs count of sample 1 was on the order of 10^8 to 10^9 (high inoculation density) while sample 2 was counted on the order of 10^4 to 10^5 (standard inoculation density) as determined at the beginning of the experiment. To be able to determine the inoculum dose at the beginning of the experiment CFUs of the cultures were measured. CFUs results of Sample 2 demonstrated that the dilution

ratio is proper for the experiments carried out at standard inoculation cell density. The samples at OD_{600} = 0.3 were added directly to the wells at high inoculation cell density.

Minimum inhibitory concentration for fluorescently labeled pVEC was determined as 200 μM at high inoculation density and 100 μM at standard inoculation density of wild-type *E. coli* K12 cells in this analysis. However, these values can change if different concentrations within the range are used. Because of 2 fold dilution of fluorescently labeled pVEC, the concentration difference between successive wells is high and MIC values can be present in that range. Therefore, other concentrations in the range should be tried to find exact MIC value of fluorescently labeled pVEC.

4.2.3. Effects of Fluorescently Labeled P4 on Bacterial Growth

To be able to determine the effect of fluorescently labeled P4 on wild-type and mutant *E. coli* K12 cells, cultures at standard ($2x10^4$-10^5) and high (10^8-10^9) inoculum cell density were treated with different fluorescently labeled P4 concentrations in the range of 6.25 – 400 μM. Since fluorescently labeled P4 stock solution was prepared in DMSO-water mixture, control samples were treated with the same concentration of this mixture, for comparison.

After 20 hours of incubation of cultures treated with fluorescently labeled P4 and control cultures, visible growth was observed in control cultures at both standard and high inoculum density of wild-type and mutant *E. coli* K12 cells. However, microplate image of wild-type *E. coli* K12 cells may be misleading because fluorescently labeled P4 precipitated at the bottom of the wells, especially at the wells containing higher concentration of fluorescently labeled P4.

At high inoculation density, visible growth was not observed in *E. coli* K12 and opp-deleted mutant *E. coli* K12 SS5013 cultures treated with 200 μM or higher concentration of fluorescently labeled P4. At standard inoculation cell density, visible growth

was not observed in *E. coli* K12 and opp-deleted mutant *E. coli* K12 SS5013 cultures treated with 100 μM or higher concentration of fluorescently labeled P4. Growth curves of both cells treated with P4 peptide at high and standard inoculum density were given in Figure 4.18.

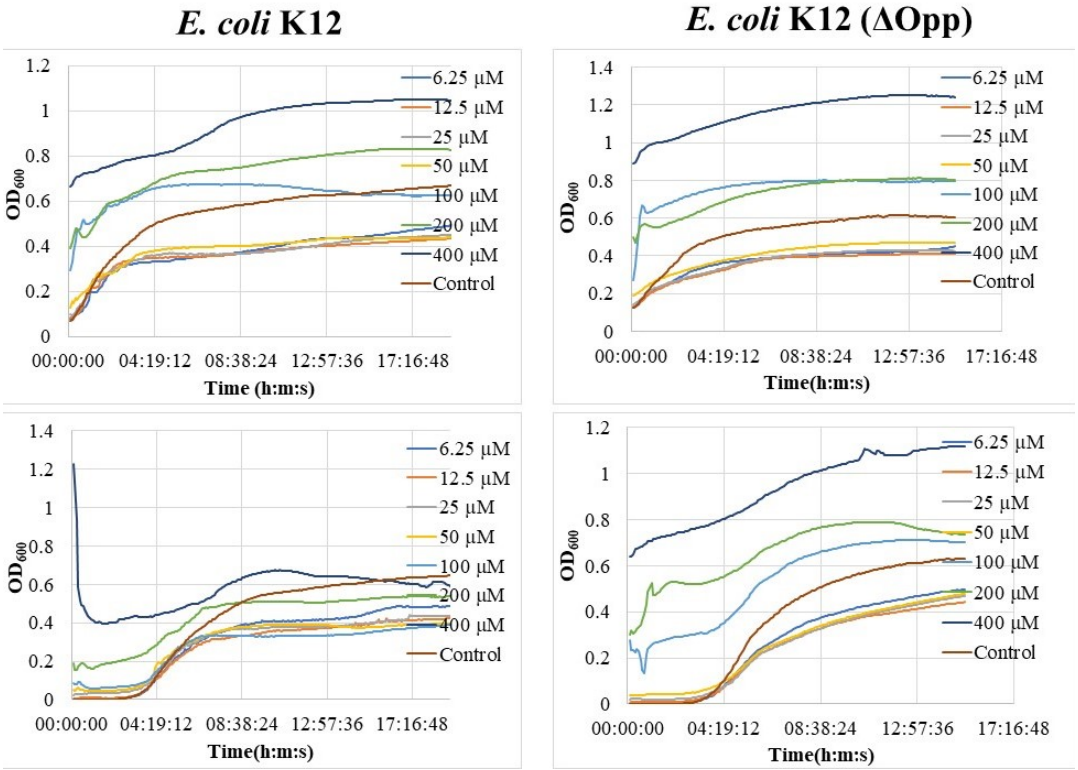

Figure 4.18. Growth curves of strains for 20 hours of incubation. Bacteria at standard inoculum (bottom) and high inoculum (top) dose were treated with different fluorescently labeled P4 concentrations.

Growth curves of wild-type and mutant cells contain some fluctuations particularly when fluorescently labeled P4 concentration increased. Minimum inhibitory concentration for fluorescently labeled P4 was determined as 200 μM at high inoculation density and 100 μM at standard inoculation density of both wild-type and mutant *E. coli* K12 cells in this analysis. However, this values can be changed if different concentrations in the range is used. Because of 2 fold dilution of fluorescently labeled P4, concentration difference between successive wells is high and MICs values can be present in that range. Therefore, other concentrations in the range should be tried to find exact MIC value of fluorescently labeled P4.

4.2.4. Effects of Fluorescently Labeled P2 on Bacterial Growth

The effects of fluoresceine-labeled P2 on opp-deleted mutant *E. coli* K12 SS5013 cells were tested by treating the cultures at standard ($2x10^4$-10^5) and high (10^8-10^9) inoculum cell density with different fluoresceine-labeled P2 concentrations in the range of 3.125 – 200 μM. Since fluoresceine-labeled P2 stock solution was prepared in DMSO-water mixture, control samples were treated with the same concentration of this mixture, for comparison. Growth curves of both cells treated with P2 peptide at high and standard inoculum density were given in Figure 4.19.

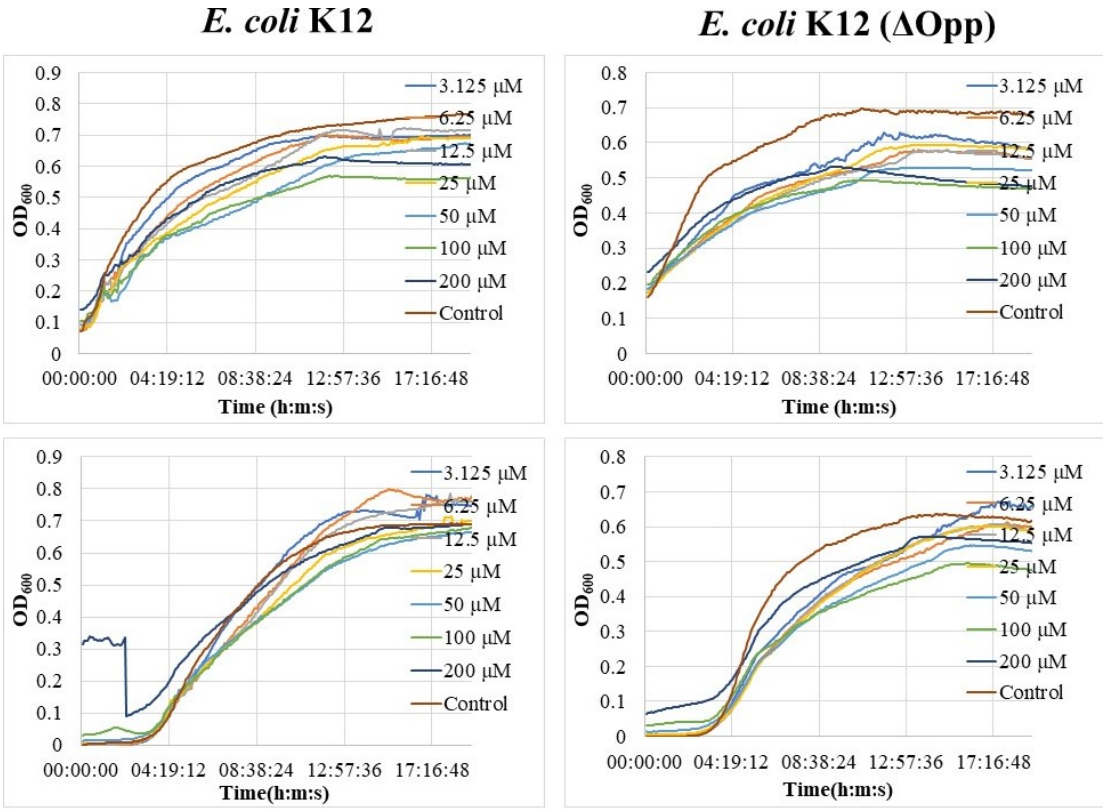

Figure 4.19. Growth curves of strains for 20 hours of incubation. Bacteria at standard inoculum (bottom) and high inoculum (top) dose were treated with different fluoresceine-labeled P2 concentrations.

After 20 hours of incubation of cultures treated with fluoresceine-labeled P2 and control cultures, visible growth was observed in control cultures at both standard and high inoculum density of wild-type and mutant *E. coli* K12 cells. Visible growth can be observed in certain wells by naked eye after 20 hours of incubation. Similar to

results of pVEC and P4 peptide, fluoresceine-labeled P2 precipitated at the bottom of the wells, especially at the wells containing higher concentration of fluoresceine-labeled P2. The dilution ratio was found convenient for the experiments carried out at standard inoculum cell density.

Minimum inhibitory concentration for fluoresceine-labeled P2 was determined as 100 μM at high inoculation density and 50 μM at standard inoculation density of both wild-type *E. coli* K12 and opp-deleted mutant SS5013 cells in this analysis. However, this values can change if different concentrations in the range is used. Because of 2 fold dilution of fluoresceine-labeled P2, concentration difference between successive wells is high and MICs values can be present in that range. Therefore, other concentrations in the range should be tried to find correct MIC value of fluoresceine-labeled P2.

4.2.5. Effects of Trypsin-EDTA Solution on Bacterial Growth

In order to determine the concentration and treatment time of trypsin, MIC experiment was performed for both wild type *E. coli* K12 and opp-deleted mutant *E. coli* K12 SS5013 cells. The effects of trypsin-EDTA solution on bacterial cells were tested by treating the cultures with different trypsin concentrations in 0.003906 – 0.125 % range. The software was adjusted to measure OD_{600} of each sample in the wells every 30 seconds. According to the growth curve of wild type *E. coli* K12 cells at OD of 0.2, trypsin effects on bacterial cells was not observed. All samples containing different trypsin concentrations displayed almost the same growth profile with control group. However, growth curve of washed bacterial cells showed that trypsin affects growth rate of bacterial cells. When trypsin concentration increases (from E1 to E6 well), growth rate decreases more. Only E6 well containing the highest trypsin concentration did not fit in with this condition.

According to the growth curve of *E. coli* (ΔOpp) K12 cells at OD of 0.2, trypsin effects on bacterial cells was not observed again. LB medium may have inhibited the trypsin effect. All samples containing different trypsin concentrations displayed

almost the same growth profile with control group. However, growth curve of washed bacterial cells showed that trypsin affects growth rate of bacterial cells. When trypsin concentration increases (from E1 to E6 well), growth rate of bacterial cells decreases more. The growth rate of the samples in E1 and E2 wells containing the least trypsin concentration was not affected by trypsin treatment.

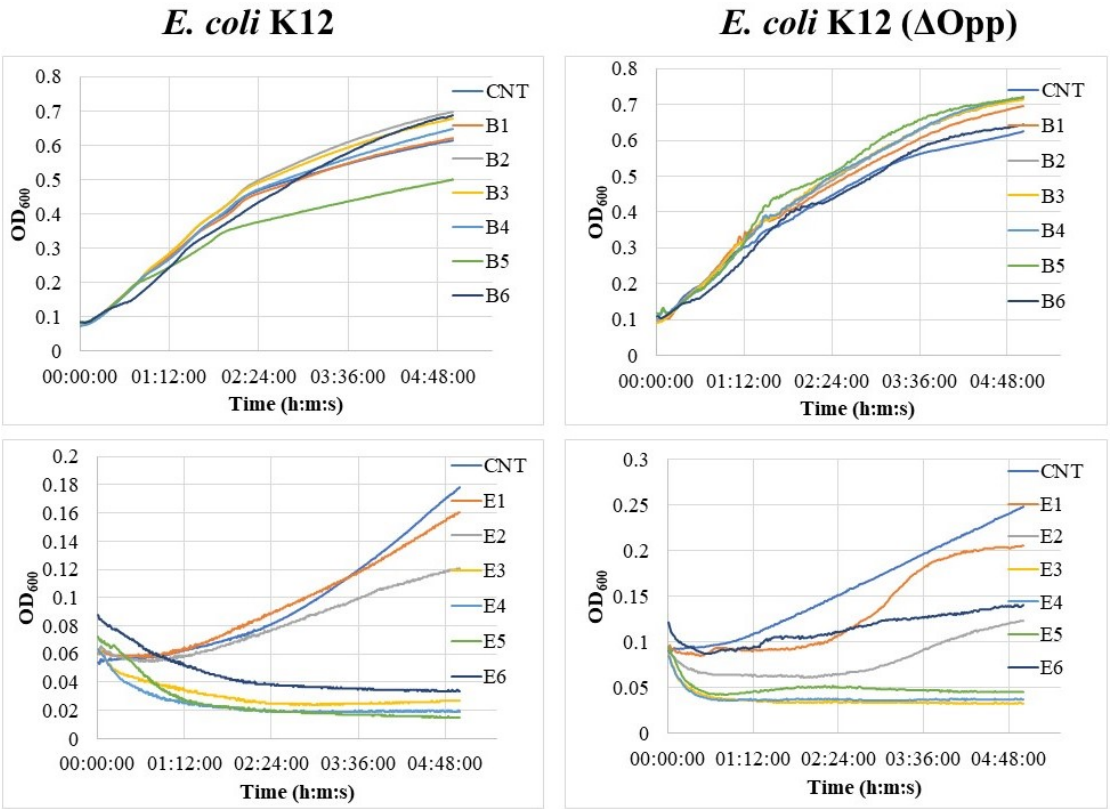

Figure 4.20. Growth curves of strains for 5 hours of incubation. Bacteria at OD_{600} of 0.2 (top) and washed bacterial cells (bottom) were treated with different trypsin concentrations.

4.2.6. Effects of Amiloride on Bacterial Growth

In order to determine the effect of DMSO and Amiloride hydrochloride hydrate on wild-type *B. subtilis* 168 cells, the cultures at standard ($2x10^4$-10^5) and high (10^7-10^8) inoculation cell density were treated with different DMSO concentrations in the 0.39% - 50% range and Amiloride hydrochloride hydrate concentrations in the 0.25 mM - 8 mM range. Since Amiloride stock solution was prepared in DMSO-water mixture, control

samples were treated with the same concentration of this mixture, for comparison. Deionized water was used for the control groups of DMSO samples.

After 20 hours of incubation of the bacterial cultures treated with DMSO, visible growth was observed in control cultures at both standard and high inoculation density of *B. subtilis* 168 (Figure 4.21). At high inoculation density, visible growth was not observed in *B. subtilis* 168 cultures treated with 25 % or higher concentration of DMSO.

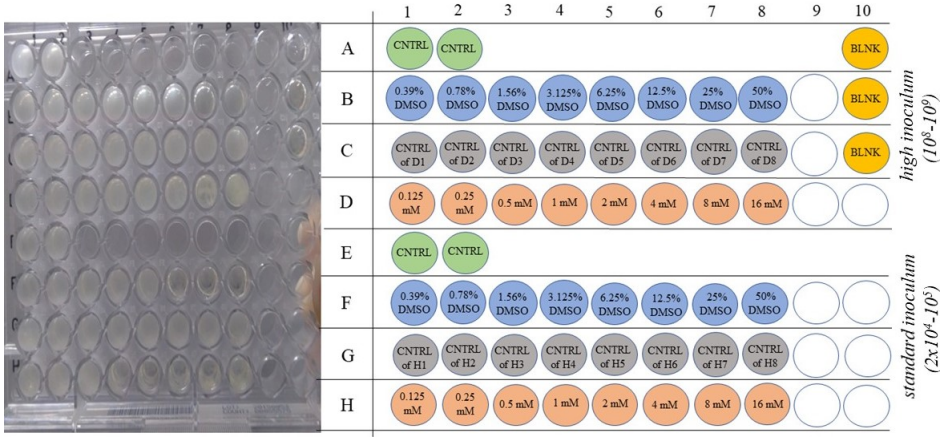

Figure 4.21. The photograph of the plate after incubation of 20 hours (left) and the plate setup used in the experiment (right). The effect of DMSO on the growth of *B. subtilis* 168 was analyzed. DMSO concentration being tested was in the 0.39 - 50 % range.

At standard inoculation cell density, visible growth was not observed in *B. subtilis* 168 cultures treated with 12.5 % or higher concentration of DMSO. Growth curves of both strains at high and standard inoculation density were given in Figure 4.22. For the experiments carried out at high inoculum cell density, the cultures at $OD_{600} = 1.4$ were added directly to the microplate wells. Minimum inhibitory concentration for DMSO was determined as 25 % (v/v DMSO) at high inoculation density and 12.5 % (v/v DMSO) at standard inoculation density of *B. subtilis* 168 cells. Minimum inhibitory concentration of amiloride was determined as 4 mM at high inoculation density and 1 mM at standard inoculation density of wild-type *B. subtilis* 168 cells in this analysis (Figure 4.22). However, this values can be changed if different concentrations in the range is used. Because of 2 fold dilution of Amiloride, the concentration difference

between successive wells is high and MICs values can be present in that range. Therefore, other concentrations in the range should be tried to find correct MIC value of Amiloride.

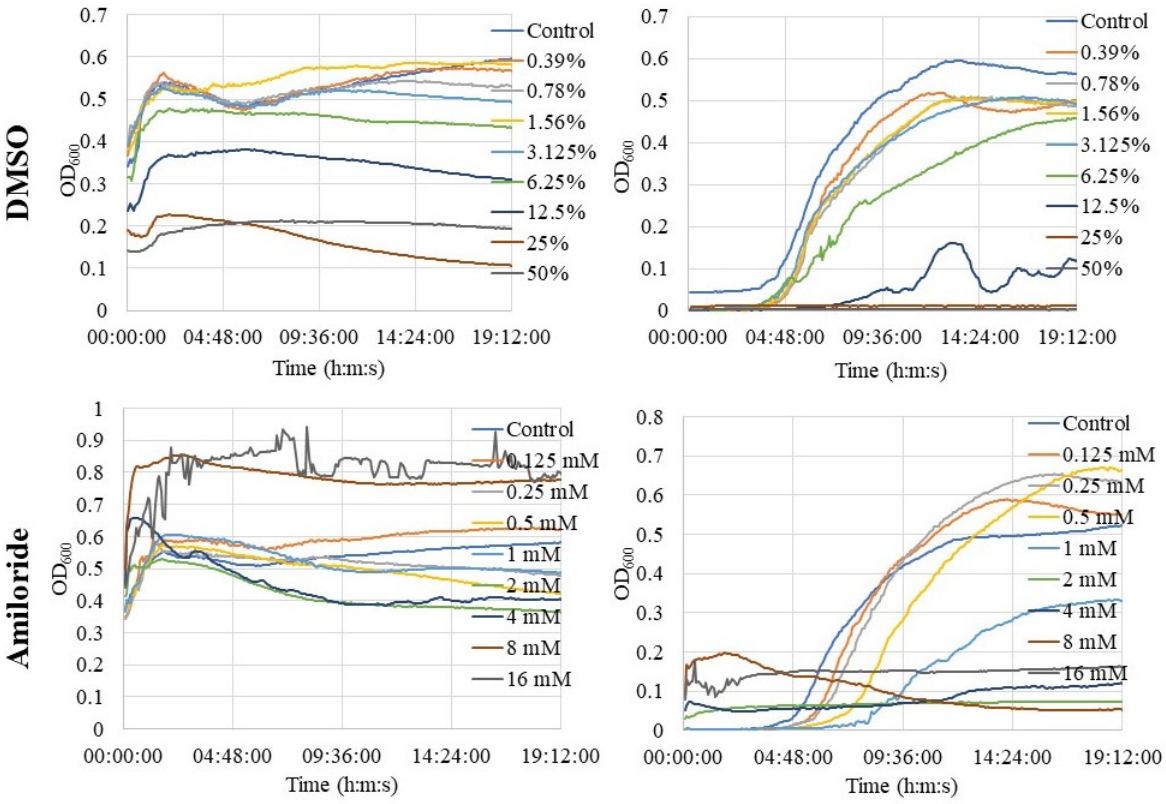

Figure 4.22. Growth curve of *B. subtilis* 168 strain for 20 hours of incubation. *B. subtilis* 168 cells at standard inoculum (bottom-right) and high inoculum (bottom-left) density incubated with different amiloride concentrations.

4.3. Monitoring of Cell Heterogeneity of *Bacillus* Cells

During the growth of *B. subtilis* population bifurcates such that cells are either joined end-to-end in long sessile cell chains which are predominant in the exponential phase of growth or grow as single motile individuals. Motile cells represent a small proportion of the population during growth but are known to become prevalent during the transition to stationary phase in which motile cells seek new sources of nutrients while the sessile chains exploit an existing niche. Cell chaining and motility are controlled by the alternative sigma factor σ^{D}, which directs the transcription of genes (lytC, lytD,

and lytF) for autolytic enzymes that mediate the separation of sister cells after cell division [55–57]. To be able to monitor cell heterogeneity, samples were taken from the culture every hour and added on the microscopy glass and covered with a coverslip to visualize under Nikon inverted microscopy. Bright field images were captured at 60x zoom and movies were recorded.

4.3.1. Monitoring of Cell Heterogeneity of *B. subtilis* 168 Cells

Images were captured at specific times during the incubation (in lag phase, early log phase, middle log phase and early stationary phase) to be able to observe transition from sessile chain structure to single motile cells. Images of *B. subtilis* 168 strain in lag phase were given in Figure 4.23.

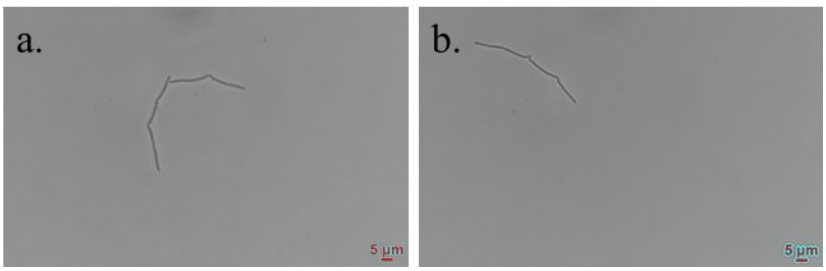

Figure 4.23. Images of *B. subtilis* 168 strain captured in lag phase (a) captured at the second hour after inoculation (b) captured at the third hour after inoculation.

Long sessile chains were observed in the images captured at the lag phase. Although cells continued to reproduce, they did not dissociate mostly because of the inactivation of alternative sigma factor σ^{D}. Image processing was performed by using Fiji-ImageJ software. The number of the cells, area, perimeter and cell length in the images were measured. In Figure 4.23a, two sessile chains are recognized. Average length of these cells was measured as 42 μm. The area and perimeter were measured as 34 $\mu\mathrm{m}^2$ and 90 μm, respectively. As mentioned above, if the food is plentiful, σ^{D} is not activated and therefore, cells grow as long nonmotile chains. Cells continued to reproduce but sister cells did not disassociate and formed long chains. Similar trend was observed at the third hour after inoculation (Figure 4.23b). The length of this chain was measured as 58 μm. The area and perimeter of the cell were found as 151

μm^2 and 123 μm, respectively. Images of *B. subtilis* 168 strain in the early log phase were given in Figure 4.24.

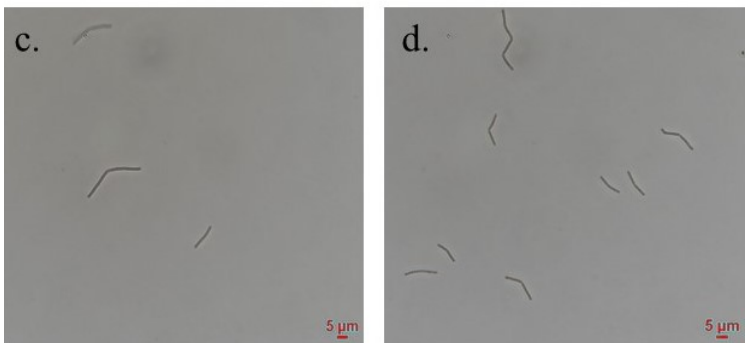

Figure 4.24. Images of *B. subtilis* 168 strain in the early log phase (c) captured at the fourth hour after inoculation (d) captured at the fifth hour after inoculation.

In the images given in Figure 4.24, cell heterogeneity was observed. Distinct differences between longitudinal axis length of the cells can be noticed. In the long chain structures, joint points can be observed clearly. These cells did not dissociate because of the inactivation of alternative sigma factor σ^{D}. In logarithmic phase, *B. subtilis* cells were found as a mixture of both sessile chains and single motile cells, which can be also seen in Figure 4.24. There are three cells in Figure 4.24a. The average cell length, perimeter and area were measured as 20 μm, 50 μm and 66 μm^2, respectively. At the fifth hour after inoculation, the cell density increased. The average cell length, perimeter and area of the eight cells given in Figure 4.24b were measured as 15 μm, 39 μm, and 49 μm^2, respectively. Images of *B. subtilis* 168 strain in the middle log phase were given in Figure 4.25.

Cell heterogeneity was continued in the images captured in the middle logarithmic phase. Distinct differences between longitudinal axis length of the cells can be also observed. In this phase, cell length began to decrease, which can be seen in Figure 4.25b clearly. While the number of motile cell increases, the decrease in sessile chain structures was observed. The average cell length, perimeter and area of the 22 cells given in Figure 4.25a were measured as 13 μm, 32 μm, and 36 μm^2, respectively.

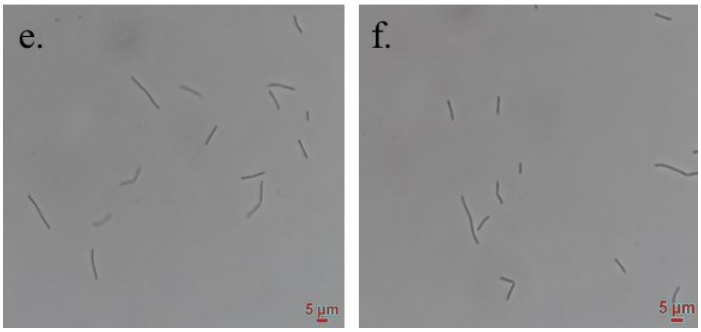

Figure 4.25. Images of *B. subtilis* 168 strain in the middle log phase (e) captured at the sixth hour after inoculation (f) captured at the seventh hour after inoculation.

The dimesion of the cells began to decrease in the middle logarithmic phase compared to previous images. The average cell length, perimeter and area of the 37 cells given in Figure 4.25b were measured as 9 μm, 23 μm, and 20 μm^2, respectively. Images of *B. subtilis* 168 strain in the early stationary phase were given in Figure 4.26.

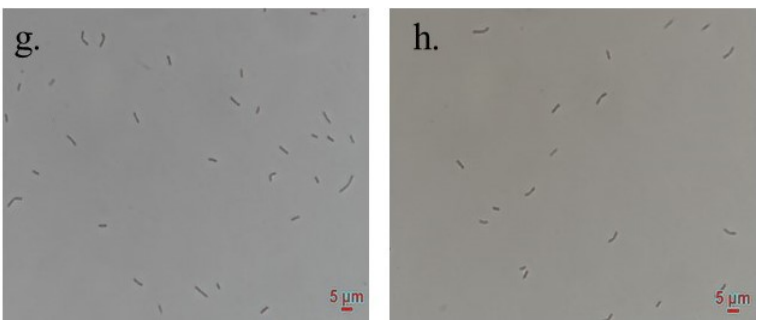

Figure 4.26. Images of *B. subtilis* 168 strain in the early stationary phase (g) captured at the tenth hour after inoculation (h) captured at the twelfth hour after inoculation.

At the beginning of the stationary phase, motile cells became predominant. The number of sessile chains decreased dramatically. In this case, food is insufficient, and therefore σ^D may become ON and flagella synthesis occur in order to seek new sources of nutrients. Reproduction of the cells continued during the experiment, which led to increase in cell density in the chamber. In addition, cell size was smaller in these images captured in the stationary phase. The average cell length, perimeter and area of the 40 cells given in Figure 4.26a were measured as 4 μm, 12 μm, and 9 μm^2, respectively. The dimension of the cells decreased considerably in the early stationary phase. The average cell length, perimeter and area of the 36 cells were measured as 4 μm, 13 μm,

and 11 μm^2, respectively. Cell heterogeneity of *B. subtilis* strain can be also observed in the videos recorded at 40x zoom.

In literature, the mean diameter of the *B. subtilis* strain was reported as 0.86 μm [44]. In the studies, it was reported that the length of the *B. subtilis* cells varies between 3 and 5 μm [58]. Compared to experimental results, the length of the cells in the early stationary phase was found consistent with the reported value in the literature. However, diameter of the cells is greater than one measured in the previous study. Supposing that the area was calculated by multiplying the length with the diameter of the cell, the average diameter of the cells given in Figure 4.25a is calculated as 2.8 μm. As a result, the diameter of the cells was found between 2 and 3 μm.

4.3.2. Monitoring of Cell Heterogeneity of *B. subtilis* 3610 Cells

In order to monitor cell heterogeneity, samples were taken from *B. subtilis* 3610 culture every hour, added on the microscopy glass and covered with a coverslip to visualize under Nikon inverted microscopy. Bright field images were captured at 60x zoom and movies were recorded. Images were captured at every hour to be able to observe transition from sessile chain structure to single motile cells. Images of *B. subtilis* 3610 strain in lag phase were given in Figure 4.27.

Figure 4.27. Images of *B. subtilis* 3610 strain captured in in lag phase (a) captured at the first hour after inoculation (b) captured at the second hour after inoculation (c) captured at the third hour after inoculation.

Long sessile chains were observed in the images captured in the lag phase. Although cells continued to reproduce, they did not dissociate mostly because of the

inactivation of alternative sigma factor σ^{D} during the first and second hour of the incubation. At the third hour of the incubation, sister cells began to disassociate. Therefore, single motile cells were observed in the image capture at the third hour of the incubation (Figure 4.27c).

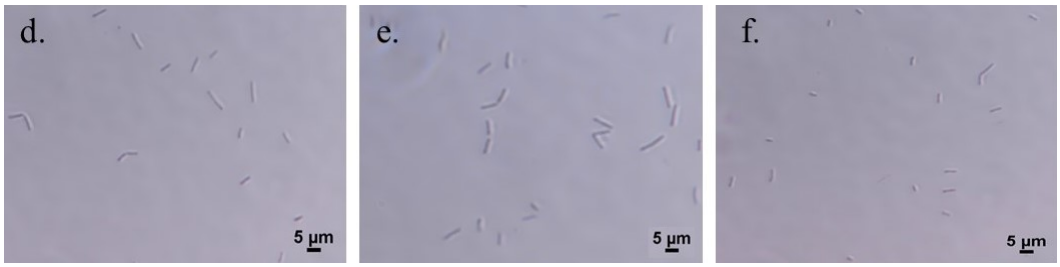

Figure 4.28. Images of *B. subtilis* 3610 strain captured in log phase (d) captured at the fourth hour after inoculation (e) captured at the fifth hour after inoculation (f) captured at the sixth hour after inoculation.

In log phase, motile *B. subtilis* 3610 cells were observed. Reproduction of the cells continued during the experiment, which led to increase in cell density in the chamber. In addtition, cell size was smaller in these images captured in the exponential phase. Cell density continued to increase in late exponential phase. Cell size also began to decrease in this phase compared to previous images. The dissociation of the sister cells are obvious in bright field images.

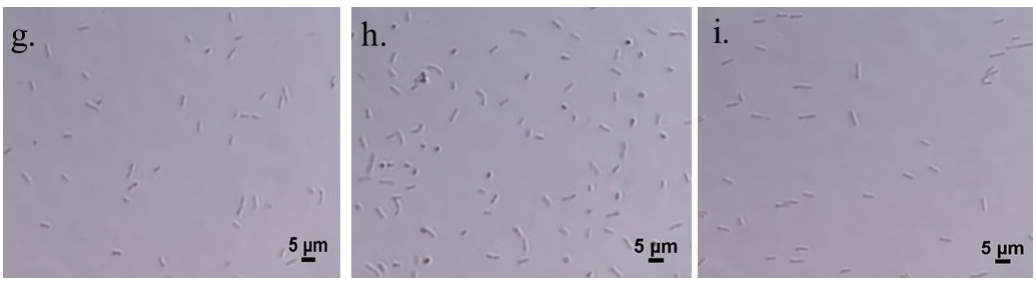

Figure 4.29. Images of *B. subtilis* 3610 strain captured in late exponential phase (g) captured at the seventh hour after inoculation (h) captured at the eight hour after inoculation (i) captured at the ninth hour after inoculation.

4.3.3. Monitoring of Cell Heterogeneity of DS222 Strain

Long sessile chains were observed in the images captured at the lag phase. Bacterial cells continued to reproduce and became long sessile chains which can be clearly observed in Figure 4.30.

Figure 4.30. Images of DS222 strain captured in lag phase (a) captured at the first hour after inoculation (b) captured at the second hour after inoculation (c) captured at the third hour after inoculation.

Due to the inactivation of alternative sigma factor σ^{D} during the first, second and third hour of the incubation, sister cells were unable to dissociate from each other. At the third hour of the incubation, DS222 cells were found as a mixture of both sessile chains and single motile cells, which can be also seen in Figure 4.30c.

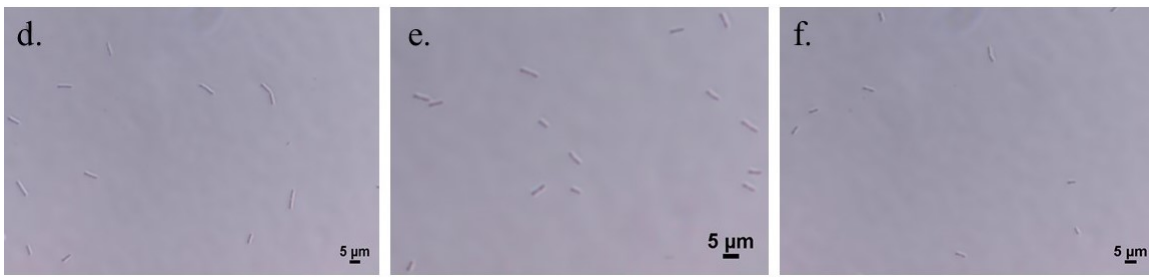

Figure 4.31. Images of DS222 strain captured in log phase (d) captured at the fourth hour after inoculation (e) captured at the fifth hour after inoculation (f) captured at the sixth hour after inoculation.

From the fourth hour of the incubation, alternative sigma factor σ^{D} became active and single motile cells were formed by the dissociation of the sister cells (Figure 4.31). Bacterial cell density continued to increase in exponential phase. Cell size of DS222 strain decreased toward to the late exponential phase, while the cell density increased.

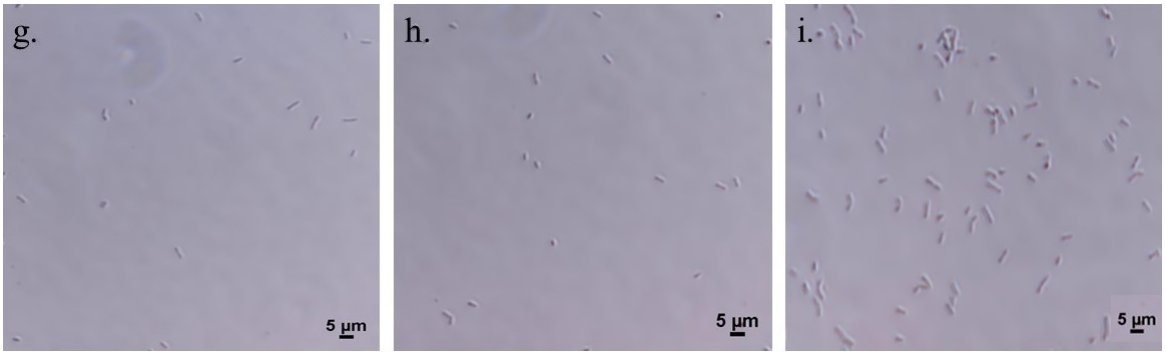

Figure 4.32. Images of DS222 strain captured in late exponential phase (g) captured at the fourth hour after inoculation (h) captured at the fifth hour after inoculation (i) captured at the sixth hour after inoculation.

4.3.4. Monitoring of Cell Heterogeneity of DS223 Strain

Long sessile chains were observed in the images captured in the lag phase. Although cells continued to reproduce, they did not dissociate mostly because of the inactivation of alternative sigma factor σ^{D} during the lag phase (Figure 4.33).

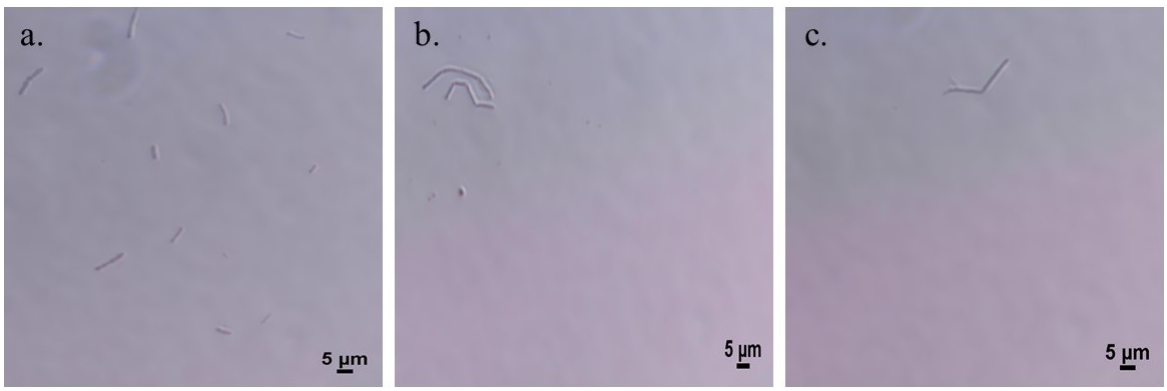

Figure 4.33. Images of DS223 strain captured in lag phase (a) captured at the first hour after inoculation (b) captured at the second hour after inoculation (c) captured at the third hour after inoculation.

Both long sessile chains and single motile cells were observed in the images captured in the log phase. Due to the inactivation of alternative sigma factor σ^{D} during the fourth hour of the incubation, sister cells were unable to dissociate from each other.

At the fifth hour of the incubation, DS223 cells became single motile cells with the activation of alternative sigma factor σ^{D}.

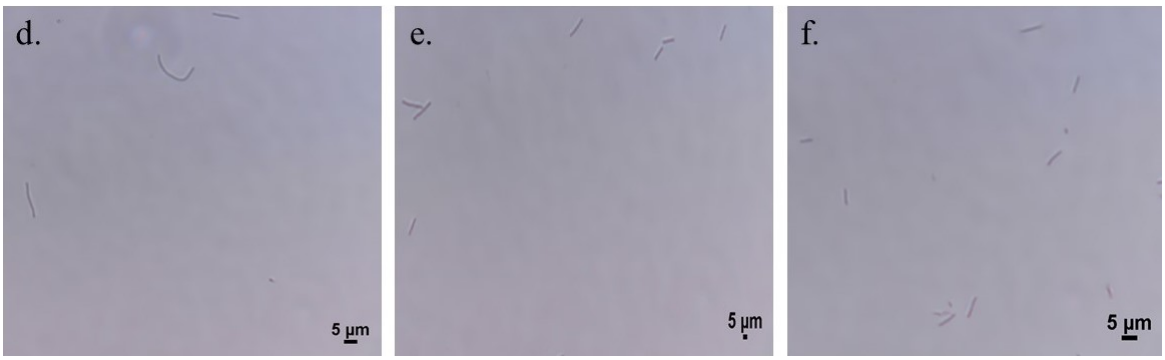

Figure 4.34. Images of DS223 strain captured in log phase (d) captured at the fourth hour after inoculation (e) captured at the fifth hour after inoculation (f) captured at the sixth hour after inoculation.

At the late log phase, motile cells are predominant and density of motile cells continued to increase. In this phase, food is insufficient, and therefore σ^{D} may become ON and flagella synthesis occur in order to seek new sources of nutrients. Moreover, cell size became smaller in these images captured in the late exponential phase.

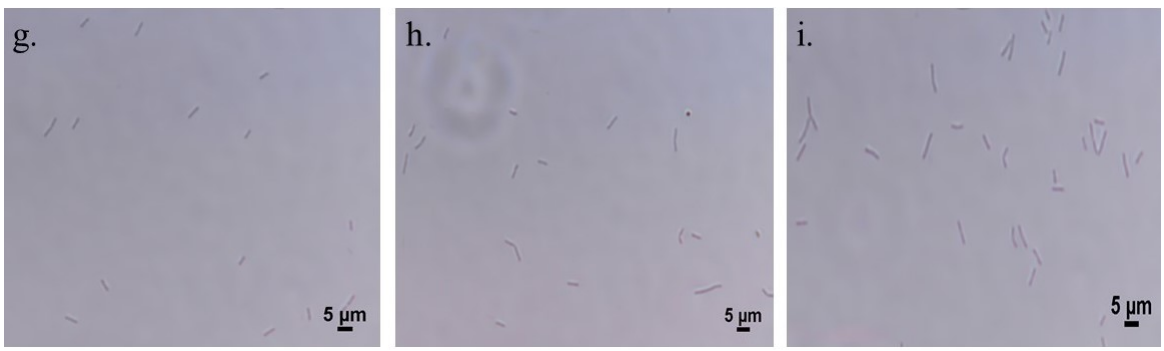

Figure 4.35. Images of DS223 strain captured in late log phase (g) captured at the seventh hour after inoculation (h) captured at the eight hour after inoculation (i) captured at the ninth hour after inoculation.

4.3.5. Monitoring of Cell Heterogeneity of *B. marmarensis sp. nov.* Strain

In order to monitor cell heterogeneity, samples were taken from the culture every hour, added on the microscopy glass and covered with a coverslip to visualize under

Nikon inverted microscopy. Bright field images captured at 40x zoom were given in Figure 4.36.

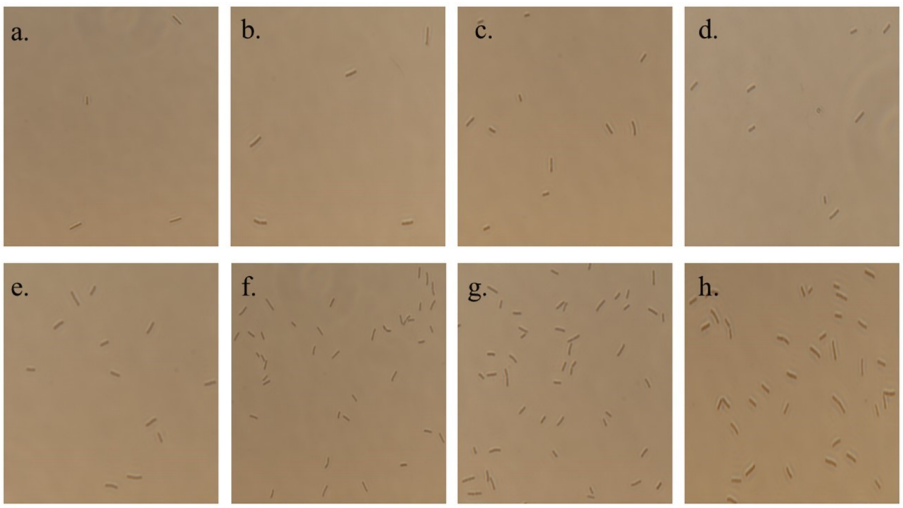

Figure 4.36. Images of *B. marmarensis* strain captured at every hour of incubation throughout eight hours.

Unlike *B. subtilis* 168 cells, cell heterogeneity (transition from long sessile chains to single motile cells) was not observed in *B. marmarensis* strain during the incubation in NB media. As seen in Figure 4.36, only single motile cells exist in the culture. Even if both *B. subtilis* 168 and *B. marmarensis* strains are gram positive, their cell structure are different from each other. Reproduction of the cells continued during the experiment, which led to increase in cell density over time. As reproducing, internodes between daughter cells are explicit and daughter cells dissociated from each other unlike the case observed in *B. subtilis* 168 cells.

In amiloride treatment experiments carried out with *B. subtilis* cells, cell heterogeneity was determinant in which period the bacterial cell solution should be perfused into the microfluidic chamber. Because single motile cells become dominant at the late logarithmic phase, sample is taken approximately the 7^{th} hour of the incubation of *B. subtilis* 168 cells. However, *B. marmarensis* cells can be perfused into the chamber when they in early or middle logarithmic phase of the incubation because they did not display long sessile chains during the growth.

4.4. Effects of Drugs on Swimming and Swarming Motility of Neutrophilic and Alkaliphilic Bacillus Cells

The effects of high Na^+ concentration and amiloride on the flagellar motility of *B. subtilis* 168, undomesticated *B. subtilis* 3610, DS222 (*B. subtilis* 3610 with a deletion of MotAB gene), and DS223 (*B. subtilis* 3610 with a deletion of MotPS gene) cells and *B. marmarensis sp. nov.* cells were monitored in zeonor microchips- reaction chambers of 10 μL.

4.4.1. Effect of Amiloride on the Motility of *B. subtilis* 168 Cells

Swim plates are supplemented with low concentrations of agar (less than 0.5 % (w/v)) in order to provide porous medium for the movement and colonization of bacteria. Swarm plates containing agar concentration more than 0.3 % (w/v) force the bacteria to move over the agar surface [59]. A compound leading a colony diameter greater than the control is considered stimulatory and if a reverse situation occurs, it is accepted as an inhibitory substance [53].

B. subtilis has two forms of active movement, swimming and swarming motility that are powered by rotating flagella. In *B. subtilis*, MotAB is more dominant than MotPS mostly, however high Na^+ concentration enables MotPS to make a contribution to motility as much as MotAB does. In previous studies, it was reported that amiloride inhibits the Na^+ driven flagellar motors of alkalophilic Bacillus by competing with Na^+ ions in the medium [60]. In this regard, swim and swarm plates were prepared to observe motility of *B. subtilis* 168 laboratory strain and the aim is to investigate the effects of different amiloride concentrations on the flagellar motility.

From the swim plate images, it was observed that amiloride has an inhibitory effect on swimming motility. As the amiloride concentration increased, the diameter of the colonization decreased in swim plates (Figure 4.37). Maximum swimming was observed in WT plate that does not contain Amiloride. Swarming motility was not

observed in *B. subtilis* 168 laboratory strain just as reported previously [52]. Swarming motility is required the production of a surfactant to reduce surface tension and swrA to increase the flagella biosynthesis. Due to the multiple genetic alterations during domestication, laboratory strains are defective in both surfactant production and swrA, so they remained unable to swarm [61]. *B. subtilis* 168 laboratory strain is swimming proficient, whereas it is swarming deficient and the colonization is restricted to the center of the swarm plate (Figure 4.37). Each test was performed using triplicate plates.

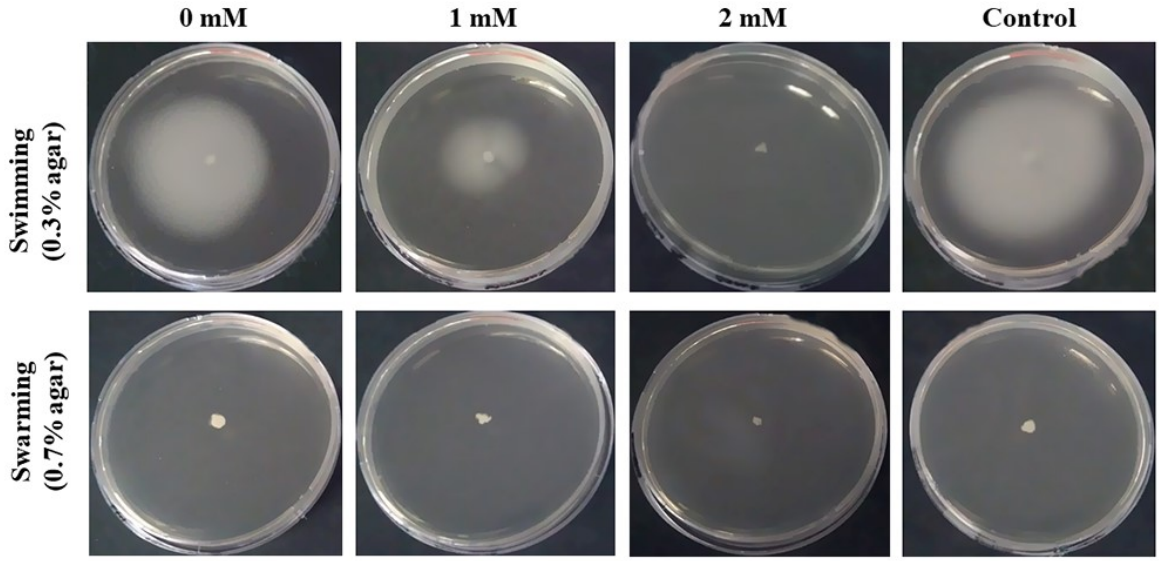

Figure 4.37. Swimming and swarming motility on LB-agar media supplemented with different concentrations of amiloride. In qualitative images of the plates, colonized agar appears white and uncolonized agar appears black on LB media.

In the following motility assay experiments, agar media containing different concentrations of NaCl were prepared to determine if high concentrations of NaCl in the medium affects the motility of *B. subtilis* 168 strain or not. Swim and swarm plates containing 170 mM NaCl were prepared as described above and supplemented with 1 mM and 2 mM amiloride to observe the inhibitory effect of amiloride on bacterial motility. For comparison, control groups were treated with the same concentration of DMSO. In the light of the findings, it was observed that amiloride has a striking inhibitory effect on swimming motility. As the amiloride concentration increases, the diameter of the colonization declined in swim plates dramatically. Maximum swim-

ming was observed in control plates containing DMSO instead of amiloride. Swarming motility was not observed in *B. subtilis* 168 laboratory strain as indicated previously. Colonization is limited to the center of the swarm plate (Figure 4.38).

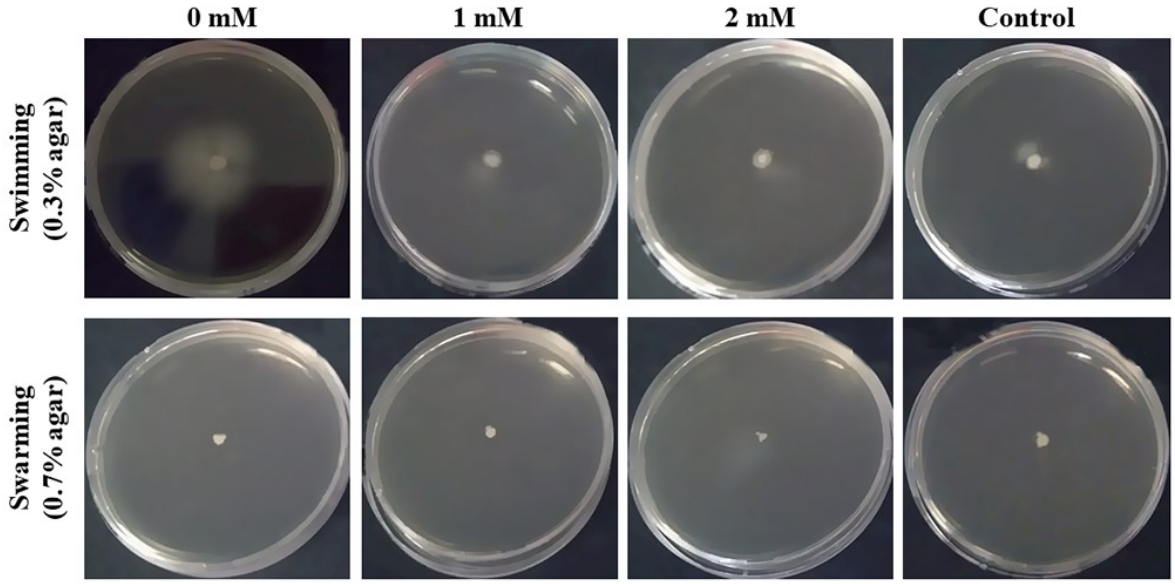

Figure 4.38. Swimming and swarming motility on LB-agar (550 mM NaCl) and supplemented with different concentrations of amiloride. In qualitative images of the plates, colonized agar appears white and uncolonized agar appears black.

B. subtilis has a single flagellar rotor which is powered by two Mot complexes, H^+ coupled MotAB and Na^+ coupled MotPS, respectively. MotAB is dominant in laboratory strains of *B. subtilis*, which are only slightly motile when motAB is disrupted [62]. However, MotPS dependent swimming on agar plates was reported at elevated pH and NaCl concentration [63]. To observe whether Na^+ concentration affects the MotPS-dependent swimming motility, swim and swarm plates were prepared with 550 mM NaCl concentration. Swimming motility decreased dramatically in the control plate in the absence of amiloride. The inhibitory effect of the amiloride on motility increased significantly at elevated NaCl concentration as reported previously [62]. Swarming motility was not observed in *B. subtilis* 168 laboratory strain even at increased NaCl concentration (Figure 4.38). The diameters of the colonization of *B. subtilis* 168 laboratory strain on the agar plates containing different concentrations of amiloride were measured after 18 hours of incubation and results were presented in Table 4.2.

Table 4.2. Diameters (cm) of *B. subtilis* 168 colonies formed on swimming and swarming agar plates supplemented with different concentrations of amiloride.

Plate	**Amiloride Concentration (mM)**				
	0	**0.25**	**0.5**	**1**	**Control**
Swimming (0.3 % agar)	9 cm	9 cm	9 cm	9 cm	9 cm
Swarming (0.7 % agar)	9 cm	9 cm	9 cm	9 cm	9 cm
Swarming (1 % agar)	6.4 ± 0.3 cm	4.3 ± 1.2 cm	3.2 ± 0.8 cm	2 ± 1.1 cm	7.6 ± 0.4 cm

4.4.2. Effect of Amiloride on Motility of *B. subtilis* 3610 Cells

Swarming motility is a flagellum-driven social form of surface locomotion that is observed in Gram-negative and Gram-positive bacteria. Due to the environmental signals, bacterial cells differentiate into the swarming proficient state, resulting in the production of surfactants and more flagella.

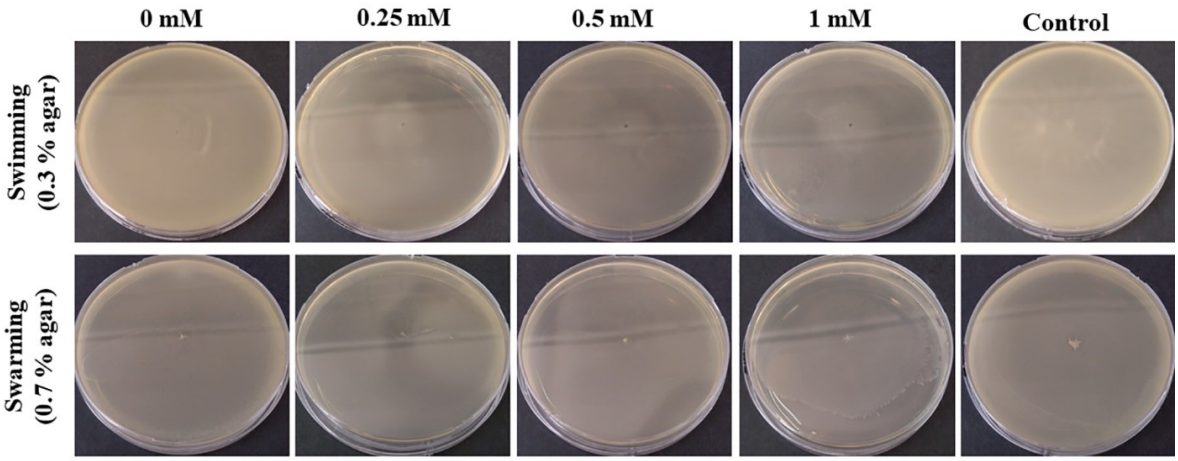

Figure 4.39. Swimming and swarming motility of *B. subtilis* 3610 on LB-agar media. In qualitative images of the plates, colonized agar appears white and uncolonized agar appears black on LB media.

Unlike *B. subtilis* 168 laboratory strain, swarming motility was identified in undomesticated wild strain, Bacillus subtilis 3610. Swarming motility has been lost in laboratory Bacillus strains because of the inability to produce surfactants associated

with multiple genetic defects [52, 64]. Swim and swarm agar plates were prepared as described above and supplemented with 0.25 mM, 0.5 mM and 1 mM amiloride to observe the inhibitory effect of amiloride on the motility of undomesticated *B. subtilis* 3610. For comparison, control groups were treated with the same concentration of DMSO.

Undomesticated *B. subtilis* 3610 completely colonized both swim (0.3 % agar) and swarm (0.7 % agar) agar plates. Then, the agar concentration was increased to 1 % and plates were supplemented with 0.25 mM, 0.5 mM and 1 mM amiloride similarly to investigate the effects of amiloride on swarming motility. In this case, the diameter of the colonization declined in agar plates dramatically.

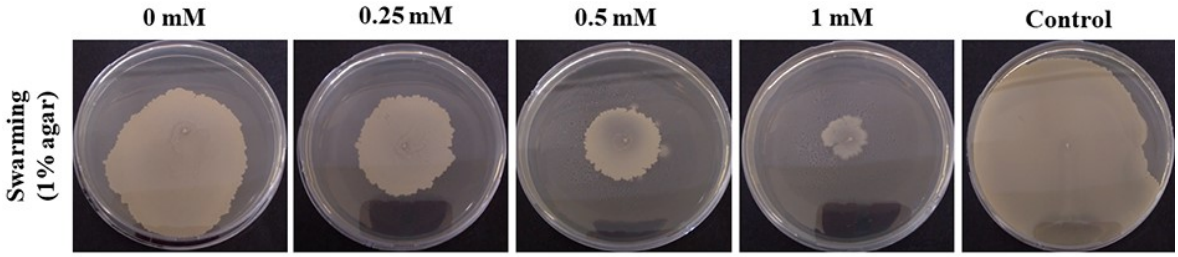

Figure 4.40. Swarming motility of *B. subtilis* 3610 on LB-agar media (1 % agar). In qualitative images of the plates, colonized agar appears white and uncolonized agar appears black on LB media.

Moreover, it was observed that amiloride has a striking inhibitory effect on swarming motility. As the amiloride concentration increases, the diameter of the colonization declined in swarm plates containing 1 % agar. Colonization is limited to the center of the swarm plate supplemented with 1 mM amiloride. Maximum swimming was observed in the control plate containing DMSO instead of amiloride (Figure 4.40.). Swarming motility was observed in *B. subtilis* 3610 strain as indicated previously [52]. Each motility assay was performed as triplicate and results were given in Table 4.3.

Table 4.3. Diameters (cm) of *B. subtilis* 3610 colonies formed on swimming and swarming agar plates supplemented with different concentrations of amiloride.

Plate	**Amiloride Concentration (mM)**				
	0	**0.25**	**0.5**	**1**	**Control**
Swimming (0.3 % agar)	9 cm	9 cm	8.2 ± 0.4 cm	7.3 ± 0.5 cm	9 cm
Swarming (0.7 % agar)	3.1 ± 0.6 cm	2.2 ± 0.3 cm	1.3 ± 0.4 cm	0.6 ± 0.1 cm	3.4 ± 0.4 cm

4.4.3. Effect of Amiloride on Motility of DS222 (containing only Na^+-driven MotPS stator)

Swim and swarm agar plates of DS222 strain (*B. subtilis* 3610 with a deletion of MotAB gene) were prepared as described above and supplemented with 0.25 mM, 0.5 mM and 1 mM amiloride to observe the inhibitory effect of amiloride on the motility of DS222 strain.

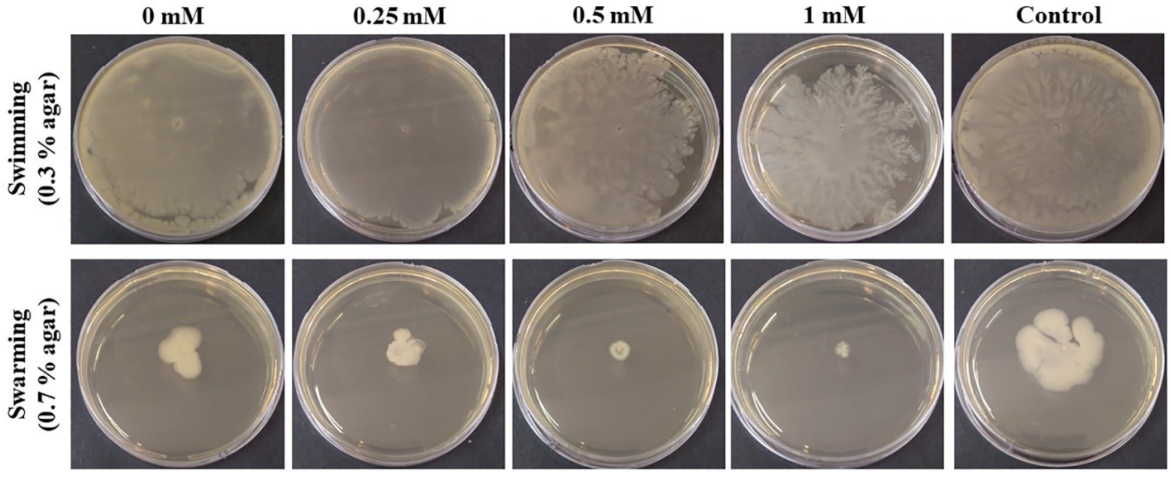

Figure 4.41. Swimming and swarming motility of DS222 strain on LB-agar media. In qualitative images of the plates, colonized agar appears white and uncolonized agar appears black on LB media.

For comparison, control groups were treated with the same concentration of DMSO. DS222 strain completely colonized swim plates supplemented with amiloride up to 0.25 mM concentration. When the amiloride concentration increased to 0.5 mM,

the diameter of the colonization started to decline in agar plates. Futhermore, the decrease in the colonization was obvious in swim agar plates supplemented with 1 mM amiloride. On the other hand, amiloride effects on motility was clearly observed in swarm agar plates (Figure 4.41). When the amiloride concentration was increased, the colonization was restricted to the center of the swarm plate, which indicates that amiloride has a striking inhibitory effect on swarming motility of DS222 strain. These results were expected because DS222 strain is constructed by the deletion of MotAB gene of undomesticated *B. subtilis* 3610 strain. Therefore, DS222 strain has only Na^+-driven MotPS stator and behaves as alkaliphilic bacillus.

As amiloride has an inhibitory effect on motility of alkaliphilic bacillus as reported previously [60], the diameter of the colonization decreased dramatically in swarm plates supplemented with amiloride. Each motility assay was performed as triplicate and results were given in Table 4.4.

Table 4.4. Diameters (cm) of DS222 colonies formed on swimming and swarming agar plates supplemented with different concentrations of amiloride

Plate	**Amiloride Concentration (mM)**				
	0	**0.25**	**0.5**	**1**	**Control**
Swimming	9 cm	9 cm	8.2 ± 0.4 cm	7.3 ± 0.5 cm	9 cm
Swarming	3.1 ± 0.6 cm	2.2 ± 0.3 cm	1.3 ± 0.4 cm	0.6 ± 0.1 cm	3.4 ± 0.4 cm

4.4.4. Effect of Amiloride on Motility of DS223 (containing only H^+-driven MotAB stator)

Swim and swarm agar plates of DS223 strain (*B. subtilis* 3610 with a deletion of MotPS gene) were prepared as described above and supplemented with 0.25 mM, 0.5 mM and 1 mM amiloride to observe the inhibitory effect of amiloride on the motility of DS223 strain. For comparison, control groups were treated with the same concentration of DMSO.

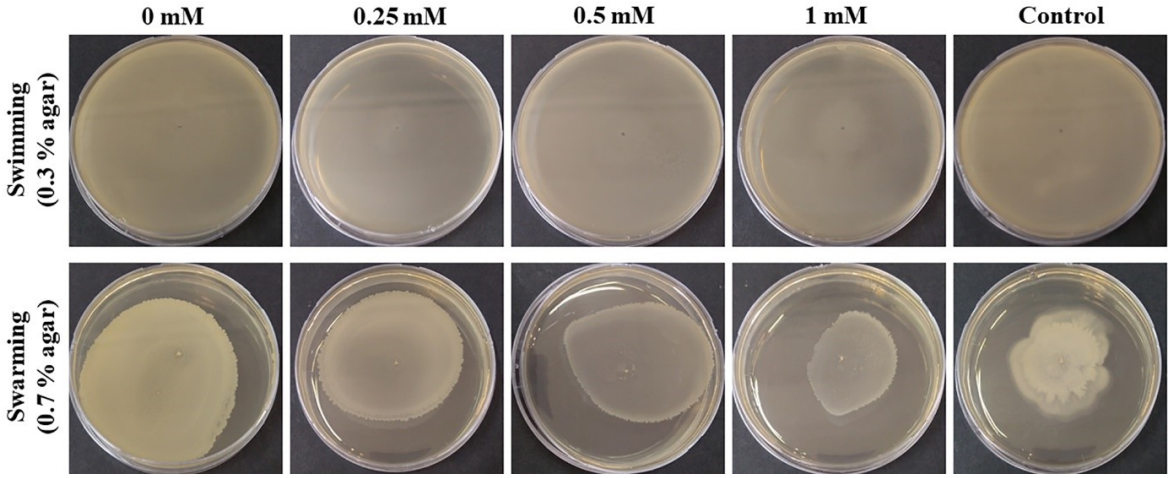

Figure 4.42. Swimming and swarming motility of DS223 strain on LB-agar media. In qualitative images of the plates, colonized agar appears white and uncolonized agar appears black on LB media.

DS223 strain completely colonized swim (0.3 % agar) agar plates. Amiloride has almost no effect on swarming motility. DS223 strain is constructed by the deletion of MotPS gene of undomesticated *B. subtilis* 3610 strain. Because DS223 strain has H^+-driven MotAB stator and amiloride does not affect MotAB dependent motility, these results were expected. The diameter of the colonization in swarm plates are close each other, which also indicates that DS223 strain has swarming motility as undomesticated *B. subtilis* 3610 strain does. Each motility assay was performed as triplicate and results were given in Table 4.5.

Table 4.5. Diameters (cm) of DS223 colonies formed on 0.3 % (swimming) and 0.7 % (swarming) agar plates supplemented with different concentrations of amiloride

Plate	**Amiloride Concentration (mM)**				
	0	**0.25**	**0.5**	**1**	**Control**
Swimming	9 cm	9 cm	9 cm	9 cm	9 cm
Swarming	7.5 ± 0.5 cm	6.5 ± 0.3 cm	6.2 ± 0.4 cm	5.6 ± 0.7 cm	4.5 ± 0.2 cm

4.4.5. Effect of Amiloride on Motility of *B. marmarensis sp. nov.*

B. marmarensis sp. nov. strain belongs to alkalophilic *Bacillus*, so this strain uses Na^+-driven MotPS stator for motility. Previously, it was reported that amiloride inhibits the Na^+ driven flagellar motors of alkalophilic *Bacillus* by competing with Na^+ ions in the medium [52]. In this regard, swim and swarm plates that contain different amount of agar were prepared to observe motility of *B. marmarensis sp. nov.* strain and the aim is to investigate the effects of different amiloride concentrations on the motility of this strain. Images of the swim and swarm plates obtained from the first motility assay experiment were given in Figure 4.43. From swim and swarm plate images, it was observed that amiloride has an inhibitory effect on swimming and swarming motility. For swim plates, if amiloride is not added to the plates (0 mM), the diameter of the colonization is equal to almost the diameter of the plate.

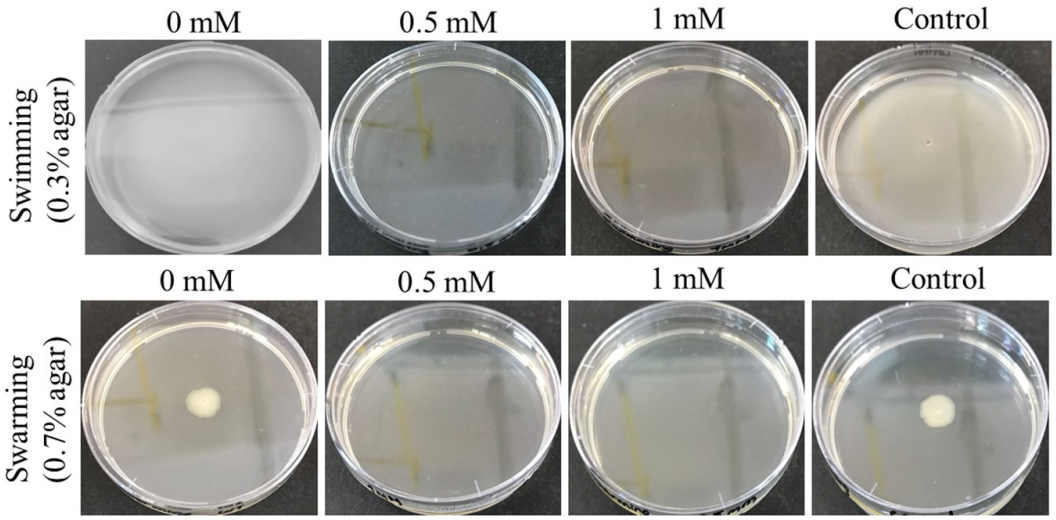

Figure 4.43. Swimming and swarming motility of *B. marmarensis* strain on NB-agar media. In qualitative images of the plates, colonized agar appears white and uncolonized agar appears black on NB-agar media.

Control plates contain the same concentration of DMSO, for comparison and the diameter of the colonization in these plates also reached to the diameter of the plates. When 0.5 mM and 1 mM amiloride was added to the plates, colonization of *B. marmarensis* cells did not occur. For swarm plates, the colonization of *B. marmarensis*

cells is restricted to the center of the swarm plate, which represents that *B. marmarensis* strain is swimming proficient whereas it is swarming deficient. Each motility assay was performed as triplicate. The diameters of the colonization of *B. marmarensis* strain on the NB-agar plates containing different concentrations of amiloride were measured after 18 hours of incubation and results were presented in Table 4.6.

Table 4.6. Diameters (cm) of *B. marmarensis* colonies formed on NB agar plates supplemented with different concentrations of amiloride

Plate	**Amiloride Concentration (mM)**			
	0	**0.5**	**1**	**Control**
Swimming	7.2 ± 0.1 cm	0 cm	0 cm	7.3 ± 0.6 cm
Swarming	1.4 ± 0.1 cm	0 cm	0 cm	1.4 ± 0.1 cm

In the following motility assay experiments, to be able to determine the concentration of amiloride at which colonization of *B. marmarensis* strain did not occur, different amiloride concentrations between 0 mM and 1 mM were tested in swarm and swarm plates. Images of the swim plates containing amiloride concentratios of 0 mM, 0.2 mM, 0.4 mM, 0.6 mM, 0.8 mM and 1 mM were given in Figure 4.44.

Similar results were also obtained from the second motility assay analysis. Amiloride has an inhibitory effect on the swimming motility of *B. marmarensis* strain. If amiloride is not added to the plates (0 mM), the diameter of the colonization is equal to the diameter of the plate. When 0.2 mM and 0.4 mM amiloride was added to the plates the diameter decreased somewhat. 0.6 mM and higher concentrations of amiloride totally ceased the swimming motility, resulting in no colonization of *B. marmarensis* cells on agar plates. As the amiloride concentration increased, the diameter of the colonization decreased in swim plates (Figure 4.44). Maximum swimming was observed in 0 mM and control plates that do not contain amiloride. Control plates contain the same concentration of DMSO for comparison and the diameter of the colonization in these plates reached to the diameter of the plates.

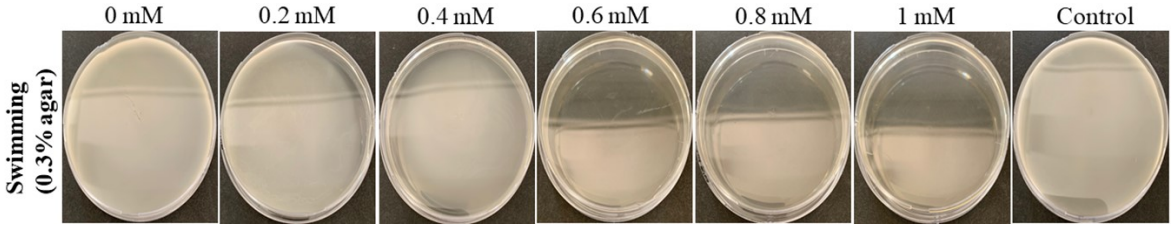

Figure 4.44. Swimming motility of *B. marmarensis* strain on NB-agar media. In the images, colonized agar appears white and uncolonized agar appears black on NB-agar media. Swim plates are supplemented with different concentrations of amiloride.

On the other hand, the results of swarm motility assay for *B. marmarensis* strain given in Figure 4.45 are different from the first motility assay. From the swarm plates, it can be said that amiloride has no effect on the swarming motility of *B. marmarensis* strain, while amiloride caused no colonization on swarm plates in the first experiment.

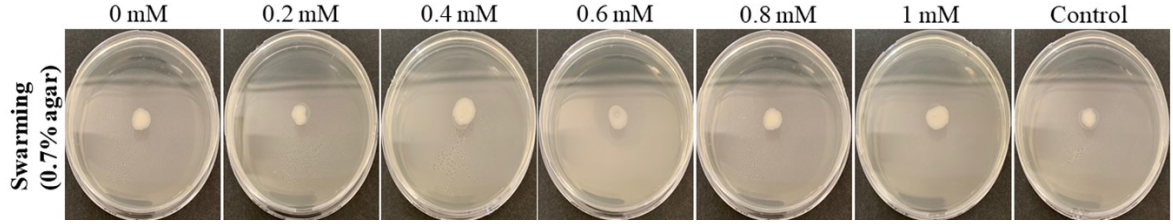

Figure 4.45. Swarming motility of *B. marmarensis* strain on NB-agar media. In the images, colonized agar appears white on NB-agar media. Swarm plates are supplemented with different concentrations of amiloride.

The diameters of the colonization of *B. marmarensis* strain on the agar plates containing different concentrations of amiloride were measured after 18 hours of incubation and results of the second motility assay experiment were presented in Table 4.7. The colonization of *B. marmarensis* cells is restricted to the center of the swarm plate. Amiloride concentration tested between 0 mM and 1 mM did not change significantly the diameters of the colonization of *B. marmarensis* strain. As a result, amiloride has an inhibitory effect on the swimming motility, whereas it has no effect on the swarming motility of *B. marmarensis* strain. Each motility assay was performed as triplicate.

Table 4.7. Diameters (cm) of *B. marmarensis* colonies formed on NB agar plates supplemented with different concentrations of amiloride

Plate	Amiloride Concentration (mM)						
	0	**0.2**	**0.4**	**0.6**	**0.8**	**1**	**Control**
Swimming (0.3 % agar)	8 ± 0.1 cm	7.7 ± 0.4 cm	7.6 ± 0.1 cm	0 cm	0 cm	0 cm	8 ± 0.1 cm
Swarming (0.7 % agar)	1 ± 0.1 cm	1.1 ± 0.4 cm	1 ± 0.3 cm	0.9 ± 0.1 cm	0.9 ± 0.1 cm	1.2 ± 0.2 cm	1 ± 0.1 cm

4.5. Monitoring of Bacterial Cells Using Microfluidic Systems

4.5.1. Growth of Bacterial Cells in Zeonor Microchips-Reaction Chambers of 10 μL Volume

Growth of wild type *E. coli* K12 and opp-deleted mutant *E. coli* K12 SS5013 cells was analyzed in zeonor microchips-reaction chambers of 10 μL (Figure 4.46). Cell density of both wild type and mutant cells increased over time due to the cellular division, which is called as binary fission. The bacterium starts this process by elongation of the cell size.

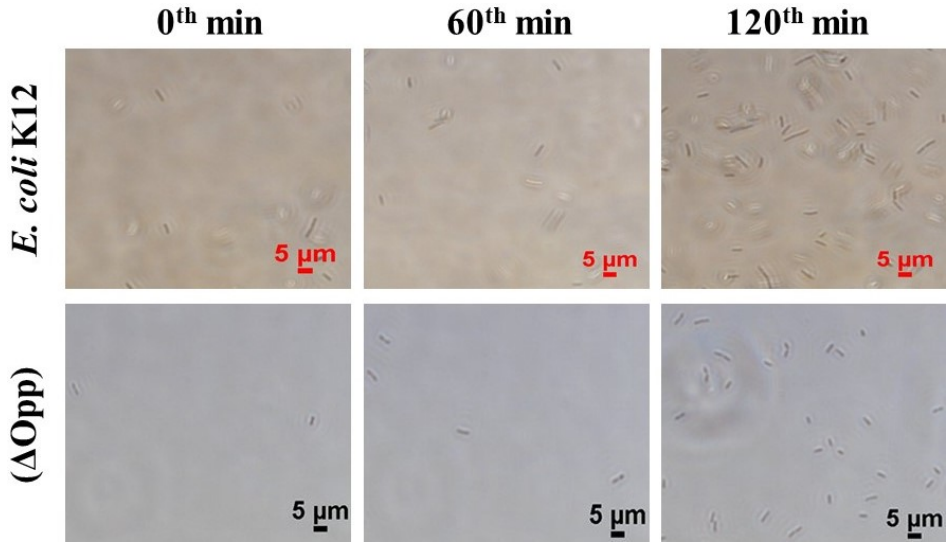

Figure 4.46. Growth of wild type *E. coli* K12 and opp-deleted mutant SS5013 cells. Microscopy images were captured at 40X zoom at 60 min intervals. Scale bars, 5 μm.

Afterwards, bacterial genome is replicated. The cell continues to enlarge, which is followed by cell division and two identical copies were generated. Two copies of the bacterium are called as daughter cells. As a result, a million of bacterial cells can be generated from a single cell within several hours. The sizes of the mutant cells were smaller than that of wild type cells as can be seen in the images. In this regard, the set-up used in this study provides suitable conditions which mimic the physiological environment of bacterial cells.

4.5.2. Bacterial Uptake of Fluoresceinamine Dye in Zeonor Microchips-Reaction Chambers of 10 μL Volume

The aim of this study was to determine whether the fluoresceinamine dye (100 μM, in distilled water) was spontaneously internalized by wild type *E. coli* K12 cells or not, before testing the suitability of the reaction chambers for the visualization of fluorescently labeled peptides. Nikon inverted microscope was used to visualize the bacterial cells in the chambers at room temperature continuously. Bright field and fluorescence images captured using the FITC filter were given in Figure 4.47.

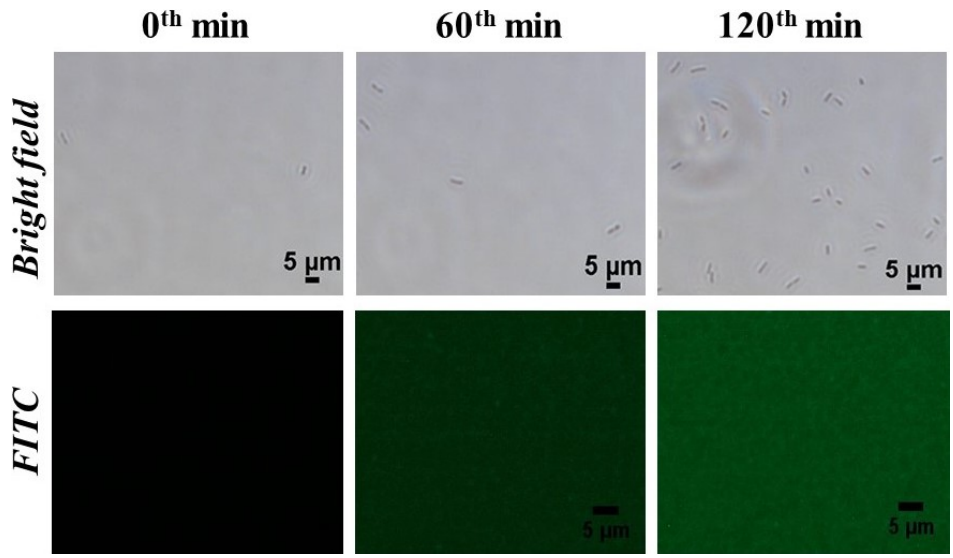

Figure 4.47. Microscopy images of bacterial uptake of fluoresceinamine dye captured at 40X zoom. Images were captured from the same spot at 1 hour intervals. Scale bars, 5 μm.

This experiment lasted 4 hours. Because wild-type *E. coli* K12 cells are motile, cell density in the chamber changed continuously. As seen in the fluorescence images, no fluorescence intensity was observed in the bacterial cells. This result was expected since fluoresceinamine is not able to penetrate into the bacteria spontaneously, but it can be carried through the membrane as a cargo [65]. As bacterial uptake of fluoresceinamine was not observed, the fluorescence intensity in the background increased continuously.

4.5.3. Bacterial Uptake of Fluorescently Labeled pVEC in Zeonor Microchips-Reaction Chambers of 10 μL Volume

It was demonstrated above that fluoresceinamine was not able to penetrate into wild type *E. coli* K12 cells spontaneously. After that, microfluidic bioreactors (reaction chips) were tested whether fluorescently labeled pVEC (H-RRRIRKQAHAHSKK(HF-488)-NH_2) was internalized by wild type *E. coli* K12 and opp-deleted mutant cells or not.

4.5.3.1. Penetration Into Wild Type *E. coli* K12 Cells. Microscopy images from the same spot were captured every 10 minutes during a time interval of 1.5 hours. The chamber was monitored continuously and the number of fluorescent cells increased from one image to another. As the number of fluorescent cells increased from one image to another, fluorescence density of the background increased as well due to the continuous fluorescently labeled pVEC perfusion into the chamber.It seems that fluorescently labeled pVEC was able to penetrate into the wild type E. coli K12 cells, meaning that fluorescently labeled pVEC carries fluoresceinamine into plasma membrane whereas it can not be internalized spontaneously [66, 67].

Fluorescence intensity of these bacterial cells was analyzed via Fiji-ImageJ software. The corrected total cell fluorescence was calculated by subtracting background intensity from integrated density of bacterial cells. The sum of the corrected total cell fluorescence was calculated for each image and both integrated density and CTCF were shown on the same graph.

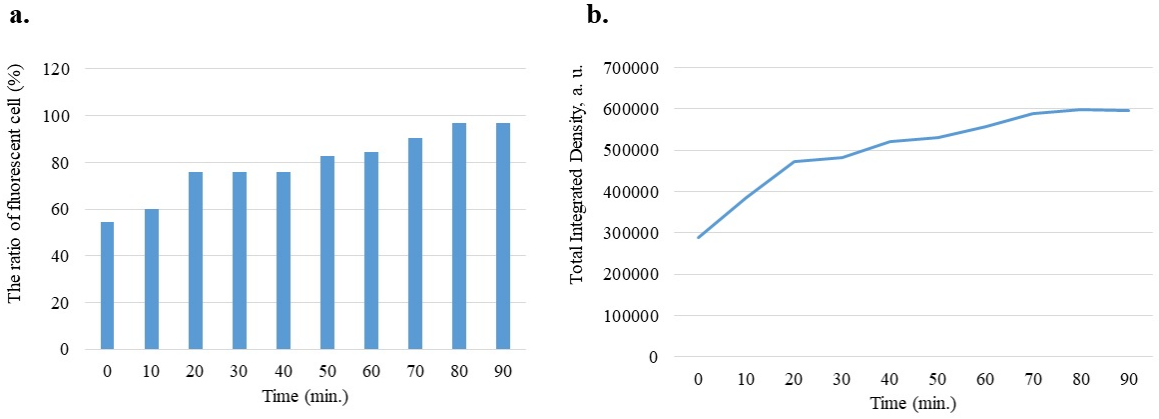

Figure 4.48. a. The ratio of fluorescent cell versus time graph for wild type *E. coli* K12 cells incubated with pVEC in reaction chambers. b. the sum of the integrated density of bacterial cells in each image versus time.

To be able to observe the difference between integrated density and corrected total cell fluorescence (obtained by subtracting the fluorescence intensity of background from integrated density), both of them were displayed on the same graph. Even the number of fluorescent cells increased in the chamber over time, total integrated density showed a fluctuation. The reason for that may be the motility of bacterial cells.

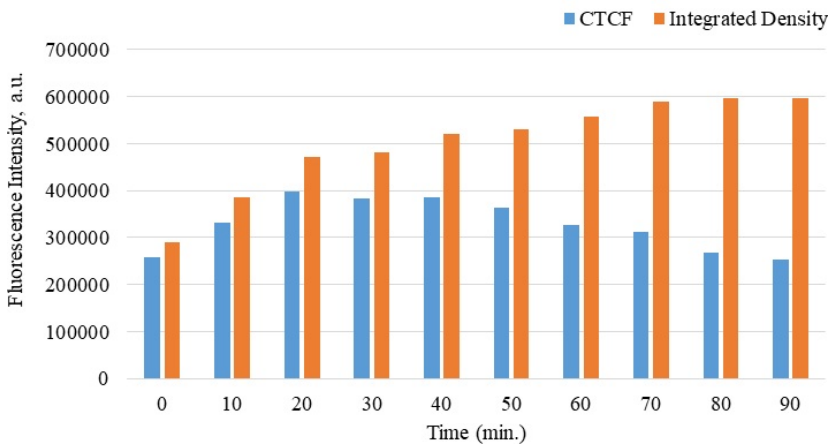

Figure 4.49. Time profile for fluorescence intensity of wild type *E. coli* K12 cells incubated with pVEC in reaction chambers.

During the experiment, some bacterial cells entered to the region we focused on while some of them exited from the chamber. In addition, bacterial cells move in the z stage due to the 3D environment of reaction chips, so they may become invisible after

a while during the image capture. Because the fluorescence intensities of the bacterial cells are different from each other, the sum of the integrated density and corrected total cell density is expected to change over time.

Upon fluorescently labeled pVEC perfusion into the chamber, the fluorescence intensity of the background and integrated density of bacterial cells increased in time. Even if the number of fluorescent cells increased in the chamber, the cell size and fluorescence intensity of bacterial cells are different, resulting in the fluctuation of total integrated density. Due to the increase in background fluorescence, the difference between the corrected total cell density and integrated density increased as well.

4.5.3.2. Penetration into Opp-deleted Mutant *E. coli* K12 SS5013 Cells. The outer membrane of gram negative bacteria limits the size of the peptides that can be taken up, and only peptides up to five or six amino acids long can freely diffuse across the outer membrane. Oligopeptide permease (Opp) system is a protein-dependent ABC transport system, which mediates the transportation of peptides. Opp system is found to allow peptides, the amino acid residues of which varies between three and eighteen depending on bacterial strains, pass through the membrane. OppA protein is essential part of the Opp system, which has a role in binding peptides. OppB and OppC are the integral membrane proteins, which form translocation pores for the transition of peptides from the membrane. OppD and OppF proteins are membrane-bound cytoplasmic ATP binding proteins that provide energy for this process [68–70].

In this experiment, the aim was to analyze whether fluorescently labeled pVEC was internalized via Opp system or not. For this aim, opp-deleted mutant *E. coli* K12 SS5013 cells were used. The similar procedure used for wild type cells was also followed for the mutant SS5013 cells. After a 30 minute time interval, brightfield and fluorescence images were captured from the same spot every 15 minutes at 40X zoom using a 16.25 megapixel Nikon microscope camera (DS-Ri2). FITC filter was used for fluorescence microscopy images and Nikon inverted microscope was used to visualize cells in the chamber continuously.

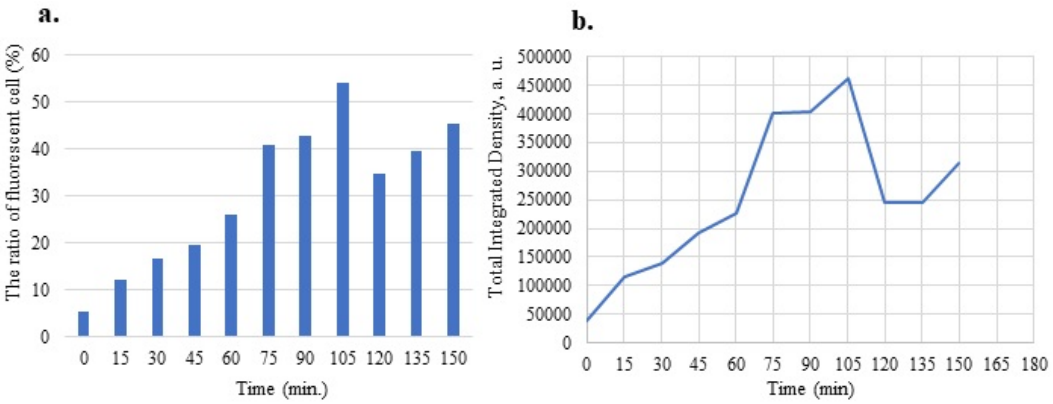

Figure 4.50. a. The ratio fluorescent cell versus time graph for mutant *E. coli* K12 (ΔOpp) cells incubated with pVEC in reaction chambers. b. The sum of the integrated density of bacterial cells in each image versus time

Image capturing process was carried out for 2.5 hours. After that, the experiment was obliged to be finished because of the increase in fluorescence intensity of the background, resulting in the decline in the visibility of bacterial cells in the chamber.

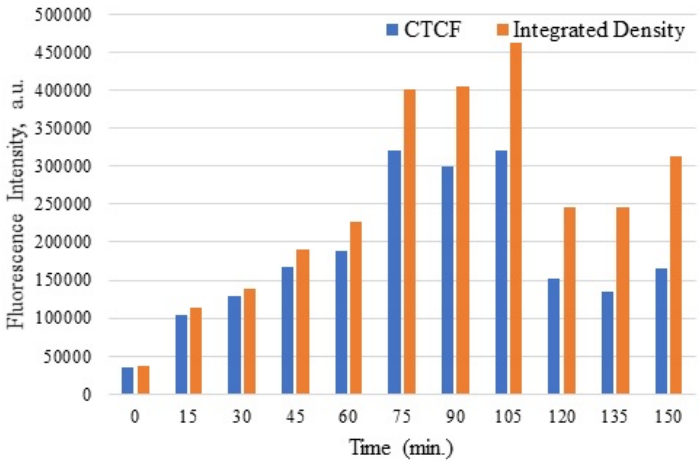

Figure 4.51. Time profile of fluorescence intensity of mutant *E. coli* K12 (ΔOpp) cells incubated with pVEC in reaction chambers.

The ratio of fluorescent cell in the chamber was calculated by dividing the number of fluorescent cell to the total cell in the image. The ratio of fluorescent cell reached to 95 % for wild type cells, but this value was found only 54 % for mutant cells. Therefore, deletion of opp system caused the decrease in the uptake of fluorescently

labeled pVEC. Fluorescence density of background increased over time owing to the continuous pVEC perfusion to the chamber, but the increase of background fluorescence was slow compared to that of wild type cells.

The increase in fluorescence density of background occurs slowly compared to wild type cells, resulting in the increase in CTCF values of bacterial cells in parallel with total integrated density values. As a result, the fluorescently labeled pVEC penetrated into the mutant cells, meaning that fluorescently labeled pVEC is not internalized only by the opp system. Besides the opp system, there must be other mechanisms for the internalization of these peptides. Both integrated density and corrected total cell fluorescence values were displayed on Figure 4.51. The increase in the number of fluorescent cells during the experiment was found to be consistent with the rise in the fluorescence intensity of cells.

The number of fluorescent cells increased until the 105^{th} minutes but then, a significant decrease in the count of the fluorescent cells was observed. The reason of that could be the exit of the cells from the point we focused on. Another reason may be the pressure difference occurred in the chamber due to the volume change occurred between the tubings and the chamber. This pressure difference may lead to sweeping of the cells out the chamber.

Similar to the case observed in wild type cells, fluorescence intensity of bacterial cells differs from each other, so the sum of the corrected total cell density changed over time as expected. The corrected total cell fluorescence and integrated density values were very close at the beginning, however the difference between them increased in time due to the increase in fluorescence intensity of background. The longitudinal axis length of wild type cells is bigger than that of mutant cells. In addition, mutant cells were usually at upright position in the chamber. For this reason, that seems as a stain rather than a bacterium. This difference may cause the decrease in the uptake of fluorescently labeled pVEC, because the peptide uptake of bacterial cells is limited by the size of them [71]. Even the corrected total cell fluorescence values of wild type and

mutant cells were on the same order, the maximum CTCF value of wild type cells was $5x10^5$, whereas this value was $3x10^5$ for mutant *E. coli* K12 (ΔOpp) cells. In order to be sure whether fluorescent peptide is internalized by bacterial cells or it stucks on the surface of them, trypsin treatment should be performed after the incubation of bacterial cells with fluorescently labeled pVEC. Trypsin enzyme damages peptides especially C-terminal side of lysine and arginine, and it is mostly used to discard mammalian cells from flask [72]. Therefore, trypsin treatment can be used to analyse fluorescence intensity change of bacterial cells for future studies.

4.5.4. Bacterial Uptake of Fluorescently Labeled pVEC in Zeonor Microchips-Rhombic Chambers of 6 μL Volume

Zeonor microchips-reaction chambers of 10 μL volume used in previous section consisted of one inlet and one outlet for each chamber. For this reason, the solutions perfused into the chamber were seperately sent from syringe pumps but they are combined before connecting to the inlet. A time delay occurs during the perfusion of fluorescent peptide solution into the chamber. As a result of this fact, the perfusion of the peptide and bacterial cell solutions was decided to be performed from separate inlets to the chamber. Bacterial uptake of fluorescently labeled pVEC and P4 peptides and fluorescein-labeled P2 peptide was analyzed using rhombic chambers of 6 μL volume.

4.5.4.1. Bacterial Uptake of Fluorescently Labeled pVEC by *E. coli* K12 Cells. When bacterial cell and fluorescent peptide solutions were perfused from separate inlets into the chamber, fluorescence background increased at the beginning of the experiment even when the peptide pump was not switched on. Afterwards, the concentration of fluorescent peptide was decreased from 100 μM to 50 μM and 25 μM, respectively. However, the fluorescence background problem could not be overcome. For this reason, similar tubing system used in previous experiments was used, but only difference was that the length of the tubing part connected to the inlet was decreased from 4 cm to 2.5 cm in order to decrease the arrival time of the peptide solution into the

chamber. The other inlet was plugged in with a Mini Luer fluid plug for these uptake experiments but it was used for the perfusion of trypsin solution into the chamber later. The experiment was carried out for 3 hours. The concentration of fluorescently labeled pVEC to be tested on bacterial cells was 50 μM. The images from the same spot were captured every 15 minutes during a time interval of 3 hours. In the first fluorescent image, only 2 fluorescent cells were observed. Over time, the number of fluorescent cells increased in the chamber. The last image captured after 2 hours following the fluorescently labeled pVEC perfusion contained 21 fluorescent cells.

As the number of fluorescent cells increased from one image to another, fluorescence density of background increased as well due to the continuous fluorescently labeled pVEC perfusion into the chamber. Due to the increase in background fluorescence, the difference between the corrected total cell density and integrated density increased as well. The chamber was monitored continuously and over time, the number of fluorescent cells increased.

Fluorescence intensity of bacterial cells is consistent with the number of fluorescent cells in the chamber. Both integrated density and CTCF values increased until 45th minutes. After that, a decrease was observed and then fluorescence intensity continued to increase. The ratio of fluorescent cell in the images increased over time and reached to 92 % in the last image. However, the number of fluorescent cells showed a fluctuation over time.

Total integrated density increased continuously, however CTCF values started to decrease after 45^{th} minutes because of the increase in fluorescence intensity of the chamber. The size of the bacterial cells causes a difference between the fluorescence intensity of them. Thus, the sum of the corrected total cell density changed over time as expected. The corrected total cell fluorescence and integrated density values were very close at the beginning, however the difference between them increased in time due to the increase in fluorescence intensity of background.

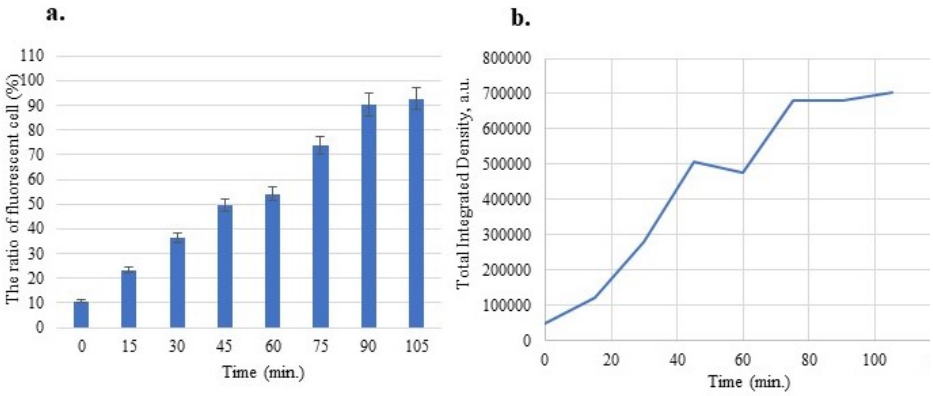

Figure 4.52. a. The ratio of the number of fluorescent cells to the total number of *E. coli* K12 cells incubated with pVEC in rhombic chambers. b. Corrected total cell fluorescence per a fluorescent cell versus time graph.

The maximum CTCF value of wild type *E. coli* K12 cells is 4.4×10^5. From the same spot, microscopy images were captured every 10 minutes during a time interval of 1.5 hours. The experiment was carried out for 4.5 hours. Cell density in the chamber increased over time.

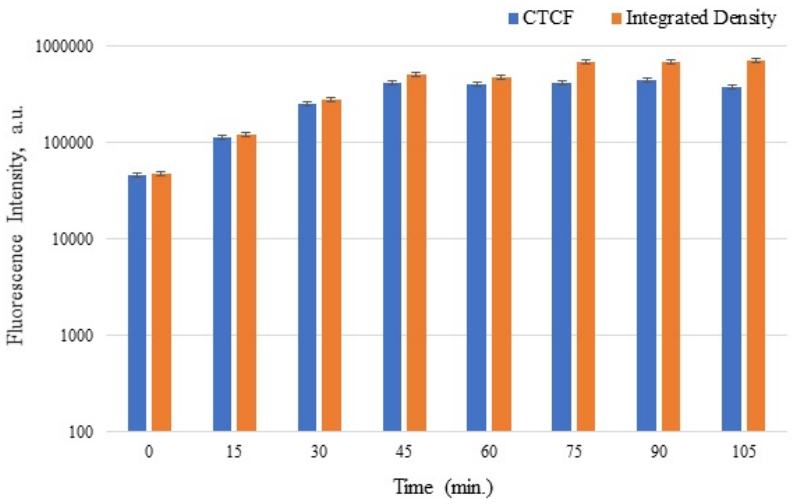

Figure 4.53. Time profile of fluorescence intensity of *E. coli* K12 cells incubated with pVEC in rhombic chambers.

In the first fluorescent image, 12 fluorescent cells were detected. Over time, the number of fluorescent cells increased in the chamber. The last image captured after 1.5 hours following the fluorescently labeled pVEC perfusion contained 29 fluorescent cells.

As the number of fluorescent cells increased from one image to another, fluorescence density of the background increased as well due to the continuous fluorescently labeled pVEC perfusion into the chamber.

4.5.4.2. Bacterial Uptake of Fluorescently Labeled pVEC by Mutant Cells. Images from the same spot were captured every 15 minutes during a time interval of 3 hours. Microscopy images involve both bright field and fluorescence images captured using the FITC filter. The experiment was carried out approximately for 4 hours.

In the first fluorescent image, only 2 fluorescent cells were observed. Over time, the number of fluorescent cells increased in the chamber. The last image captured after 3 hours following the fluorescently labeled pVEC perfusion contained 14 fluorescent cells. As the number of fluorescent cells increased from one image to another, fluorescence density of background increased as well due to the continuous fluorescently labeled pVEC perfusion into the chamber.

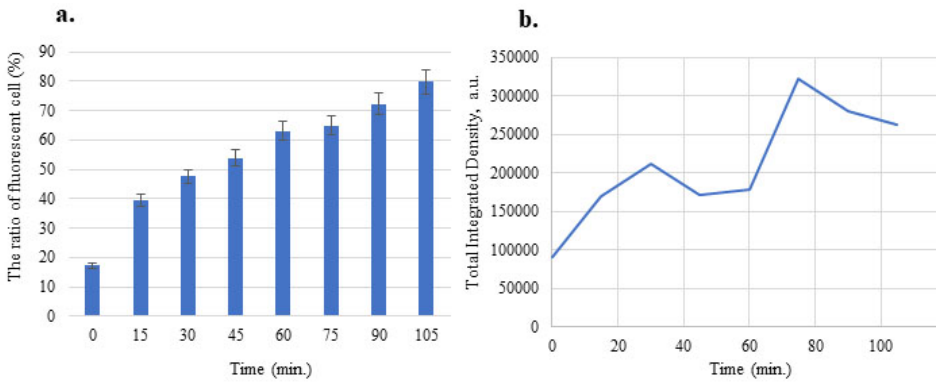

Figure 4.54. a. The ratio of the number of fluorescent cells to the total number of opp-deleted mutant cells incubated with pVEC in rhombic chambers. b. Corrected total cell fluorescence per a fluorescent cell versus time graph.

Upon fluorescently labeled pVEC perfusion into the chamber, the fluorescence intensity of the background increased in time. Due to the increase in background fluorescence, the difference between the corrected total cell density and integrated density increased as well.

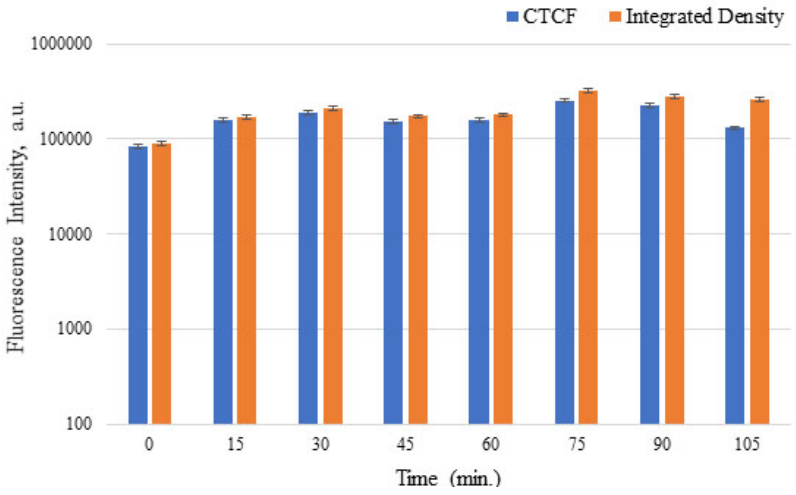

Figure 4.55. Time profile of fluorescence intensity of opp-deleted mutant cells incubated with pVEC in rhombic chambers.

The fluctuation in fluorescence intensity profile of bacterial cells were found consistent with the number of fluorescent cell in the image. As the wild type cells, opp-deleted mutant cells are also motile and they can enter and exit from the point we focused on. Therefore, the number of fluorescent cell in the images changes in time. Because of the pressure difference occurring occasionally in tubings, bacterial cells can be swept from the chamber, leading to change of fluorescent cell ratio in the chamber. Even if the number of fluorescent cells is the same in the images, fluorescence intensity of wild type and mutant cells changes. The maximum CTCF value of mutant *E. coli* K12 cells is $2.5\text{x}10^5$. The size of bacterial cells changes over time, resulting in difference between the fluorescence intensity of bacterial cells. It was concluded that opp system has a role in the uptake of florescent peptide but this is not the only way for the penetration of florescent cells into the bacterial cells.

4.5.5. Bacterial Uptake of Fluorescently Labeled P4 in Microchips-Rhombic Chambers of 6 μL Volume

After the bacterial uptake of fluorescently labeled pVEC was tested on both *E. coli* K12 and opp-deleted mutant SS5013 cells, the bacterial uptake of fluorescently labeled P4 (H-LLIILRRGHYYK(HF488)-NH_2) was investigated on these cells.

4.5.5.1. Bacterial Uptake of Fluorescently Labeled P4 by *E. coli* K12 Cells. The concentration of fluorescently labeled P4 to be tested on bacterial cells was 50 μM. Images from the same spot were captured every 15 minutes during a time interval of 3.5 hours. The experiment was carried out approximately for 5 hours. Bacterial cell density in the chamber increased over time as it is seen from the brightfield images. Due to the depth of the rhombic chamber, the movement of bacterial cells in z direction is limited and the images of the bacterial cells became more clear. In the first fluorescent image, only 1 fluorescent cell was observed. Over time, the number of fluorescent cells increased in the chamber. The last image captured after 3.5 hours following the fluorescently labeled P4 perfusion contained 15 fluorescent cells. The number of fluorescent cells was small at the beginning of the experiment, however, a sharp increase was observed after 60^{th} minutes.

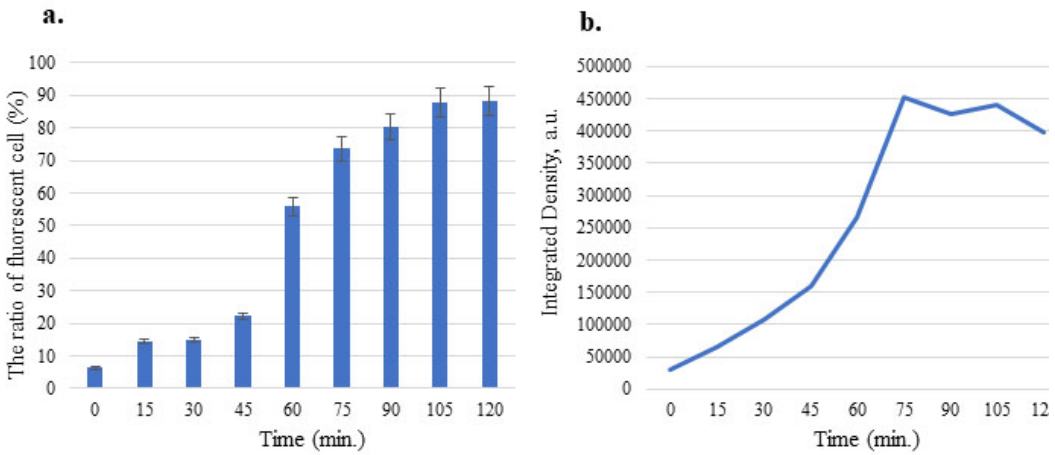

Figure 4.56. a. The ratio of the number of fluorescent cells to the total number of *E. coli* K12 cells incubated with P4 in rhombic chambers.. b. Corrected total cell fluorescence per a fluorescent cell versus time graph.

The number of fluorescent cells in the chamber increased in time. However, the integrated density values fluctuated especially towards the end of the experiment. Upon fluorescently labeled P4 perfusion into the chamber, the fluorescence intensity of the background increased in time. Due to the increase in background fluorescence, the difference between the corrected total cell density and integrated density increased as well. Fluorescently labeled P4 tended to precipitate in the chamber compared to

fluorescently labeled pVEC, so the increase in background intensity of the chamber occurred quickly.

The ratio of fluorescent to nonfluorescent cells was low at the beginning, but it increased noticeably after 60^{th} minutes. The reason of that could be the exit of the cells from the point we focused on. Another reason may be the pressure difference occurred in the chamber due to the sudden volume change between tubings and the chamber. This pressure difference may lead to sweeping of the cells from the chamber at that moment. The size of the bacterial cells changes over time, resulting in difference between the fluorescence intensity of bacterial cells. Thus, the sum of the corrected total cell density changed over time as expected.

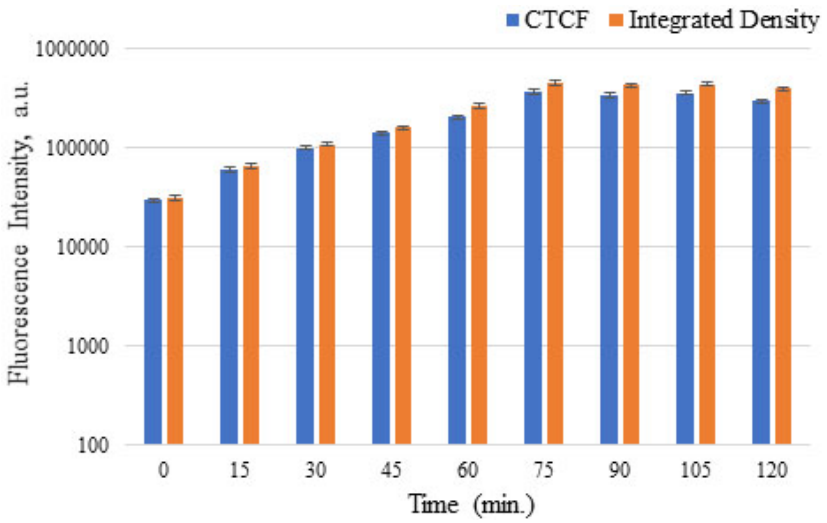

Figure 4.57. Time profile of fluorescence intensity of *E. coli* K12 cells incubated with P4 in rhombic chambers.

The corrected total cell fluorescence and integrated density values were very close at the beginning, however the difference between them increased in time due to the increase in fluorescence intensity of background. The maximum CTCF value of wild type *E. coli* K12 cells is 3.7×10^5. The bacterial uptake of fluorescently labeled P4 peptide was low compared to uptake of fluorescently labeled pVEC peptide by *E. coli* K12 cells according to fluorescence intensity values.

4.5.5.2. Bacterial Uptake of Fluorescently Labeled P4 by Mutant Cells. Images from the same spot were captured every 15 minutes during a time interval of 4 hours. Microscopy images involve both brightfield and fluorescence images captured using the FITC filter. The experiment was carried out for 5 hours and cell density in the chamber increased over time as it is seen from brightfield images. In the first fluorescent image, only 1 fluorescent cell was observed. Over time, the number of fluorescent cells increased in the chamber. The last image captured after 3 hours following the fluorescently labeled P4 perfusion contained 32 fluorescent cells. The increase in fluorescence intensity of the background happened quickly.

The chamber was monitored continuously and over time, the number of fluorescent cells increased and the fluorescence intensity of the bacterial cells changed consistently with the number of fluorescent cell in the chamber.

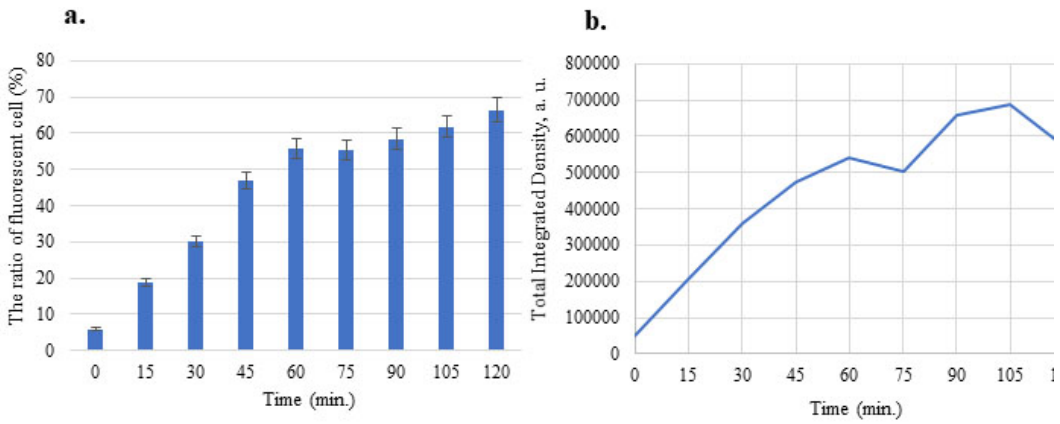

Figure 4.58. a. The ratio of the number of fluorescent cells to the total number of opp-deleted mutant SS5013 cells incubated with P4 in rhombic chambers. b. Corrected total cell fluorescence per a fluorescent cell versus time graph.

Upon fluorescently labeled P4 perfusion into the chamber, the fluorescence intensity of the background increased in time, resulting in the increase in the difference between the corrected total cell density and integrated density towards the end of the experiment. The ratio of fluorescent to nonfluorescent cells increased until the 60th minutes quickly but then, a slight increase in the count of fluorescent cells was observed. The maximum ratio of fluorescent cell in the chamber was found 66 % for

mutant cells which is less than the ratio of wild type *E. coli* K12 fluorescent cells (88 %). It can be said that the absence of opp system limited the uptake of fluorescent P4 peptide by mutant cells. The uptake of fluorescently labeled P4 peptide by both bacterial cells is less than the uptake of fluorescently labeled pVEC according to the ratio of fluorescent cell in the chamber, implying that the penetration of pVEC into bacterial cells is easier than that of P4 peptide.

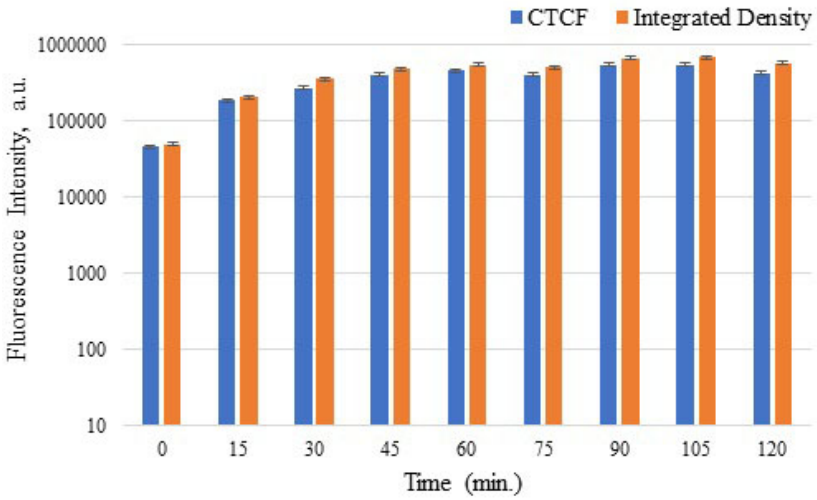

Figure 4.59. Time profile of fluorescence intensity of opp-deleted mutant SS5013 cells incubated with P4 in rhombic chambers.

The size and density of bacterial cells at that moment in the chamber affects the fluorescence intensity values. The sum of the integrated density of bacterial cells increased mostly but due to the change in the number of fluorescent cells in the chamber, fluorescence intensity values showed fluctuation. The reason of the change of fluorescent cell density in the chamber could be the pressure difference occurred in the tubings and the motility of bacterial cells. Integrated density and CTCF values were close at the beginning but the difference between them increased over time due to the fluorescence intensity of the background. The maximum integrated density and CTCF values of mutant cells are 6.8×10^5 and 5.4×10^5, respectively.

4.5.6. Bacterial Uptake of Fluoresceine-labeled P2 in Microchips-Rhombic Chambers of 6 μL Volume

After the bacterial uptake of fluorescently labeled pVEC and P4 peptides were analyzed, the bacterial uptake of fluoresceine-labeled P2 (5(6)-Fluoresceine-NH-LLIILHA-AGDYYAY-$CONH_2$) was investigated on both wild type *E. coli* K12 and opp-deleted mutant *E. coli* K12 SS5013 cells. When 50 μM of fluoresceine-labeled P2 was analyzed on *E. coli* K12 cells, fluorescence intensity was low in the bacterial cells. For this reason, the concentration of fluoresceine-labeled P2 was increased to 100 μM.

4.5.6.1. Bacterial Uptake of Fluoresceine-labeled P2 by *E. coli* K12 Cells. The concentration of fluoresceine-labeled P4 to be tested on bacterial cells was 100 μM. Images from the same spot were captured every 15 minutes during a time interval of 3 hours. The experiment was carried out for 5 hours. Bacterial cells are more distinct in bright field images mostly because the depth of the chamber decreased and so the movement of bacterial cells in z direction was restricted. In the first fluorescent image, 5 fluorescent cells were observed. Over time, the number of fluorescent cells increased in the chamber.

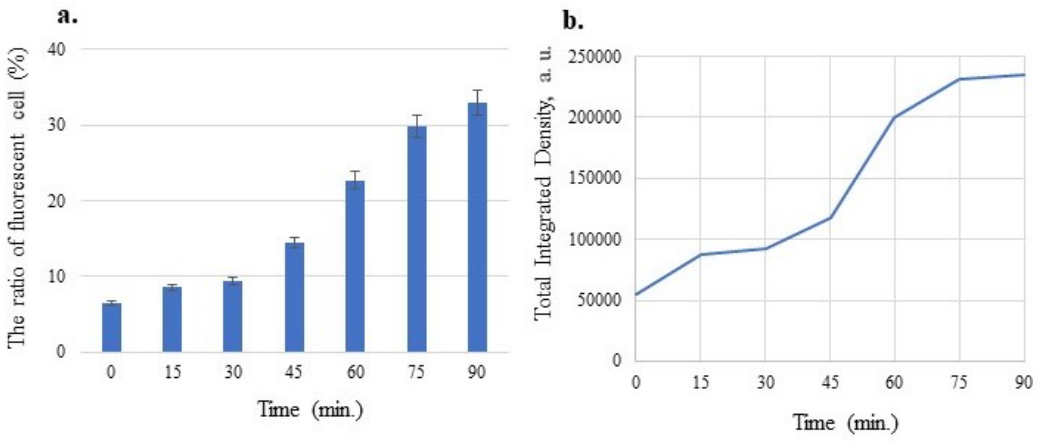

Figure 4.60. a. The ratio of the number of fluorescent cells to the total number of *E. coli* K12 cells incubated with P2 in rhombic chambers. b. Corrected total cell fluorescence per a fluorescent cell versus time graph.

The last image captured after 3 hours following the fluorescently labeled P2 perfusion contained 13 fluorescent cells. As the number of fluorescent cells increased from one image to another, fluorescence density of background increased as well due to the continuous fluoresceine-labeled P2 perfusion into the chamber. The ratio of fluorescent to nonfluorescent cells in the images was mainly low, and at the end of the experiment, the fluorescent to nonfluorescent cell ratio was found only 33 % in the last image. Compared to bacterial uptake of fluorescently labeled pVEC and P4 peptides, internalization of fluoresceine-labeled P2 peptide decreased noticeably. The fluorescence intensity of the background increased slowly in time. Therefore, the difference between the integrated density and CTCF values did not increase too much towards the end of the experiment.

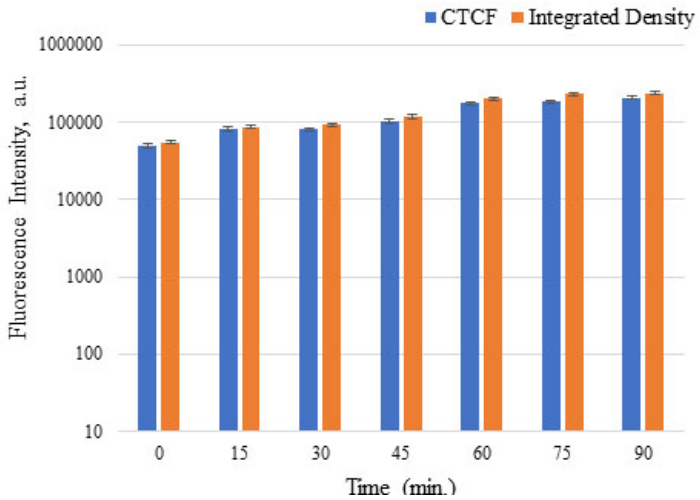

Figure 4.61. Time profile of fluorescence intensity of *E. coli* cells incubated with P2 in rhombic chambers.

The number of fluorescent and nonfluorescent cells in the chamber changed in time. However, the percentage of fluorescent cell increased continuously. The integrated density profile of bacterial cells is consistent with the number of fluorescent cells in the chamber at that moment. The maximum integrated density and CTCF values of mutant cells are 2.3×10^5 and 2×10^5, respectively. These values are very low compared to that found for fluorescent pVEC and P4 peptides. The reason of that may be the type of fluorescent dye used for the labeling of peptide. PVEC and P4 peptides were labelled with HiLyte^{TM} Fluor 488 dye, whereas P2 peptide was labelled

with fluoresceinamine dye. HiLyte^{TM} Fluor 488 conjugates are brighter than fluorescein conjugates, and they emit maximum fluorescence, which may clarify the difference between the fluorescence intensity of bacterial cells when they were subjected to these peptides [73].

4.5.6.2. Bacterial Uptake of Fluorescein-labeled P2 by Mutant Cells. The concentration of fluoresceine-labeled P4 to be tested on mutant bacterial cells was 100 μM. Images from the same spot were captured every 15 minutes during a time interval of 3 hours. The cell density in the chamber increased over time. Bacterial cells are more distinct in bright field images mostly because the depth of the chamber decreased and so the movement of bacterial cells in z direction was restricted. As the cell density increased from one image to another, fluorescence density of background increased as well due to the continuous fluoresceine-labeled P2 perfusion into the chamber. However, bacterial uptake of fluoresceine-labeled P2 peptide did not occurred, so no fluorescent bacterial cell was observed in the chamber.

Table 4.8. Summary of the bacterial uptake of fluorescent peptides.

Chamber	**Peptide**	**Bacterium**	**Fluo. cell ratio**	**Integrated dens. (a.u.)**	**CTCF (a.u.)**	**change (%)**
Reaction (10 μL)	pVEC (100 μM)	*E. coli* K12	55% - 97%	26053	18551	39.2
		Δopp	5% - 53%	14130	11281	
Rhombic (6 μL)	pVEC (50 μM)	*E. coli* K12	10% - 92%	280755	252283	37.98
		Δopp	17% - 72%	179265	156449	
	P4 (50 μM)	*E. coli* K12	6% - 88%	434823	356649	43.5
		Δopp	5% -66 %	243780	201539	
	P2 (50 μM)	*E. coli* K12	6% - 33%	199793	174641	100
		Δopp	-	-	-	

4.5.7. Confirmation of Bacterial Uptake of Fluorescently Labeled pVEC Using Trypsin-EDTA in Zeonor Microchips-Rhombic Chambers of 6 μL Volume

After the bacterial uptake of fluorescently labeled pVEC, fluorescently labeled P4 and fluoresceine-labeled P2 were analyzed, the confirmation of bacterial uptake of fluorescently labeled pVEC was analyzed using trypsin-EDTA following the incubation of bacterial cells with fluorescent peptide in a rhombic chamber of 6 μL volume. To prevent the immense fluorescent background in the chamber, the concentration of the fluorescent peptide decreased to 25 μM to be used in the experiments.

4.5.7.1. Confirmation of Bacterial Uptake of pVEC by *E. coli* K12 Cells. To prevent the increase of the fluorescence intensity of the background before trypsin perfusion into the chamber, the concentration of fluorescently labeled pVEC to be tested on bacterial cells decreased to 25 μM. The experiment was carried out for 4.5 hours.

In the first fluorescent image, 6 fluorescent cells were observed. Over time, the number of fluorescent cells increased in the chamber and the last image captured after 2 hours following pVEC perfusion contained 21 fluorescent cells. After trypsin treatment, the number of fluorescent cells was found 30. The ratio of fluorescent cell in the chamber increased continuously. Fluorescence intensity of these bacterial cells was analyzed via Fiji-ImageJ software to determine whether fluorescence intensity changed after trypsin treatment or not.

To be able to control the increase of the fluorescence intensity of the background, fluorescent peptide was perfused into the chamber at a rate of 0.2 μL/min. Upon fluorescently labeled pVEC perfusion into the chamber, the fluorescence intensity of the background increased slowly. The corrected total cell fluorescence and integrated density values were very close at the beginning, however the difference between them increased slightly over time due to the increase in fluorescence intensity of background. The brightness of fluorescent cells decreased in this experiment.

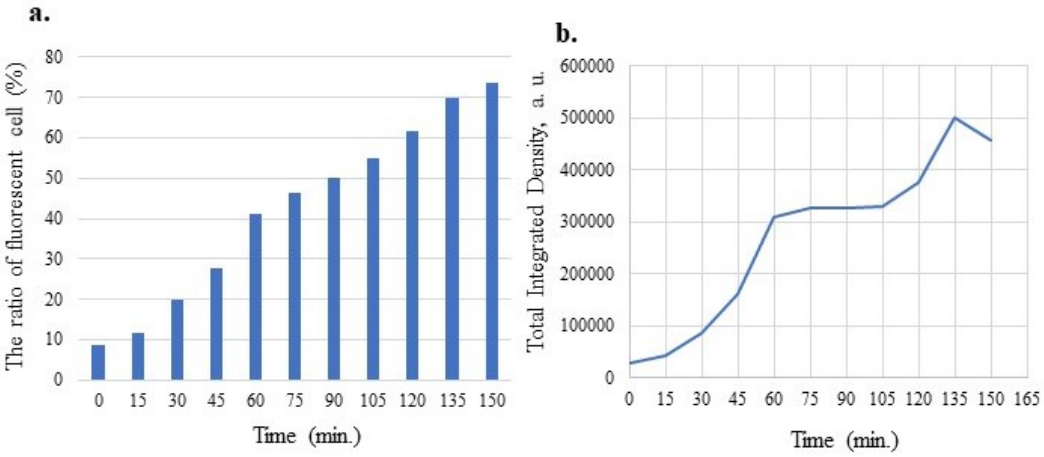

Figure 4.62. a. The ratio of the number of fluorescent cells to the total number of *E. coli* K12 cells incubated with pVEC and trypsin. b. Corrected total cell fluorescence per a fluorescent cell versus time graph.

The reason could be the decrease of the concentration of fluorescent peptide from 50 μM to 25 μM. Trypsin solution was perfused from separate inlet. Even if the trypsin pump was switched off, the trypsin solution may diffuse to the cell-drug solution.

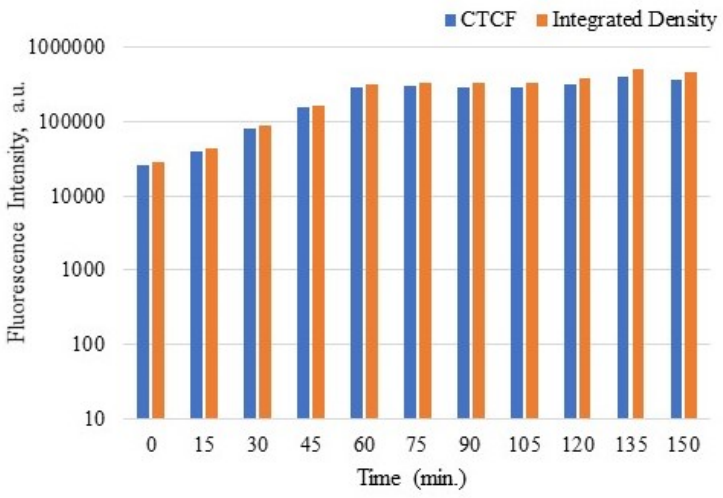

Figure 4.63. Time profile of fluorescence intensity of *E. coli* K12 cells incubated with pVEC and trypsin.

As trypsin damages the peptides in the chamber, the bacterial uptake of fluorescently labeled pVEC may be restricted in the presence of trypsin [74]. In addition, trypsin solution may underlie the decrease of bacterial cell size. The maximum inte-

grated density and CTCF values of wild type cells are $3.3x10^5$ and $3x10^5$ at the end of the peptide perfusion , respectively. These values were found as $4.6x10^5$ and $3.7x10^5$ at the end of the trypsin perfusion, respectively. This increase is consistent with the increase in the number of fluorescent cells. Because the fluorescence intensity of bacterial cells did not change after trypsin treatment, it can be deduced that fluorescently labeled pVEC was internalized by wild type *E. coli* K12 cells rather than stuck on the cellular membrane.

4.5.7.2. Confirmation of Bacterial Uptake of pVEC by Mutant Cells. Mutant cells are smaller and stand upright in the z direction. As a result, being able to separate bacterial cells from impurities of the chamber become difficult. In the first fluorescent image, 6 fluorescent cells were observed. Over time, the number of fluorescent cells increased in the chamber. The last image captured after 3 hours following the fluorescently labeled pVEC perfusion contained 29 fluorescent cells. Total integrated density profile was consistent with the number of fluorescent cells in the chamber. When the fluorescence intensity decreased (75^{th} minutes), the number of fluorescent cells decreased from 28 to 21. Due to the increase in the background fluorescence, the difference between the corrected total cell density and integrated density increased especially towards to end of the experiment as well.

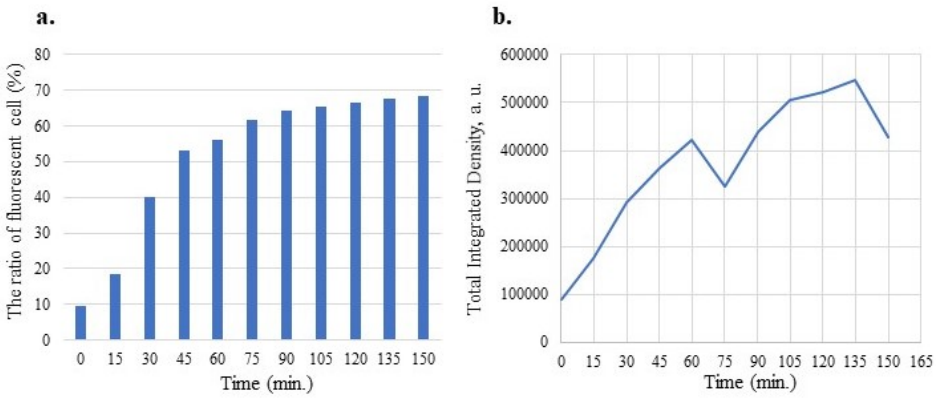

Figure 4.64. a. The ratio of the number of fluorescent cells to the total number of mutant SS5013 cells incubated with pVEC and trypsin. b. Corrected total cell fluorescence per a fluorescent cell versus time graph.

The percentage of fluorescent cell increased continuously. The brightness of mutant cells was also low due to the concentration of of fluorescent peptide. Similar to the case observed in wild type cells, the perfusion of the trypsin solution from the second inlet may lead to the decrease in the fluorescence intensity of the background and also to the decrease of the brightness of the bacterial cells.

The maximum integrated density and CTCF values of mutant cells are $4.3x10^5$ and $4.1x10^5$ at the end of the peptide perfusion, respectively. These values were found $5.5x10^5$ and $4.9x10^5$ at the end of the trypsin perfusion, respectively. This increase is consistent with the the number of fluorescent cells in the images. Because the fluorescence intensity of bacterial cells did not change significantly after trypsin treatment, it can be deduced that fluorescently labeled pVEC was internalized by opp-deleted mutant *E. coli* K12 SS5013 as it was observed in wild type cells.

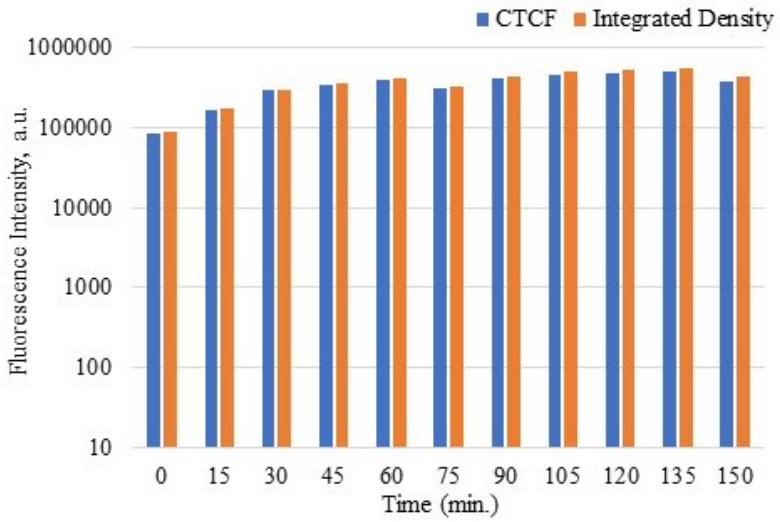

Figure 4.65. Time profile of fluorescence intensity of mutant SS5013 cells incubated with pVEC and trypsin

4.5.8. Confirmation of Bacterial Uptake of Fluorescently Labeled P4 Using Trypsin-EDTA in Zeonor Microchips-Reaction Chambers of 6 μL Volume

After the confirmation of bacterial uptake of fluorescently labeled pVEC was analyzed using trypsin-EDTA following the incubation of bacterial cells with fluorescent peptide in a rhombic chamber of 6 μL volume, the bacterial uptake of fluorescently labeled P4 peptide was investigated as well. To prevent the immense fluorescent background in the chamber, the concentration of the fluorescent peptide decreased to 25 μM to be used in the experiments.

4.5.8.1. Confirmation of Bacterial Uptake of P4 by *E. coli* K12 Cells. As in the case of fluorescently labeled pVEC, to be able to prevent the increase of fluorescence intensity of the background before trypsin perfusion into the chamber, the concentration of fluorescently labeled P4 to be tested on bacterial cells decreased to 25 μM. The experiment was carried out for 4.5 hours.

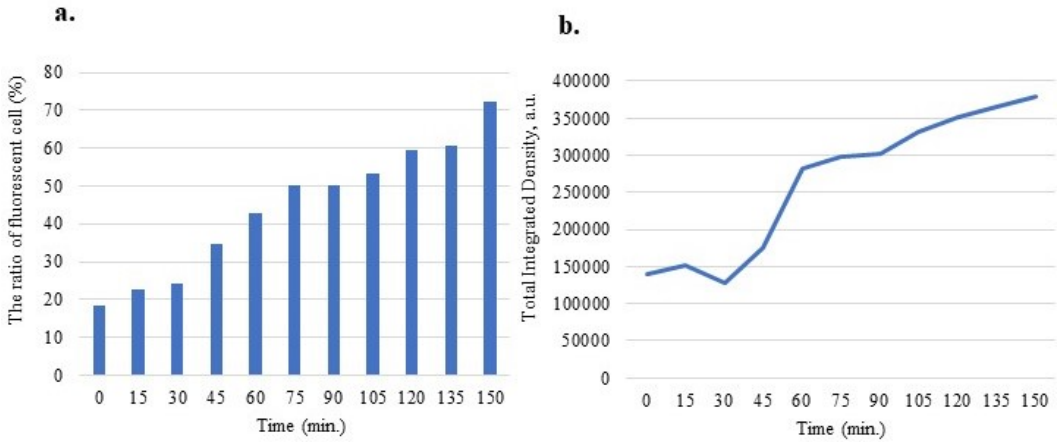

Figure 4.66. a. The ratio of the number of fluorescent cells to the total number of *E. coli* K12 cells incubated with P4 and trypsin. b. Corrected total cell fluorescence per a fluorescent cell versus time graph.

6 fluorescent cells were observed in the first fluorescent image. Over time, the number of fluorescent cells increased in the chamber. The last image captured after

2 hours following the fluorescently labeled P4 perfusion contained 17 fluorescent cells. Although the number of fluorescent cells increased from one image to another, fluorescence density of background did not change significantly. The ratio of fluorescent cell in the chamber increased continuously.

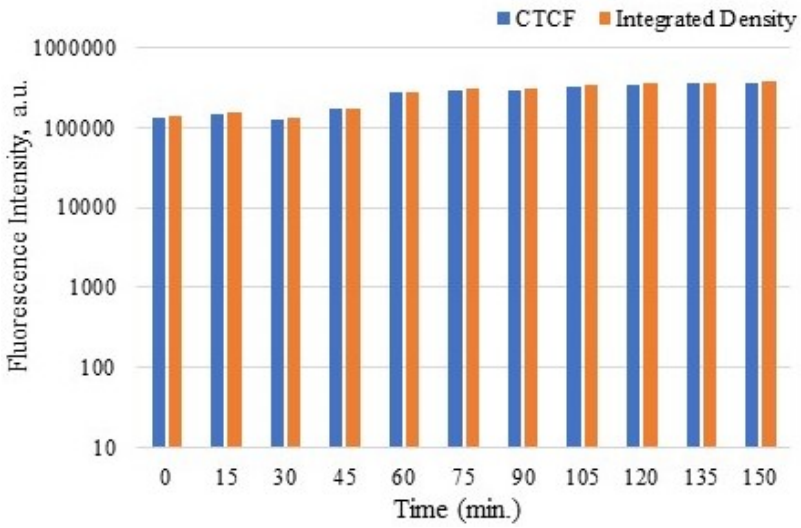

Figure 4.67. Time profile of fluorescence intensity of *E. coli* K12 cells incubated with P4 and trypsin

Total integrated density profile was consistent with the number of fluorescent cells in the chamber again. Upon fluorescently labeled P4 perfusion into the chamber, the fluorescence intensity of the background did not change interestingly and so the the corrected total cell density and integrated density values were very close to each other. The brightness of wild type cells incubated with P4 peptide was also low due to the concentration of fluorescent peptide.

Bacterial uptake of fluorescently labeled P4 peptide is lower than the uptake of fluorescently labeled pVEC. In addition to the low capability of the internalization of P4 peptide, trypsin perfusion may decrease the uptake of this peptide by bacterial cells and could be the reason of the low fluorescence intensity of the background. Fluorescently labeled P4 peptide is disposed to precipitate like pVEC peptide [75]. For this reason, some peptide residuals were noticed in the chamber during the image capturing. The maximum integrated density and CTCF values of wild type cells are $3x10^5$ and $2.8x10^5$

at the end of the peptide perfusion, respectively. These values were found $3.8x10^5$ and $3.6x10^5$ at the end of the trypsin perfusion, respectively. This increase is consistent with the number of fluorescent cells in the images. Because the fluorescence intensity of bacterial cells did not change significantly after trypsin treatment, it can be deduced that fluorescently labeled P4 was internalized by wild type *E. coli* K12 cells.

4.5.8.2. Confirmation of Bacterial Uptake of P4 by Mutant *E. coli* Cells. The concentration of fluorescently labeled P4 to be tested on mutant bacterial cells was also determined as 25 μM. Cell density in the chamber increased over time. In the first fluorescent image, 5 fluorescent cells were observed. Over time, the number of fluorescent cells increased in the chamber. The last image captured after 2 hours following the fluorescently labeled P4 perfusion contained 17 fluorescent cells. Although the number of fluorescent cells increased from one image to another, fluorescence density of background did not change significantly. The ratio of fluorescent cell in the chamber increased continuously.

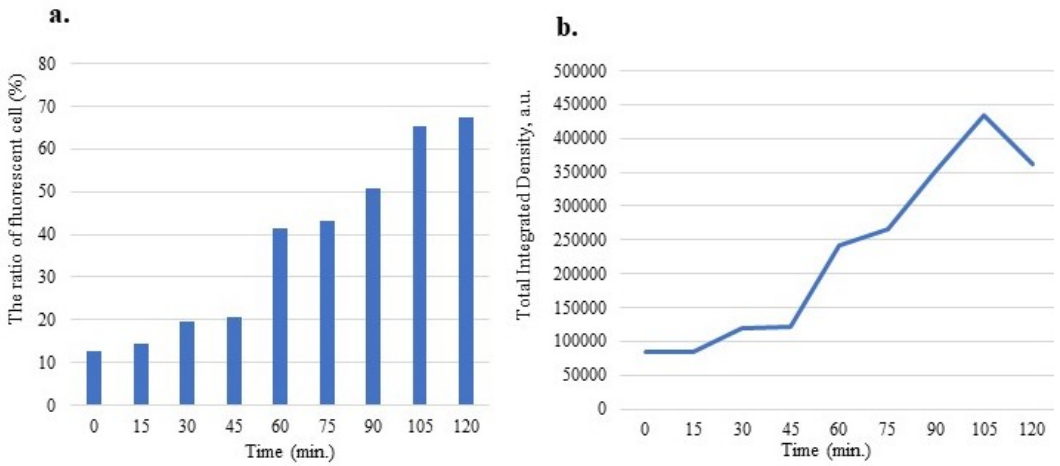

Figure 4.68. a. The ratio of the number of fluorescent cells to the total number of mutant SS5013 cells incubated with P4 and trypsin. b. Corrected total cell fluorescence per a fluorescent cell versus time graph.

Total integrated density profile was consistent with the number of fluorescent cells in the chamber. Upon fluorescently labeled P4 perfusion into the chamber, the fluorescence intensity of the background increased a little and the difference between

the corrected total cell density and integrated density values increased very slightly towards the end of the experiment. The brightness of mutant cells incubated with fluorescent P4 peptide was also low due to the concentration of fluorescent peptide and the presence of trypsin-EDTA solution. The maximum integrated density and CTCF values of mutant cells are 2.4×10^5 and 2.1×10^5 at the end of the peptide perfusion, respectively.

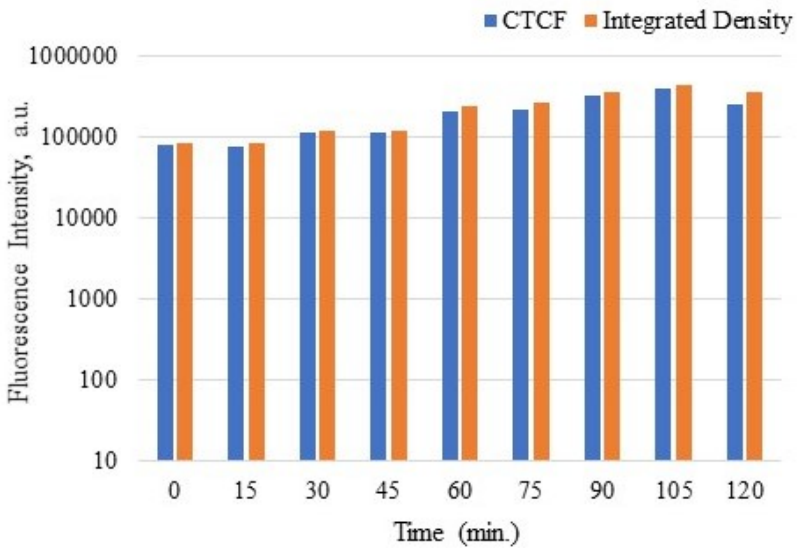

Figure 4.69. Time profile of fluorescence intensity of mutant SS5013 cells incubated with P4 and trypsin

These values were found 4.3×10^5 and 3.9×10^5 at the end of the trypsin perfusion, respectively. This increase is consistent with the number of the fluorescent cells in the images. Because the fluorescence intensity of bacterial cells did not change significantly after trypsin treatment, it can be deduced that fluorescently labeled P4 was internalized by opp-deleted mutant *E. coli* K12 SS5013 cells. Summary of the validation of pVEC and P4 uptake by bacterial cells was given in Table 4.9.

4.5.9. Monitoring of Motility of *E. coli* K12 Cells in Zeonor Microchips-Reaction Chambers of 10 μL Volume

Microscopy images of wild-type *E. coli* K12 and flagella-deleted mutant *E. coli* HCB137 cells taken 5 min. intervals were given in Figure 4.70. As illustrated in Figure

Table 4.9. Summary of validation of bacterial uptake of fluorescent peptides.

Chamber	Peptide	Bacterium	Fluo. cell ratio	$\log_2$ (int. dens.), (a.u.)		CTCF (a.u.)		change (%)
				before tryp.	after tryp.	before tryp.	after tryp.	
Rhombic (6 μL)	pVEC	*E. coli* K12	0% - 86%	14	14.16	13.91	13.85	0.43
		ΔOpp	0% - 68%	13.88	13.79	13.90	13.75	1.08
	P4	*E. coli* K12	0% - 80%	14.20	14.14	14.15	14.09	0.42
		ΔOpp	0% - 67%	14.06	13.61	13.99	13.54	3.22

4.70, the wild-type *E. coli* K12 cells are in constant motion. Due to their fast motion, it is almost impossible to trace a single cell from one panel to the next at 5 min intervals as they move and divide. The same cell can be traced if images are captured at short time periods. On the other hand, the non-motile *E. coli* cells do not display any measurable movement during the same time frame (Figure 4.70). Selected cells were marked with unique geometrical shapes in consecutive snapshots to follow them. The only indication that non-motile cells are still viable is the evidence for their division. This stark and easily identifiable difference in cell location between motile and non-motile cells as a function of time coupled with the ability to co-verify cell viability makes this lab-on-a chip technique a much more versatile and robust approach for monitoring flagellar motility.

Swimming speed of the cells was calculated taking time-lapse images in the chambers of 2800 μm width and 500 μm depth. Since the depth of these commercially available smallest microchips is far larger than the diameter of the bacterial cells, bacterial movement was not one-dimensional. As the camera was focused on a single cell, this cell would sometime pass to anther z stage and get out of focus. Therefore, swimming speed of the wild-type cells was calculated as 14 ± 6 μm/s, taking the average from different time-lapse images of different periods. This value is pretty close to values reported in other studies [44, 76]. Since the non-motile cells were not moving, their swimming speed rate was not calculated.

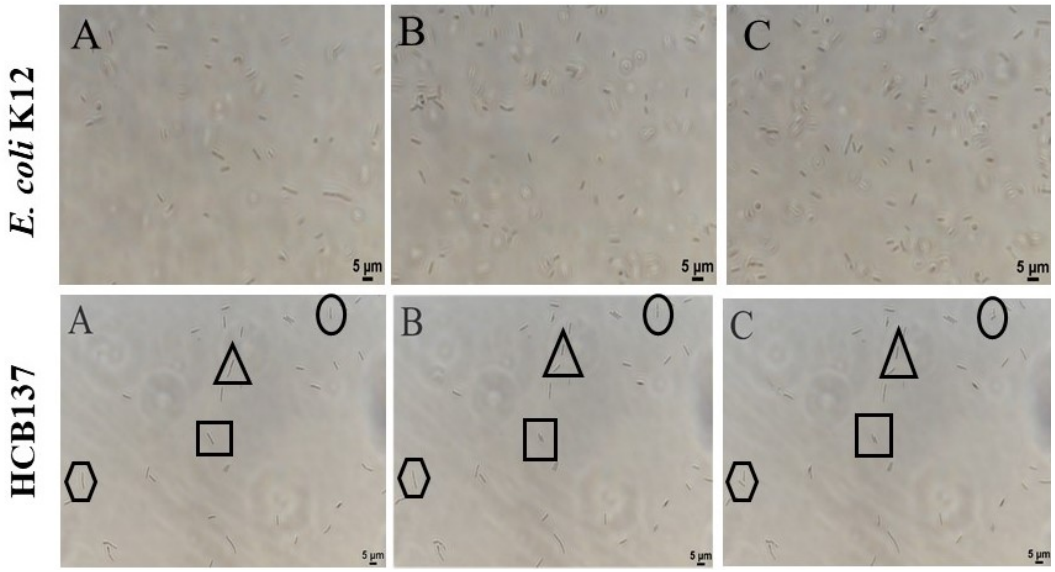

Figure 4.70. Microscopy images of *E. coli* K12 and mutant HCB137 cells grown in LB media in the chamber captured at 60x zoom and 5-minute intervals.

Then microscopy images were processed via ImageJ to determine cell count, cell area, cell perimeter, and longitudinal axis length of the bacterial cells in the chamber. As previously mentioned, wild type cells were moving very fast, continuously entering and leaving a given area. Dynamic analysis of quantitative values required tracing of a single cell in time but unfortunately most cells were blurred in the images due to their fast displacement. On the other hand, it was possible to select and trace the movement of a single non-motile cell during the same time period. An example of the measurements taken for a non-motile cell is presented in Table 4.10. Gradually each parent cell grows until it is cleaved into two daughter cells. Until division, cell area, cell perimeter and longitudinal axis length increase, which reflect growth. As expected, these three parameters are smaller for the obtained daughter cells. From this dynamics, the doubling time (t_d) was calculated as 20 minutes, which is consistent with the values reported in literature [77]. In general, the measured sizes were consistent with the reported average values for *E. coli* cells [78]. Moreover, they gave a good indication for the dynamics of cells growth and division.

Table 4.10. Dynamic analysis a selected single non-motile cell.

Time (min)	**Cell identitiy**	**Area (μm^2)**	**Perimeter (μm)**	**Length (μm)**
0	Parent cell	1.4	5.65	2.28
5	Parent cell	1.51	6.36	2.51
10	Parent cell	1.74	7	2.82
15	Parent cell	1.85	7.47	3.06
20	Cell division at this time			
25	Daughter cell	1.265	5.21	2
	Daughter cell	0.88	3.73	1.2

4.5.10. Monitoring of Motility of *B. subtilis* 168 Cells in Zeonor Microchips-Reaction Chambers of 10 μL Volume

Before monitoring of the flagellar motility of *bacillus* cells in reaction chambers, growth of these cells was analyzed in LB media. When cell solution was perfused into the chamber, sessile chains were observed and sessile chain ratio decreased while the ratio pf motile cells increased over time. Wild type *B. subtilis* 168 cells are quite motile, whereas sessile chains were not motile. As a result, this microfluidic chip platform provides a continuous and controlled flow system for the bacterial cells. In addition, the proposed system enables live imaging, it may also be extended to capture the dynamic and micro-scale imaging on a single cell level in controlled microbial environments. Afterwards, the flagellar motility of bacillus cells was analyzed and effects of amiloride and high Na^+ concnetration on *bacillus* cells were monitored in microdevices-reaction chambers of 10 μL.

To understand whether amiloride affects motility of *B. subtilis* 168 cells, the bacterial cells were grown until 7^{th} hour (mid log phase) following the inoculation and then the chip setup was established. At the beginning, the bacterial cells were monitored without amiloride treatment and the time-lapse images were captured to calculate the swimming rate of the bacterial cells.

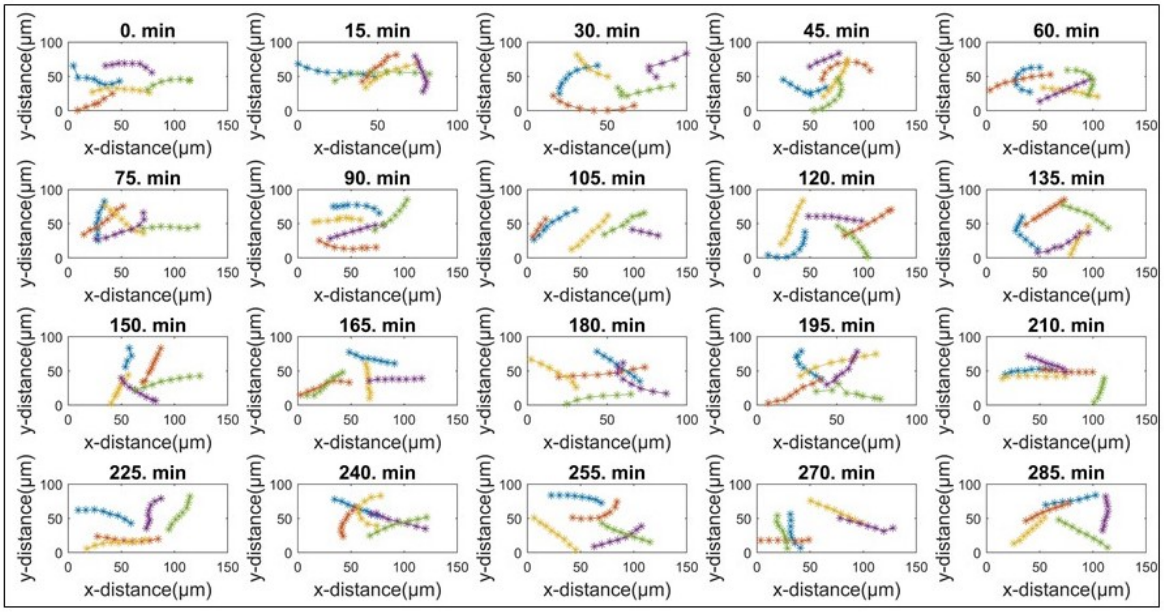

Figure 4.71. Trajectories of *B. subtilis* 168 cells grown in LB media in the chamber obtained from the analysis of time-lapse images captured every 15 minutes.

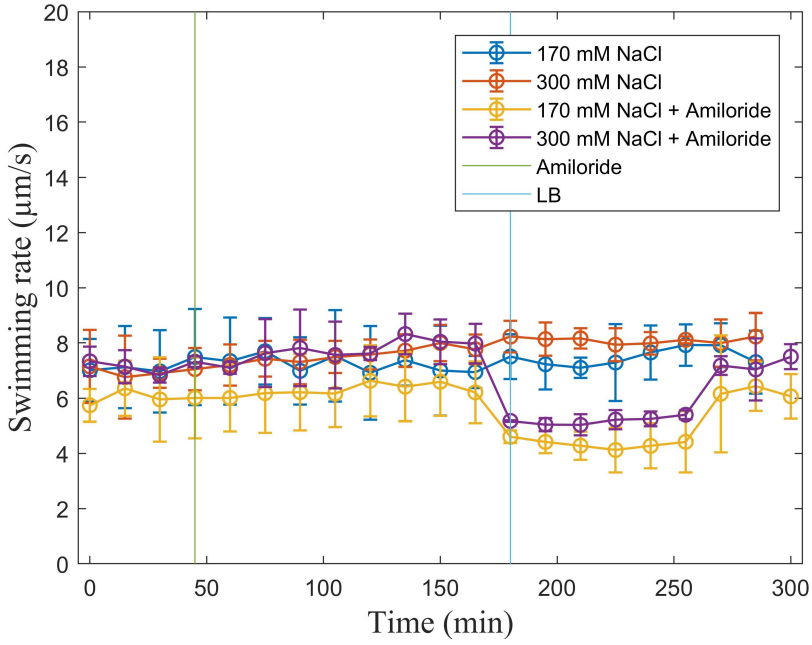

Figure 4.72. Swimming rate vs time graph of *B. subtilis* 168 cells analyzed in four different conditions. The data represent the average of n=3 replicate experiments. Mean values and error bars are shown.

Table 4.11. Summary of the swimming rate values of *B. subtilis* 168 cells incubated in LB and supplemented with amiloride.

Bacteria	**Na^+ concentration**	**Drug**	**Swimming rate (μm/s)**			**Change (%)**
			During LB perfusion	**Before Amiloride perfusion**	**After Amiloride perfusion**	
B. subtilis 168	170 mM	-	7.31			4.79
	300 mM	-	7.66			
	170 mM	Amiloride (1 mM)		6.21	4.35	29.95
	300 mM	Amiloride (1 mM)		7.56	5.18	31.48

Then, amiloride was perfused into the chamber after cell perfusion and the motility of bacterial cells were monitored in the presence of amiloride. To analyze whether the addition of Na^+ into the medium increases the MotPS-based motility which affects the overall motility, *B. subtilis* 168 cells were grown in LB medium containing 300 mM NaCl. Nikon inverted microscope was used to visualize cells in the chamber at room temperature continuously. Sessile chain ratio was low at the beginning, but it increases towards the end of the experiment. 8 second-time-lapse images of *B. subtilis* 168 cells grown in LB media captured every 15 minutes at 1 second intervals during the experiment were analyzed via Fiji-ImageJ software. The positions of *B. subtilis* 168 cells grown in LB media in x-direction and y-direction in time-lapse images were determined and collected in an excel file. Since the time-lapse images were captured at 1 second intervals, the total path of the cell was divided by elapsed time (7 seconds) to calculate the swimming rate of the bacterial cells.

The path of 5 cells in every image were recorded and then displayed in Figure 4.71. Swimming rate vs time profile of *B. subtilis* 168 cells was given in Figure 4.72. Mean values and error bars belongs to three experiments. Average swimming rate of the five bacterial cells were given in Table 4.11. When the Na^+ concentration increased,

a little increase in the swimming rate of *B. subtilis* 168 cells was observed. When amiloride was perfused into the chamber, swimming rate of these cells decreased by approximately 30 %.

4.5.11. Monitoring of Motility of *B. subtilis* 3610, DS222 and DS223 Cells in Zeonor Microchips - Reaction Chambers of 10 μL

After the motility of *B. subtilis* 168 cells was tested in zeonor microchips, the motilities of *B. subtilis* 3610 (an undomesticated derivative of *B. subtilis* 168 strain), DS222 (*B. subtilis* 3610 with a deletion of MotAB gene), and DS223 (*B. subtilis* 3610 with a deletion of MotPS gene) in the presence of amiloride drug were also investigated in these microdevices to observe the effects of amiloride on MotPS stator directly.

To understand whether amiloride affects the motility of undomesticated *B. subtilis* 3610 cells, these bacterial cells were grown until mid-log phase following their inoculation and then, they were treated with amiloride and the change in motility was monitored in zeonor microchips. Sessile chain ratio of undomesticated *bacillus* cells was lower than that of laboratory strain. The averages of the swimming rates of five cells at every image (15-minute intervals) were taken and the average swimming rate values of two experiments were shown in Figure 4.73. Mean values and error bars belong to two experiments.

Amiloride perfusion was started at 30th minutes of the incubation of bacterial cells in the chamber. However, the swimming rate of the bacterial cells began to decrease at nearly 120^{th} minutes of the incubation. This time delay (80-90 minutes) results from the arrival of drug amiloride from the tubings to the chamber. Moreover, a specific time is necessary for the interaction of the drug with the bacterial cells. When we take into these two factors, the observation of this time delay is inevitable. Mean swimming rate values of the bacterial cells at 15 minute-intervals varied between 7.5 μm/s and 8 μm/s until their interaction with the drug. After the interaction of *B. subtilis* 3610 cells with amiloride, the swimming rate values decreased slightly and

varied between 6.4 μm/s and 7.2 μm/s. The drop resulting from amiloride interaction is apparent on the graph.

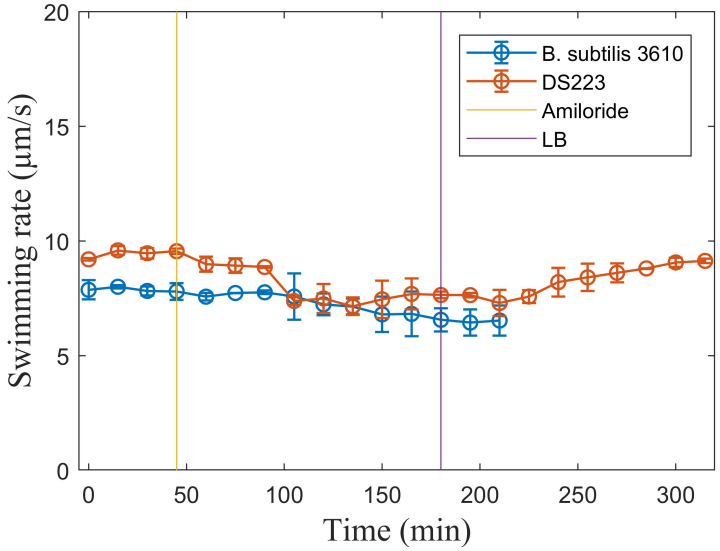

Figure 4.73. Swimming rate vs time graph of *B. subtilis* 3610 and DS223 cells grown in LB media and treated with amiloride. The data represents the average of n=2 replicate experiments. Mean values and error bars are shown.

To investigate the effects of amiloride on MotPS-dependent swimming rate, DS222 (*B. subtilis* 3610 with a deletion of MotAB gene) strain was grown until mid-log phase and monitored in zeonor microchips. The position of four bacterial cells did not change throughout time-lapse image capturing interval. DS222 cells lack MotAB gene, and that is the reason of becoming nonmotile in the chamber. It was expected that DS222 cells have swimming motility because they have MotPS gene [79]. However, these bacterial cells were monitored for approximately three hours in the microchip and the movement of bacterial cells was only observed because of the movement of the medium in the chamber. This result again showed that MotAB is dominant in the motility of bacterial cells. Experiments were repeated for 2 times and these bacterial cells were nonmotile in the chamber and so amiloride treatment was not performed.

Afterwards, Na^+ concentration of the medium was increased to investigate whether high Na^+ concentration stimulates MotPS-based motility, and DS222 cells become

motile even a little or not. DS222 cells were grown in LB media supplemented with 300 mM NaCl until mid-log phase. After that, they were perfused into the chamber and monitored continuously. Although the Na^+ concentration in the medium was increased, DS222 cells were still nonmotile. The positions of four DS222 cells were the same throughout the time-lapse image capturing interval. Since DS222 cells have only MotPS gene, they were to become motile due to the high Na^+ concentration. However, they were nonmotile in the chamber again. It can be said that MotAB gene is dominant in the motility of undomesticated *B. subtilis* 3610 cells and they become nonmotile when this gene was deleted.

To investigate the effects of amiloride on MotAB-dependent swimming rate, DS223 (*B. subtilis* 3610 with a deletion of MotPS gene) strain was grown until mid-log phase and then, they were treated with amiloride and the change in motility was monitored in zeonor microdevices. Morphology of *B. subtilis* 3610 and mutant cells is highly similar. Sessile chain ratio was lower than that observed in laboratory strain.

Amiloride perfusion was started at 30^{th} minutes of the incubation of DS223 cells in the chamber. Swimming rate of bacterial cells began to decrease at nearly 120^{th} minutes of the incubation. If the arrival time of the drug into the chamber is taken into consideration, approximately 30-45 minutes is necessary for the accession of the drug into the inlet of the microchip. In addition, a particular time is necessary after the drug solution reached to the inlet in order to observe the effects of amiloride on the bacterial cells. For this reason, this time delay between the amiloride perfusion point and the drop point of the swimming rate was expected. Mean swimming rate values of the bacterial cells at 15 minute-intervals varied between 8.86 μm/s and 9.58 μm/s until drug interaction. After amiloride interaction with DS223 cells, the swimming rate values decreased slightly and varied between 7.15 μm/s and 7.68 μm/s. After 2.5 hour interval of drug perfusion, fresh LB pump was switched on. After 60 minutes interval of fresh LB medium perfusion, the swimming rate values began to increase and varied between 8.20 μm/s and 9.12 μm/s. The drop point resulting from amiloride interaction and the rise point due to the fresh LB perfusion are apparent on the graph.

Table 4.12. Summary of the swimming rate values of *B. subtilis* 3610, DS222 and DS223 cells incubated in LB and supplemented with amiloride

Bacteria	**Na^+ concentration**	**Drug**	**Swimming rate (μm/s)**			**Change (%)**
			During LB perfusion	**Before Amiloride perfusion**	**After Amiloride perfusion**	
B. subtilis 3610	170 mM	Amiloride (1 mM)	-	7.59	6.63	17.13
DS222	170 mM	-	Nonmotile			
	300 mM	-	Nonmotile			
DS223	170 mM	Amiloride (1 mM)	-	8.86	7.55	14.78

Average swimming rate values of the bacterial cells were given in Table 4.12. When amiloride was perfused into the chamber, swimming rate of *bacillus* 3610 cells decreased 17 %, implying that Na^+-dependent motility was decreased in the presence of amiloride. DS222 cells were nonmotile and even Na^+ concentration of the medium increased, they were nonmotile. When amiloride was perfused into the chamber, swimming rate of DS223 cells decreased 14 %, implying that Na^+-dependent motility was decreased slightly in the presence of amiloride. Swimming rate of DS223 cells were higher than that of wild type cells.

4.5.12. Monitoring of Motility of *B. marmarensis* Cells in Zeonor Microchips - Reaction Chambers of 10 μL

To understand whether amiloride affects motility of *B. marmarensis* strain, the bacterial cells were grown until mid-exponential phase following inoculation and then they were treated with amiloride and the change in motility was monitored in zeonor microchips. Afterwards, the effect of high NaCl concentration on the motility of *B. marmarensis* strain was analyzed. The standard NB medium (8 g/L NB, pH adjusted to 9.7 using 0.1 M Na_2CO_3 and 0.1 M Na_2HCO_3) contain 103 mM NaCl.

NaCl concentration in standard NB media was increased to 120 mM by adding extra NaCl to the media. *B. marmarensis* cells were incubated in this NB media supplemented by 120 mM NaCl. Similarly, the motility of *B. marmarensis* strain was first monitored in the absence of amiloride in the microfluidic reaction chambers. Thereafter, *B. marmarensis* cells incubated in zeonor microchips were treated with amiloride drug and the alterations in motility was monitored in these reaction chambers of 10 μL volume.

Because *B. marmarensis* cells are motile, it is impossible to monitor the same cell throughout 8-second time interval during the time-lapse image capture. We focused only a spot in the reaction chamber while capturing the images, and the bacterial cells enter and exit from this spot continuously. Therefore, the trajectories of the bacterial cells at 15-minute intervals are different from each other. Using a matlab code, the swimming rates of *B. marmarensis* cells were calculated from the time-lapse images. Fluctuations can be observed in the swimming rate values of the 5 bacterial cells.

Taking the average of the swimming rates of five cells, the mean values were obtained. Swimming rate vs time graphs were obtained from the swimming rates of selected five *B. marmarensis* cells in each image, so the mean values and errorbars represent the divergence of the swimming rates of these selected cells (Figure 4.74). As it can be understood from Figure 4.74, there is a little fluctuation between the swimming rate values varying between 4 μm/s and 5.2 μm/s, that are presented with the errorbars. Motility experiments were performed twice for the validation of the results. After that, the average of the swimming rates of five cells were taken at intervals of 15 minutes and the results of two experiments were shown in Table 4.13.

Because we focused only a small area in a reaction chamber, some of the bacterial cells can not be tracked throughout 8 seconds. For example, a bacterium can enter the focused area at the third second of the time-lapse imaging process and can be followed throughout the last five seconds. While calculating the swimming rate, the distance moved along the reaction chamber by bacterial cells and the elapsed time were taken

into account. Therefore, the swimming rates of five cells differ from each other and this divergence leads fluctuations and also large errorbars.

When the average of the swimming rates of *B. marmarensis* cells was taken, it was observed that the mean swimming rate values obtained from the five *B. marmarensis* cells incubated in standard NB medium within a zeonor microchip vary between 4.2 μm/s and 4.9 μm/s. The maximum swimming rate value was 4.7 μm/s in the first experiment. This value increased to 5.2 μm/s in the second motility analysis. Because the tracing time of bacterial cells in the reaction chambers may be different from each other as mentioned before, this increase in swimming rate may be ignored. The ratio of bacterial cells whose swimming rate values reached to 5 μm/s are low. Therefore, the swimming rates of *B. marmarensis* cells calculated in the first motility experiments were consistent with those obtained in the second motility analysis. Mean values and errorbars belong to two motility analyses. Errorbars become shorter when the mean values of the swimming rates were taken. As a result, the mean swimming rate values of the bacterial cells change between 4.2 μm/s and 4.9 μm/s when they were incubated in standard NB medium containing 103 mM NaCl.

A study was conducted by Sugiyama *et al.* (1988) based on the inhibition of the motility of alkalophilic *Bacillus* strain by using amiloride. A concentration of 0.5 mM amiloride was found to be sufficient to completely inhibit motility of alkaliphilic Bacillus cells in that study [60]. Taking this result and our MIC analysis as a starting point, we investigated the effect of amiloride on the motility of *B. marmarensis* cells (alkaliphilic). After the motility of *B. marmarensis* cells was analyzed in standard NB medium using the microfluidic technology, amiloride treatment was applied to observe whether amiloride inhibits motility of *B. marmarensis* cells or not.

Amiloride, a potent inhibitor of Na^+ channels of various organisms, inhibits the motors by competing with Na^+ at the Na^+-interacting site located on the external side of the force-generating unit [80–82]. Time-lapse images obtained from the first motility analysis in the reaction chambers were analyzed via Fiji-ImageJ and the average

swimming rates of *B. marmarensis* cells incubated in NB medium, and then treated with amiloride were presented in Table 4.13. After the bacterial cell and NB perfusion into the reaction chamber were completed, amiloride was perfused into the chamber at a rate of 0.5 μL/min for 2 hours. If the diameters and lengths of the tubings and accuracy of the syringe pumps were taken into account, the solutions in the tubings should arrive to the reaction chamber approximately in 60 minutes. After amiloride perfusion was switched on, the motility of the bacterial cells began to decrease nearly in 75 minutes. As a result, the motility decreased when bacterial cells were incubated in the reaction chamber with amiloride at time intervals of 15-30 minutes. Taking the average of the swimming rates of five cells, the mean swimming rate values of the five *B. marmarensis* cells obtained from the time-lapse images captured at 15 minute-intervals vary between 4.5 μm/s and 4.9 μm/s before the amiloride perfusion. After 75 minute-interval of amiloride perfusion into the reaction chamber, the motility of *B. marmarensis* cells began to decrease. The swimming rate of the bacterial cells was found to be between the 0.5 μm/s and 0.8 μm/s, which may be the result of amiloride perfusion into the chamber continuously. After the time interval of 2 hours, the amiloride pump was switched off and NB medium pump was switched on to be able to observe whether the motility increases with fresh NB medium or not. NB medium was perfused at a rate of 0.5 μL/min for 2 hours.

Creeping flow dominates in microdevices and bacterial cells move within the reaction chambers. *B. marmarensis* cells affected by amiloride at the inlet of the chamber can enter the focused area, from which the time-lapse images were taken or exit from this area easily. As a consequence of that, fluctuations occur as the motility of these cells decreases. Amiloride treatment decreased the motility of bacterial cells and the swimming rate was found to be between the 0.4 μm/s and 0.6 μm/s. After the time interval of 2 hours, the amiloride pump was switched off and NB medium pump was switched on again. Approximately 75 minutes later, the motility of the bacterial cells began to increase. Taking the average values, the mean swimming rates of *B. marmarensis* cells grown in standard NB medium and then treated with amiloride were presented in Table 4.13.

Swimming rates of *B. marmarensis* cells grown in standard NB medium, and treated with amiloride were plotted versus time and displayed in Figure 4.74. The mean swimming rate values of *B. marmarensis* cells before amiloride perfusion change between 4.7 μm/s and 4.8 μm/s when they were incubated in standard NB medium containing 103 mM NaCl. After amiloride perfusion of 75 minutes, the swimming rates of bacterial cells decreased to 0.4-0.6 μm/s. Upon NB media perfusion of 75 minutes, the motility of *B. marmarensis* cells increased and swimming rates were changed between 4.6 μm/s and 5.1 μm/s.

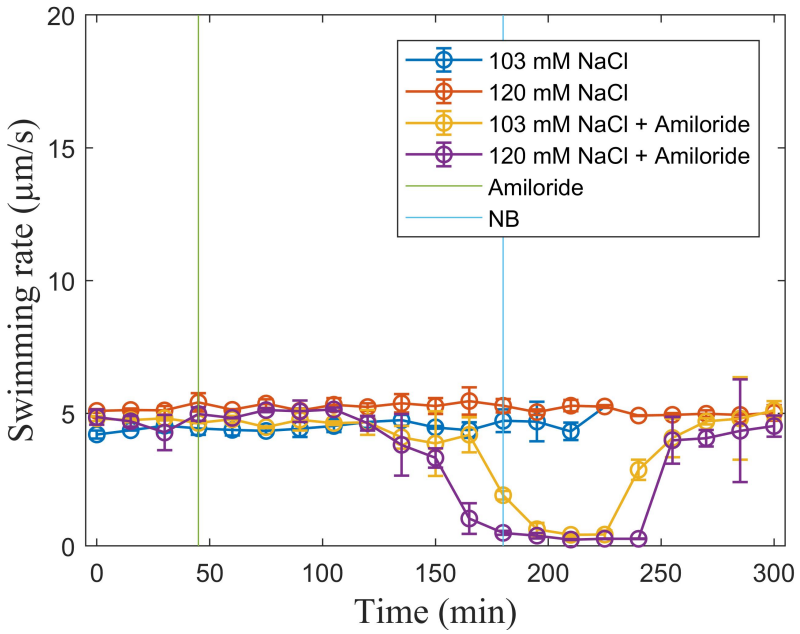

Figure 4.74. Swimming rate vs time graph of *B. marmarensis sp. nov.* cells grown in NB media and treated with amiloride. The data represents the average of n=2 replicate experiments. Mean values and error bars are shown.

To analyze whether Na^+ concentration affects the motility of *B. marmarensis* cells, bacterial cells were grown in NB media supplemented by 120 mM NaCl. Swimming rates of *B. marmarensis* cells incubated in NB media supplemented by 120 mM NaCl were calculated. Taking the average values, mean swimming rate values of selected five *B. marmarensis* cells were obtained. Compared to swimming rates of *B. marmarensis* cells incubated in standard NB media, swimming rates of *B. marmarensis* cells increased when they were incubated in NB media containing higher concentra-

tions of NaCl as it can be understood from the swimming rate vs time graph. As a result, the existence of high amount of NaCl in the medium increases MotPS-dependent motility of alkaliphilic *B. marmarensis* cells [63, 81]. The mean swimming rate values of *B. marmarensis* cells change between approximately 4.9 μm/s and 5.5 μm/s given in Table 4.13. Swimming rate of *B. marmarensis* cells increased when they were grown in NB media supplemented by 120 mM NaCl.

To analyze the effects of both high Na^+ concentration and amiloride on the motility of *B. marmarensis* cells, bacterial cells were first grown in NB media supplemented by 120 mM NaCl, and then treated with amiloride. Before amiloride perfusion, the mean swimming rate values of the selected five *B. marmarensis* cells obtained from the time-lapse images captured at 15 minute-intervals varies between 4.6 μm/s and 5.3 μm/s in the first motility assay. After 75 minute-interval of amiloride perfusion into reaction chamber, the motility of *B. marmarensis* cells began to decrease. When amiloride was completely ceased the motility, swimming rate of bacterial cells was found between the 0.2 μm/s and 0.5 μm/s, which may be the result of amiloride perfusion into the chamber continuously. After the time interval of 2 hours, the amiloride pump was switched off and NB pump was switched on. NB media was perfused at a rate of 0.5 μL/min for 2 hours. Approximately 75 minutes later, motility of *B. marmarensis* cells began to increase and the swimming rate values were changed between 4.2 μm/s and 4.8 μm/s. This result confirms that *B. marmarensis* cells belonging to alkaliphilic bacillus have MotPS-dependent motility, affected by Na^+ concentration and amiloride directly [83, 84].

Compared to the decrease in the swimming rates of *B. marmarensis* cells grown in standard NB medium, the swimming rate values of *B. marmarensis* cells grown in NB (120 mM NaCl) decreased further when they were treated with amiloride. Moreover, NB perfusion after amiloride treatment increased the swimming rates of *B. marmarensis* cells but the swimming rate values of *B. marmarensis* cells did not reach to old values at the end of the experiment. However, the swimming rates can reach to those calculated before amiloride perfusion if the duration of the experiments is extended.

Table 4.13. Summary of the swimming rate values of *B. marmarensis sp. nov.* cells incubated in LB and supplemented with amiloride

Chamber	**Bacterium**	**Na^+ concentration**	**Drug**	**Swimming rate (μm/s)**			**Change (%)**
				During LB perfusion	**Before Amiloride perfusion**	**After Amiloride perfusion**	
Reaction (10 μL)	*B. marmarensis sp. nov.*	103 mM	-	4.55	-	-	**13.63**
		120 mM	-	5.17	-	-	
		103 mM	Amiloride (1 mM)	-	4.33	0.49	**88.68**
		120 mM	Amiloride (1 mM)	-	4.84	0.45	**90.7**

4.6. Bacterial Uptake of Fluorescent Peptides Using Confocal Microscopy

Since the uptake of fluorescent peptides by bacterial cells was not clear in fluorescence microscopy images, bacterial cells were anlyzed under confocal microscopy to observe the location of fluorescently labeled pVEC, fluorescently labeled P4 and fluorescein-labeled P2 peptides in both wild type *E. coli* K12 and opp-deleted mutant *E. coli* K12 SS5013 cells.

4.6.1. Bacterial Uptake of Fluorescently Labeled pVEC by *E. coli* K12 and Opp-deleted Mutant *E. coli* K12 SS5013 Cells

Fluorescently labeled cell-penetrating peptide, pVEC (H-LLIILRRRIRKQAHAH-SKK (HF488)-NH_2), tends to be precipitated, resulting in problems during the centrifugation steps. In the first trial, fluorescent peptide could not be removed from the bacterial cell solution via centrifugation. Therefore, fluorescence background was high in confocal images.

Since fluorescent peptide could not be removed via centrifugation, cell solution was filtered by Ultra-15 Centrifugal Filter Devices (30,000 MWCO) and fluorescent peptide was removed from bacterial cells. FITC, bright field and merged confocal im-

ages of bacterial cells incubated with pVEC peptide were given in Figure 4.75. From confocal images, it was observed that fluorescently labeled pVEC peptide was internalized by both wild type *E. coli* K12 and mutant cells. Because fluorescently labeled pVEC tends to precipitate, bacterial cells in confocal images seem like clusters. Similar observations were found for mutant cells.

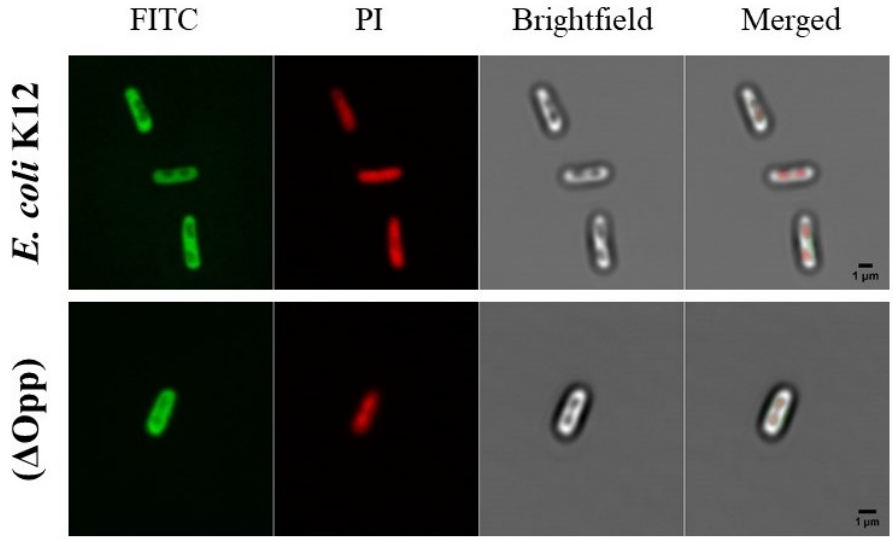

Figure 4.75. Confocal images of the internalization of fluorescently labeled pVEC by wild type *E. coli* K12 and mutant (ΔOpp) cells.

To analyze the fluorescent peptide distribution within the cell, a straight line along horizontally of a bacterium was drawn using Fiji-ImageJ and plot profile of fluorescence intensity was obtained. In addition, fluorescence intensity of bacterial cells were measured via Fiji-ImageJ software. Plot profiles of both wild type *E. coli* K12 and mutant (ΔOpp) cells were given in Figure 4.76.

From plot profiles, it was observed that fluorescence intensity was higher in the middle of the wild type cell; however, the fluorescence intensity was decreased in the middle of mutant cells. It can be deduced that fluorescent pVEC passes through the inner membrane; however, fluorescent pVEC peptide accumulated between inner and outer membrane of mutant cells. The size of mutant cells are smaller than that of wild type cells. Similarly, mutant cells were found as cluster due to the precipitation property of fluorescent peptide. As a result, microchip experiments performed to observe

the internalization of fluorescent peptide were confirmed with the confocal analyses and it was concluded that fluroescently labeled pVEC peptide was internalized by both wild type and mutant cells.

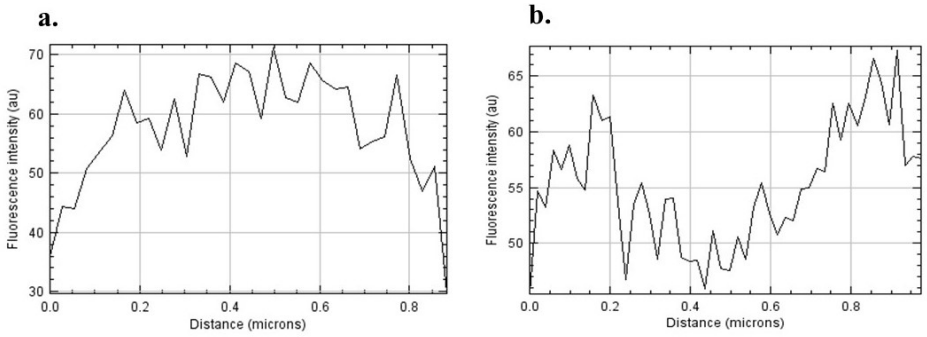

Figure 4.76. a. Plot profile of wild type *E. coli* K12 cells. b. Plot profile of mutant (ΔOpp) cells.

4.6.2. Bacterial Uptake of Fluorescently Labeled P4 by *E. coli* K12 and Opp-deleted Mutant *E. coli* K12 SS5013 Cells

Similarly, the uptake of fluorescently labeled P4 by bacterial cells was not clear in fluorescence microscopy images, bacterial cells were analyzed under confocal microscopy to observe the location of fluorescently labeled P4 peptide in both wild type *E. coli* K12 and opp-deleted mutant *E. coli* K12 SS5013 cells. Fluorescently labeled P4 peptide (H-LLIILRRGHYYK(HF488)-NH_2) also tends to be precipitated, resulting in problems during the centrifugation steps. In the first trial, fluorescent peptide could not be removed from the bacterial cell solution via centrifugation. Therefore, fluorescence background was high in confocal images.

FITC, bright field and merged confocal images of bacterial cells incubated with P4 were given in Figure 4.77. It was observed that fluorescently labeled P4 peptide was internalized by both wild type *E. coli* K12 and mutant cells and it was located between the inner and outer membrane especially. From plot profiles (Figure 4.78), it was observed that fluorescence intensity was higher in the middle of the wild type cell; however, the fluorescence intensity was decreased in the middle of mutant cells.

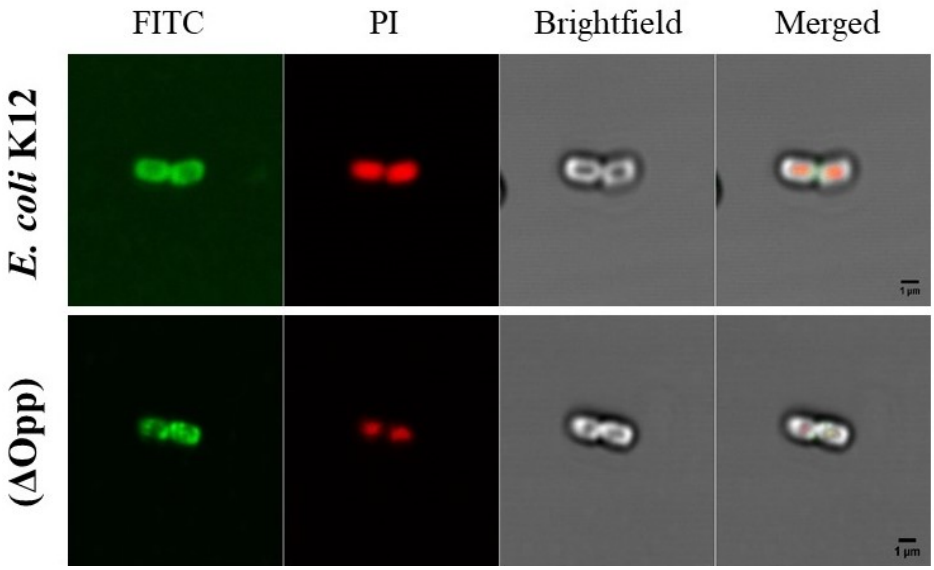

Figure 4.77. Confocal images of the internalization of fluorescently labeled P4 by wild type *E. coli* K12 and mutant (ΔOpp) cells.

Confocal images indicate nearly homogeneous distribution of fluorescent pVEC in wild type bacterial cells. However, peptide residuals were not detected in the middle of the mutant cells. Similarly, fluorescent P4 peptide was observed especially at the poles of the both cells. Plot profiles of both wild type *E. coli* K12 and mutant (ΔOpp) cells were given in Figure 4.78.

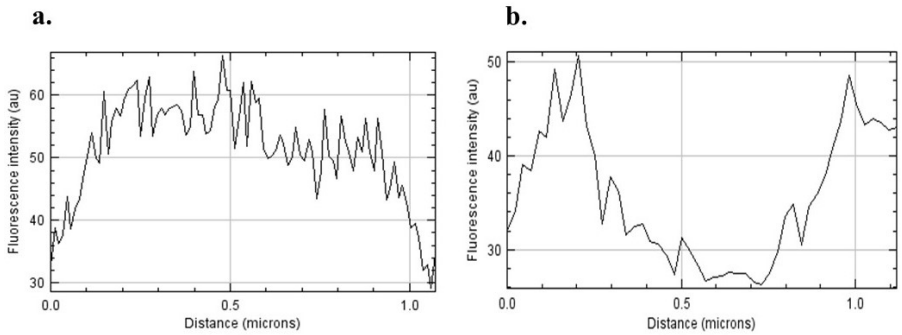

Figure 4.78. a. Plot profile of wild type *E. coli* K12 cells. b. Plot profile of mutant (ΔOpp) cells.

As a result, microchip experiments performed to observe the internalization of fluorescently labeled P4 were confirmed with the confocal analyses and it was concluded that fluroescently labeled P4 peptide was internalized by both wild type and mutant

cells. FITC, bright field and merged confocal images of bacterial cells were given.

4.6.3. Bacterial Uptake of Fluoresceine-labeled P2 by *E. coli* K12 and Opp-deleted Mutant *E. coli* K12 SS5013 Cells

In addition that the uptake of fluoresceine-labeled P2 by bacterial cells was not clear in fluorescence microscopy images, fluorescence intensity of P2 peptide was low compared to that of other peptides. Therefore, bacterial cells were anlyzed under confocal microscopy to observe the location of fluoresceine-labeled P2 peptide in both wild type *E. coli* K12 and opp-deleted mutant *E. coli* K12 SS5013 cells. Fluorescently labeled P2 peptide (5(6)-Fluoresceine-NH-LLIILHAAGDYYAY-$CONH_2$) also tends to be precipitated, resulting in problems during the centrifugation steps.

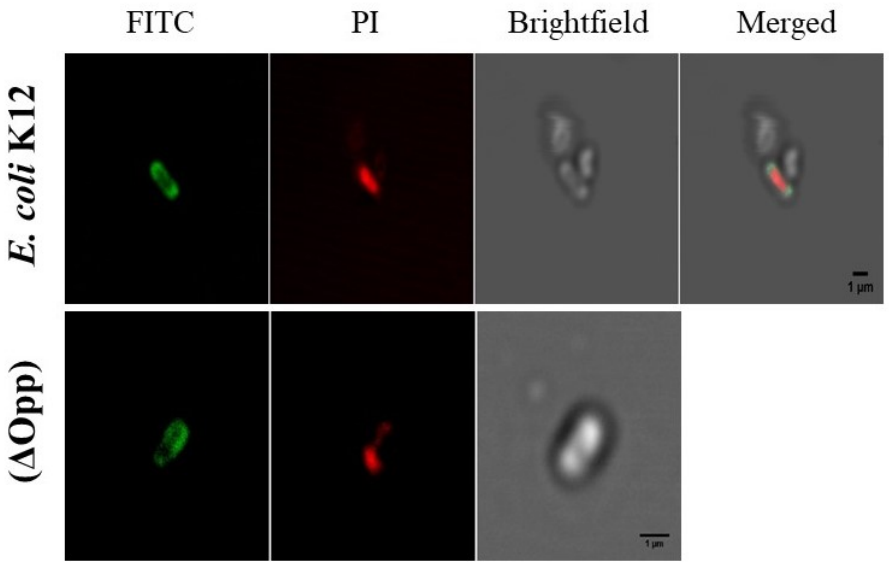

Figure 4.79. Confocal images of the internalization of fluorescently labeled P2 by wild type *E. coli* K12 and mutant (ΔOpp) cells.

FITC, bright field and merged confocal images of bacterial cells incubated with P2 peptide were given in Figure 4.79. From confocal images, it was observed that fluorescently labeled P2 peptide was internalized by both wild type *E. coli* K12 and mutant cells but fluorescence intensity of both cells were very low. From plot profiles (Figure 4.80), it was observed that fluorescence intensity was higher in the middle of

the wild type cell; however, the fluorescence intensity was decreased in the middle of mutant cells and it increased towards the membrane of the bacteral cells.

Because fluorescent peptide could not be removed in centrifugation steps, fluorescence background was high in the images. After the incubation of fluorescent peptide, bacterial cells were incubated with PI dye to be able to observe the bacterial viability. Fluorescence intensity of bacterial cells was very low as can be seen from FITC images. Almost all fluorescent cells were dead mostly due to the antimicrobial effects of this peptide on bacterial cells. The localization of this peptide in wild type cells is not clear. When mutant cells were incubated with fluorescent P2 peptide, fluorescence intensity of the cells decreased dramatically, which is not consistent with the results of microchip experiments.

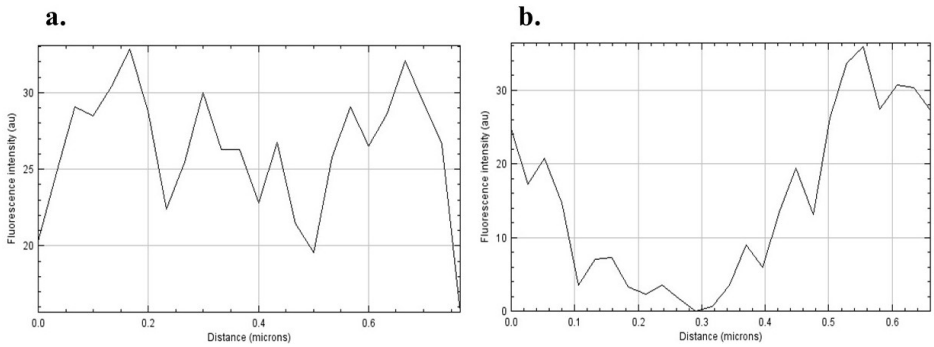

Figure 4.80. a. Plot profile of wild type *E. coli* K12 cells. b. Plot profile of mutant (ΔOpp) cells.

When mutant cells were incubated with P2 peptide and visualized under fluorescence microscopy, fluorescence intensity was not observed in bacterial cells but fluorescence intensity was detected at the least in mutant cells when they were visualized under confocal microscopy. The reason could be the usage of different fluorescent dyes for labeling of peptides. It was concluded that fluorescently labeled P2 peptide was merely internalized by both wild type and mutant cells. Fluorescence intensity was detected in the middle of wild type cells but no fluorescence intensity was observed in the middle of the mutant cells as can be seen in plot profiles (Figure 4.80).

Table 4.14. Validation of the bacterial uptake of fluorescent peptides via confocal microscopy

Analysis	**Peptide**	**Bacteria**	**Fluorescence Intensity(a.u.)**	**Change (%)**	**Localization**
Confocal Imaging	pVEC (50 μM)	*E. coli* K12	61.94	**24.66**	**Cytoplasm**
		(ΔOpp)	46.67		**Periplasm**
	P4 (50 μM)	*E. coli* K12	47.64	**24.79**	**Cytoplasm**
		(ΔOpp)	35.83		**Periplasm**
	P2 (100 μM)	*E. coli* K12	31.12	**39.43**	**Cytoplasm**
		(ΔOpp)	18.84		**Periplasm**

Confocal imaging analyses were summarized in Table 4.14. When wild type and mutant cells were compared on the basis of fluorescence intensity and location of peptides, fluorescence intensity of wild type cells higher than that of mutant cells. In wild type cells, fluorescence intensity was higher in the middle of the wild type cell; however, the fluorescence intensity was decreased in the middle of mutant cells.

Plot profiles shows that fluorescence intensity was higher in the middle of the wild type cell; however, the fluorescence intensity decreased in the middle of mutant cells. When the fluorescence intensity of wild type cells incubated with pVEC and incubated with P4 were compared, fluorescence intensity of wild type cells was higher when they incubated with pVEC. On the other hand, when wild type and mutant cell were incubated with P2, fluorescence intensity was observed in the middle of wild type cells but fluorescence intensity of bacterial cells was lower than that incubated with pVEC and P4 peptides. To summarize confocal analyses, all fluorescent peptides are able to penetrate into cytoplasm via opp system. When opp system was deleted in cells, fluorescent peptides accumulated between inner and outer membrane (periplasm) of mutant cells. If fluorescence intensities were compared, internalization of P2 peptide through outer membrane was lower than other peptides.

5. CONCLUSIONS AND RECOMMENDATIONS

In the first part of this study, the internalization of fluorescently labeled pVEC, chimeric P4 and P2 peptides by wild-type *E. coli* K12 and opp-deleted mutant *E. coli* K12 SS5013 cells was investigated in microfluidic platform, i.e. zeonor microchips-reaction chambers of 10 μL and rhombic chambers of 6 μL volume. The effects of fluorescently labeled peptides on bacterial strains were first analyzed via minimum inhibitory concentration (MIC) analysis. These analyses were carried out both at high and standard inoculum doses because MICs of drugs are highly dependent on the inoculum cell density. Minimum inhibitory concentration for fluorescently labeled pVEC was determined as 200 μM at high inoculation density and 100 μM at standard inoculation density of wild-type *E. coli* K12 cells and 200 μM at high inoculation density and 50 μM at standard inoculation density of opp-deleted mutant *E. coli* K12 SS5013 cells. Minimum inhibitory concentration for fluorescently labeled P4 was determined as 200 μM at high inoculation density and 100 μM at standard inoculation density of both wild-type *E. coli* K12 cells and opp-deleted mutant *E. coli* K12 SS5013 cells. Lastly, minimum inhibitory concentration for fluoresceine-labeled P2 was determined as 100 μM at high inoculation density and 50 μM at standard inoculation density of both wild-type *E. coli* K12 cells and opp-deleted mutant *E. coli* K12 SS5013 cells. In the light of these results, the concentration of fluorescently labeled peptide to be used in bacterial uptake studies was determined as 50 μM. Following the fluorescent peptide perfusion into the microfluidic chambers (6 and 10 6 μL volumes), the number of fluorescent cells increased from one image to another. The ratio of fluorescent wild type cells and integrated fluorescence intensity of cells in the chamber were higher than that of opp-deleted mutant cells, indicating that fluorescently labeled pVEC and P4 peptides were partially internalized through opp system. When opp system was deleted, this peptide was internalized most likely via passive diffusion. In the case of fluorescein-labeled P2 peptide, the internalization of fluoresceine-labeled P2 peptide into wild type cells decreased noticeably with time. The bacterial uptake of fluoresceine-labeled P2 peptide did not occur , so no fluorescent bacterial cell was observed in the chamber.

For the validation of bacterial uptake of fluorescently labeled pVEC, P4 and P2, trypsin-EDTA solution was perfused into the chamber just after the incubation of bacterial cells with the fluorescent peptides. Since the fluorescence intensity of bacterial cells did not change after trypsin perfusion, it can be stated that fluorescently labeled pVEC and P4 peptides were internalized by wild type *E. coli* K12 and opp-deleted mutant *E. coli* K12 SS5013 cells rather than stuck on the cellular membrane. To observe the location of fluorescently labeled pVEC, fluorescently labeled P4 and fluorescein-labeled P2 peptides in both wild type *E. coli* K12 and opp-deleted mutant E. coliz K12 SS5013 cells, these bacterial cells were analyzed under the confocal microscopy after the incubation with fluorescent peptides. Confocal images also validated the internalization of fluorescently labeled cell-penetrating peptide, pVEC and chimeric P4 peptide. These peptides were accumulated between the inner and outer membrane, periplasm. Moreover, fluorescent peptides located intensively at the poles of these bacterial cells. These results indicated that fluorescently labeled pVEC and P4 peptides are not only internalized via passive diffusion but also taken up through the cellular membrane by opp system. Therefore, opp system can be used as a tool for the permeabilization of the antimicrobial peptides and the control of infectivity and pathogenicity of bacterial cells.

In the second part of this study, the motility of *B. subtilis* 168, *B. subtilis* 3610 (an undomesticated derivative of *B. subtilis* 168 strain), DS222 (*B. subtilis* 3610 with a deletion of MotAB gene), and DS223 (*B. subtilis* 3610 with a deletion of MotPS gene) cells were investigated in microfluidic devices, i.e. zeonor microchips- reaction chambers of 10 μL. Before microfluidic studies, swimming and swarming assays were performed to determine the concentration of amiloride used to block the motility of bacterial cells. Three strains mentioned above are neutrophilic bacteria, meaning that they have both H^+- driven MotAB and Na^+-driven MotPS stators. While amiloride blocks Na^+ driven flagellar motors by competing with Na^+ ions in the medium, high Na^+ concentration in the medium was reported to increase Na^+-driven MotPS stators. Minimum inhibitory concentration of amiloride was determined as 4 mM at high inoculation density and 1 mM at standard inoculation density of wild-type *B. subtilis* 168 cells. Motility assay

results also indicated that 1 mM concentration of amiloride blocks the motility of bacterial cells and so, this concentration was used in the microchip experiments. Mean swimming rate values of *B. subtilis* 168 cells grown in standard LB media were changed between approximately 6 μm/s and 8 μm/s. When the Na^+ concentration of media increases, the swimming rate values were calculated to be between approximately 7.5 μm/s and 8.5 μm/s . As mentioned previously, high Na concentration may stimulate the Na^+-driven MotPS stator and increase the flagellar motility. In the presence of amiloride, the swimming rate of *B. subtilis* 168 cells decreased slightly.

After the motility of *B. subtilis* 168 cells was tested in microchips, the motilities of *B. subtilis* 3610 (an undomesticated derivative of *B. subtilis* 168 strain), DS222 (*B. subtilis* 3610 with a deletion of MotAB gene), and DS223 (*B. subtilis* 3610 with a deletion of MotPS gene) in the presence of amiloride drug were also investigated in these microchips. Mean swimming rate values of the *B. subtilis* 3610 cells at 15 minute-intervals varied between 7.5 μm/s and 8 μm/s until their interaction with the drug amiloride. After the interaction of amiloride with *B. subtilis* 3610 cells, the swimming rate values decreased slightly and varied between 6.4 μm/s and 7.2 μm/s. DS222 cells lacking MotAB gene are nonmotile in the chamber. Although Na^+ concentration of the medium was increased to investigate whether high Na^+ concentration stimulates MotPS-based motility, and whether DS222 cells become motile, DS222 cells were still nonmotile.

DS223 cells were first treated with amiloride and then fresh LB was perfused into the chamber. Mean swimming rate values of the bacterial cells at 15 minute-intervals varied between 8.86 μm/s and 9.58 μm/s until their interaction with the drug. After the interaction of DS223 cells with, amiloride, the swimming rate values decreased slightly and varied between 7.15 μm/s and 7.68 μm/s. After fresh LB medium perfusion, the swimming rate values increased and varied between 8.20 μm/s and 9.12 μm/s. Similar to the swimming rate results of laboratory strain, amiloride has a reducing effect on flagellar motility of undomesticated *B. subtilis* 3610 and mutant cells.

Afterwards, the motility of alkaliphilic B. marmarensis strain was analyzed in the presence of amiloride and the change in motility was monitored in microchips. The mean swimming rate values of B. marmarensis cells changed between 4.2 μm/s and 4.9 μm/s when they were incubated in standard NB medium containing 103 mM NaCl. These values varied between 4.9 μm/s and 5.5 μm/s when B. marmarensis cells were incubated in in NB medium supplemented by 120 mM NaCl.

After amiloride perfusion into the chamber, the swimming rates of B. marmarensis cells decreased to 0.4-0.6 μm/s. This result was expected because B. marmarensis cells have only Na^+-driven MotPS stator and amiloride block this stator directly. After fresh LB perfusion into the chamber, the swimming rate values increased and changed between 4.6 μm/s and 5.1 μm/s.

As a conclusion, the microfluidic chip platform used in this study provided a continuous and controlled flow system, and commercially available chips were shown to be highly reliable and versatile devices for bacterial cells. Parameters such as temperature, gas exchange, nutrition accessibility and fluidic environment can be controlled and kept constant particularly for long-term live-cell imaging analyses. This microfluidic chip platform enables live imaging, it may also be extended to capture the dynamic and micro-scale imaging on a single cell level in controlled microbial environments.

5.1. Recommendations

Commercially available microchips were demonstrated to be suitable for bacterial uptake and motility studies. However, the volume and depth of these chips are too much for bacterial cells. During the experiments, microscopy images were captured from the same spot but some bacterial cells entered to the region we focused on, while some of them exited from the chamber. In addition, bacterial cells move in the z stage due to the 3D environment of reaction chips, so they may become invisible after a while during the image capturing. For example, the size of opp-deleted mutant cells are smaller than that of wild type cells and they are observed like spots in the chamber

when they move in z stage. For future studies, microchips with small volume and less chamber depth can be designed and used in bacterial studies. In addition, some internal structures can be added to the chamber design to trap bacterial cells, so that the same bacterial cells can be monitored and analyzed throughout the experiments. Due to the fluorescent peptide perfusion into the chamber during the uptake studies, fluorescence intensity of the background increased over time, which makes the cells invisible. To be able to monitor bacterial cells in the chamber for a long time, the concentration of fluorescent peptide used in the studies can be lowered to less than 50 μM.

Fluorescent peptides tend to be precipitated, resulting in problems during the centrifugation steps. Moreover, high fluorescence intensity in the background was observed in confocal images, affecting the accuracy of the experiments. These peptides were dissolved in high amount of DMSO without damaging bacterial cells. Different solutions may be tested to dissolve these peptides, and they may be modified without changing the action mechanism of the peptides. For MIC analyses, due to 2 fold dilution of the drug solution, the concentration difference between successive wells is high. Therefore, other concentrations in the range should also be tried to find the exact MIC value of the employed drugs.

REFERENCES

1. Groshong, A. M., A. Dey, I. Bezsonova, M. J. Caimano and J. D. Radolf, "Peptide uptake is essential for borrelia burgdorferi viability and involves structural and regulatory complexity of its oligopeptide transporter", *mBio*, Vol. 8, No. 6, pp. 1–20, 2017.

2. Duan, Q., M. Zhou, L. Zhu and G. Zhu, "Flagella and bacterial pathogenicity", *Journal of Basic Microbiology*, Vol. 53, No. 1, pp. 1–8, 2013.

3. Groisman, A., C. Lobo, H. J. Cho, J. K. Campbell, Y. S. Dufour, A. M. Stevens and A. Levchenko, "A microfluidic chemostat for experiments with bacterial and yeast cells", *Nature Methods*, Vol. 2, No. 9, pp. 685–689, 2005.

4. Alberts, B., A. Johnson, J. Lewis, D. Morgan, M. Raff, K. Roberts and P. Walter, *Molecular Biology of THE CELL*, Garland Science, New York, 6th editio edn., 2014.

5. Michael Wink, *An Introduction to Molecular Biotechnology*, Wiley-Blackwell, 2nd editio edn., 2011.

6. Fuerst, J. A. and E. Sagulenko, "Protein uptake by bacteria", *Communicative & Integrative Biology*, Vol. 3, No. 6, pp. 572–575, 2010.

7. Lonhienne, T. G. A., E. Sagulenko, R. I. Webb, K.-c. Lee, J. Franke and D. P. Devos, "Endocytosis-like protein uptake in the bacterium Gemmata obscuriglobus", *PNAS*, Vol. 107, No. 29, pp. 12883–12888, 2010.

8. Fuerst, J. A. and E. Sagulenko, "Towards understanding the molecular mechanism of the endocytosis-like process in the bacterium Gemmata obscuriglobus", *BBA - Molecular Cell Research*, Vol. 1843, No. 8, pp. 1732–1738, 2014.

9. Nitschke, N., K. Atkovska and J. S. Hub, "Accelerating potential of mean force calculations for lipid membrane permeation: System size, reaction coordinate, solute-solute distance, and cutoffs", *Journal of Chemical Physics*, Vol. 145, No. 12, 2016.

10. Sonia Troeira Henriques, M. N. M. and M. A. R. B. Castanho, "Cell-penetrating peptides and antimicrobial peptides : how different are they ?", *Biochemical*, Vol. 399, pp. 1–7, 2006.

11. Guo, Z., H. Peng, J. Kang and D. Sun, "Cell-penetrating peptides : Possible transduction mechanisms and therapeutic applications", *Biomedical Reports*, Vol. 4, pp. 528–534, 2016.

12. Yu, D., B. Pi, M. Yu, Y. Wang, Z. Ruan, Y. Feng and Y. Yu, "Genomics Diversity and evolution of oligopeptide permease systems in staphylococcal species", *Genomics*, Vol. 104, No. 1, pp. 8–13, 2014.

13. Moutran, A., R. B. Quaggio, A. Balan, L. Carlos and D. S. Ferreira, "The Oligopeptide Permease (Opp) of the Plant Pathogen Xanthomonas axonopodis pv . citri", *Current Microbiology*, Vol. 48, pp. 354–359, 2004.

14. Rossez, Y., E. B. Wolfson, A. Holmes, D. L. Gally and N. J. Holden, "Bacterial flagella: twist and stick, or dodge across the kingdoms", *PLOS Pathogens*, Vol. 11, No. 1, pp. 1–15, 2015.

15. Duan, Q., M. Zhou, X. Zhu, W. Bao, S. Wu, X. Ruan, W. Zhang, Y. Yang, J. Zhu and G. Zhu, "The flagella of F18ab Escherichia coli is a virulence factor that contributes to infection in a IPEC-J2 cell model in vitro", *Veterinary Microbiology*, Vol. 160, No. 1-2, pp. 132–140, 2012.

16. Yang, Y., F. Yao, M. Zhou, J. Zhu, X. Zhang, W. Bao, S. Wu, P. R. Hardwidge and G. Zhu, "F18ab Escherichia coli flagella expression is regulated by acyl-homoserine lactone and contributes to bacterial virulence", *Veterinary Microbiology*, Vol. 165,

No. 3-4, pp. 378–383, 2013.

17. Yi, C., C.-w. Li, S. Ji and M. Yang, "Microfluidics technology for manipulation and analysis of biological cells", *Analytica Chimica Acta*, Vol. 560, pp. 1–23, 2006.

18. Wu, J., Q. Chen, W. Liu, Z. He and J.-m. Lin, "Trends in Analytical Chemistry Recent advances in micro fl uidic 3D cellular scaffolds for drug assays", *Trends in Analytical Chemistry*, Vol. 87, pp. 19–31, 2017.

19. K. Kong, L. Schneper, K. M., "NIH Public Access", *Acta Pathologica, Microbiologica et Immunologica Scandinavica*, Vol. 118, No. 1, pp. 1–36, 2011.

20. Frieri, M., K. Kumar and A. Boutin, "Antibiotic resistance", *Journal of Infection and Public Health*, Vol. 10, No. 4, pp. 369–378, 2017.

21. Macgowan, A. and E. MAcnaughton, "Antimicrobial therapy : principles of use Key points", *Medicine*, Vol. 45, No. 10, pp. 614–621, 2017.

22. Delcour, A. H., "Outer Membrane Permeability and Antibiotic Resistance", Vol. 1794, No. 5, pp. 808–816, 2010.

23. Chang, C., I. H. Huang, A. P. Hendrickx and H. Ton-That, *Visualization of gram-positive bacterial pili*, Vol. 966, 2013.

24. Splith, K. and I. Neundorf, "Antimicrobial peptides with cell-penetrating peptide properties and vice versa", *European Biophysics Journal*, Vol. 40, pp. 387–397, 2011.

25. Guidotti, G., L. Brambilla and D. Rossi, "Cell-Penetrating Peptides : From Basic Research to Clinics", *Trends in Pharmacological Sciences*, Vol. 38, No. 4, pp. 406–424, 2017.

26. Akdag, I. O. and E. Ozkirimli, "The uptake mechanism of the cell-penetrating

pVEC peptide", *Journal of Chemistry*, Vol. 2013, 2013.

27. Nan, Y. H., I.-s. Park, K.-s. Hahm and S. Y. Shin, "Antimicrobial activity , bactericidal mechanism and LPS-neutralizing activity of the cell- penetrating peptide p VEC and its analogs", *Joournal of Peptide Science*, Vol. 17, pp. 812–817, 2011.

28. Klepsch, M. M., M. Kovermann, C. Löw, J. Balbach, H. P. Permentier, F. Fusetti, J. W. D. Gier, D. J. Slotboom and R. P. Berntsson, "Escherichia coli Peptide Binding Protein OppA Has a Preference for Positively Charged Peptides", *Journal of Molecular Biology*, Vol. 414, No. 1, pp. 75–85, 2011.

29. Belas, R., "Biofilms, flagella, and mechanosensing of surfaces by bacteria", *Trends in Microbiology*, Vol. 22, No. 9, pp. 517–527, 2014.

30. Macnab, R. M., "Type III flagellar protein export and flagellar assembly", *Biochimica et Biophysica Acta - Molecular Cell Research*, Vol. 1694, pp. 207–217, 2004.

31. Li, H. and V. Sourjik, "Assembly and stability of flagellar motor in Escherichia coli", *Molecular Microbiology*, Vol. 80, No. 4, pp. 886–899, 2011.

32. Salieb-beugelaar, G. B., G. Simone, A. Arora and A. Philippi, "Latest Developments in Microfluidic Cell Biology and Analysis Systems", *Analytical Chemistry*, Vol. 82, No. 12, pp. 4848–4864, 2010.

33. Nguyen, N.-t., S. Ali, M. Shaegh, N. Kashaninejad and D.-t. Phan, "Design , fabrication and characterization of drug delivery systems based on lab-on-a-chip technology", *Advanced Drug Delivery Reviews*, Vol. 65, pp. 1403–1419, 2013.

34. Sanjay, S. T., W. Zhou, M. Dou, H. Tavakoli, L. Ma, F. Xu and X. Li, "Recent advances of controlled drug delivery using microfluidic platforms, year = 2017", *Advanced Drug Delivery Reviews*.

35. Riahi, R., A. Tamayol, S. Ali, M. Shaegh, A. M. Ghaemmaghami, M. R. Dok-

meci and A. Khademhosseini, "Microfluidics for advanced drug delivery systems", *Current Opinion in Chemical Engineering*, Vol. 7, pp. 101–112, 2015.

36. Qi-chen, Z., N. Rui-zhi, M. A. Yuan and L. I. N. Jin-ming, "Recent Developments in Microfluidic Chip for in vitro Cell [U+2010] based Research", *Chinese Journal of Analytical Chemistry*, Vol. 44, No. 4, pp. 522–532, 2016.

37. Wu, J., Z. He, Q. Chen and J.-m. Lin, "Biochemical analysis on microfluidic chips", *Trends in Analytical Chemistry*, Vol. 80, pp. 213–231, 2016.

38. Balaban, N. Q., J. Merrin, R. Chait, L. Kowalik and S. Leibler, "Bacterial Persistence as a Phenotypic Switch", *Science*, Vol. 305, pp. 1622–1626, 2004.

39. Balaban, N. Q., J. Merrin, R. Chait, L. Kowalik and S. Leibler, "Bacterial persistence as a phenotypic switch", *Science*, Vol. 305, No. 5690, pp. 1622–1625, 2004.

40. Sun, P., Y. Liu, J. Sha, Z. Zhang, Q. Tu, P. Chen and J. Wang, "High-throughput microfluidic system for long-term bacterial colony monitoring and antibiotic testing in zero-flow environments", *Biosensors and Bioelectronics*, Vol. 26, No. 5, pp. 1993–1999, 2011.

41. Mohan, R., A. Mukherjee, S. E. Sevgen, C. Sanpitakseree, J. Lee, C. M. Schroeder and P. J. A. Kenis, "A multiplexed microfluidic platform for rapid antibiotic susceptibility testing", *Biosensors and Bioelectronic*, Vol. 49, pp. 118–125, 2013.

42. Baltekin, Ö., A. Boucharin, E. Tano, D. I. Andersson and J. Elf, "Antibiotic susceptibility testing in less than 30 min using direct single-cell imaging", *PNAS*, Vol. 114, No. 34, pp. 9170–9175, 2017.

43. DiLuzio, W. R., L. Turner, M. Mayer, P. Garstecki, D. B. Weibel, H. C. Berg and G. M. Whitesides, "Escherichia coli swim on the right-hand side", *Nature*, Vol. 435, No. 7046, pp. 1271–1274, 2005.

44. Mannik, J., R. Driessen, P. Galajda, J. E. Keymer and C. Dekker, "Bacterial growth and motility in sub-micron constrictions", *Proceedings of the National Academy of Sciences*, Vol. 106, No. 35, pp. 14861–14866, 2009.

45. Baker, J. D., D. T. Kysela, J. Zhou, S. M. MAdre, A. S. Wilkens, Y. V. Brun and S. C. Jacobson, "Programmable, Pneumatically Actuated Microfluidic Device with an Integrated Nanochannel Array To Track Development of Individual Bacteria", *Analytical Biochemistry*, Vol. 88, No. 17, pp. 8476–8483, 2017.

46. Massalha, H., E. Korenblum, S. Malitsky, O. H. Shapiro and A. Aharoni, "Live imaging of root–bacteria interactions in a microfluidics setup", *Proceedings of the National Academy of Sciences*, Vol. 114, No. 17, pp. 4549–4554, 2017.

47. Russell, J. R., M. T. Cabeen, P. A. Wiggins, J. Paulsson and R. Losick, "Noise in a phosphorelay drives stochastic entry into sporulation in Bacillus subtilis", *The EMBO Journal*, pp. 1–14, 2017.

48. Balouiri, M., M. Sadiki and S. K. Ibnsouda, "Methods for in vitro evaluating antimicrobial activity: A review", *Journal of Pharmaceutical Analysis*, Vol. 6, No. 2, pp. 71–79, 2016.

49. Amsterdam, D., "Susceptibility testing of antimicrobials in liquid media", *Antibiotics in laboratory medicine*, pp. 52–111, Lippincott Williams& Wilkins, 1996.

50. Cockerill et al., F., *Methods for Dilution Antimicrobial Susceptibility Tests for Bacteria That Grow Aerobically ; Approved Standard — Ninth Edition*, Vol. 32, 2012.

51. Hartmann, M., M. Berditsch, J. Hawecker, M. F. Ardakani, D. Gerthsen and A. S. Ulrich, "Damage of the bacterial cell envelope by antimicrobial peptides gramicidin S and PGLa as revealed by transmission and scanning electron microscopy", *Antimicrobial Agents and Chemotherapy*, Vol. 54, No. 8, pp. 3132–3142, 2010.

52. Kearns, D. B. and R. Losick, "Swarming motility in undomesticated Bacillus subtilis", *Molecular Microbiology*, Vol. 49, No. 3, pp. 581–590, 2003.

53. Thampuran, N. and P. K. Surendran, "Effect of chemical agents on swarming of Bacillus species", , No. April 1995, pp. 296–302, 1996.

54. Kearns, D. B. and R. Losick, "Cell population heterogeneity during growth of Bacillus subtilis", pp. 3083–3094, 2005.

55. Kearns, D. B., F. Chu, S. S. Branda, R. Kolter and R. Losick, "A master regulator for biofilm formation by Bacillus subtilis", *Molecular Microbiology*, Vol. 55, No. 3, pp. 739–749, 2005.

56. Piggot, P., "Epigenetic Switching : Bacteria Hedge Bets about Staying or Moving", *Current Biology*, Vol. 20, No. 11, pp. 480–482, 2010.

57. Chai, Y., T. Norman, R. Kolter and R. Losick, "An epigenetic switch governing daughter cell separation in Bacillus subtilis", *Cold Spring Harbor Laboratory Press*, Vol. 24, pp. 754–765, 2010.

58. Burdett, I. D. J. and M. L. Higgins, "Study of pole assembly in Bacillus subtilis by computer reconstruction of septal growth zones seen in central, longitudinal thin sections of cells", *Journal of Bacteriology*, Vol. 133, No. 2, pp. 959–971, 1978.

59. Kearns, D. B., "A field guide to bacterial swarming motility", *Nature Reviews Microbiology*, Vol. 8, No. 9, pp. 634–644, 2010.

60. Sugiyama, S., E. J. Cragoe and Y. Imae, "Amiloride, a specific inhibitor for the Na+-driven flagellar motors of alkalophilic Bacillus", *Journal of Biological Chemistry*, Vol. 263, No. 17, pp. 8215–8219, 1988.

61. Patrick, J. E. and D. B. Kearns, "Laboratory strains of Bacillus subtilis do not exhibit swarming motility", *Journal of Bacteriology*, Vol. 191, No. 22, pp. 7129–

7133, 2009.

62. Terahara, N., M. Fujisawa, B. Powers, T. M. Henkin, T. A. Krulwich and M. Ito, "An intergenic stem-loop mutation in the Bacillus subtilis ccpA-motPS operon increases motPS transcription and the MotPS contribution to motility", *Journal of Bacteriology*, Vol. 188, No. 7, pp. 2701–2705, 2006.

63. Ito, M., D. B. Hicks, T. M. Henkin, A. A. Guffanti, B. D. Powers, L. Zvi, K. Uematsu and T. A. Krulwich, "MotPS is the stator-force generator for motility of alkaliphilic Bacillus, and its homologue is a second functional Mot in Bacillus subtilis", *Molecular Microbiology*, Vol. 53, No. 4, pp. 1035–1049, 2004.

64. Patrick, J. E. and D. B. Kearns, "Laboratory Strains of Bacillus subtilis Do Not Exhibit Swarming Motility", *Journal of Bacteriology*, Vol. 191, No. 22, pp. 7129–7133, 2009.

65. Kang, S., A. Suresh and Y. C. Kim, "A highly efficient cell penetrating peptide pVEC-mediated protein delivery system into microalgae", *Algal Research*, Vol. 24, No. May, pp. 360–367, 2017.

66. Trabulo, S., A. L. Cardoso, M. Mano and M. C. de Lima, "Cell-penetrating peptides-mechanisms of cellular uptake and generation of delivery systems", *Pharmaceuticals*, Vol. 3, No. 4, pp. 961–993, 2010.

67. Richard, J. P., K. Melikov, E. Vives, C. Ramos, B. Verbeure, M. J. Gait, L. V. Chernomordik and B. Lebleu, "Cell-penetrating peptides: A reevaluation of the mechanism of cellular uptake", *Journal of Biological Chemistry*, Vol. 278, No. 1, pp. 585–590, 2003.

68. Nakamatsu, E. H., E. Fujihira, R. C. C. Ferreira, O. P. Costa and C. S. Ferreira, "Oligopeptide uptake and aminoglycoside resistance in Escherichia coli K12", *FEMS Microbiology Letters*, Vol. 269, pp. 229–233, 2007.

69. Acosta, M. B. R., R. C. C. Ferreira, G. Padilla and S. O. P. Costa, "Altered expression of oligopeptide-binding protein (OppA) and aminoglycoside resistance in laboratory and clinical Escherichia coli strains", *Journal of Medicial Microbiology*, Vol. 49, pp. 409–413, 2017.

70. Monnet, V., "Bacterial oligopeptide-binding proteins", *Cellular and Molecular Life Sciences*, Vol. 60, No. 10, pp. 2100–2114, 2003.

71. Li, J., J. J. Koh, S. Liu, R. Lakshminarayanan, C. S. Verma and R. W. Beuerman, "Membrane active antimicrobial peptides: Translating mechanistic insights to design", *Frontiers in Neuroscience*, Vol. 11, No. FEB, pp. 1–18, 2017.

72. Duchardt, F., M. Fotin-Mleczek, H. Schwarz, R. Fischer and R. Brock, "A comprehensive model for the cellular uptake of cationic cell-penetrating peptides", *Traffic*, Vol. 8, No. 7, pp. 848–866, 2007.

73. Schreiber, G., R. Morales-Nava, A. Herrmann, J. G. Rodriguez Plaza, Z. D. Gonzalez, R. Volkmer, O. Pantoja, E. Klipp, G. Del Rio, C. Diener, I. Ortega Blake and M. T. Lara Ortiz, "Cell Penetrating Peptides and Cationic Antibacterial Peptides", *Journal of Biological Chemistry*, Vol. 289, No. 21, pp. 14448–14457, 2014.

74. Brown, M. A., C. S. Wallace, C. C. Anamelechi, E. Clermont, W. M. Reichert and G. A. Truskey, "The use of mild trypsinization conditions in the detachment of endothelial cells to promote subsequent endothelialization on synthetic surfaces", *Biomaterials*, Vol. 28, No. 27, pp. 3928–3935, sep 2007.

75. Elmquist, A., M. Hansen and Ü. Langel, "Structure-activity relationship study of the cell-penetrating peptide pVEC", *Biochimica et Biophysica Acta - Biomembranes*, Vol. 1758, No. 6, pp. 721–729, 2006.

76. Maes, A., C. Gracia, D. Bréchemier, P. Hamman, E. Chatre, L. Lemelle, P. N. Bertin and E. Hajnsdorf, "Role of polyadenylation in regulation of the flagella

cascade and motility in Escherichia coli", *Biochimie*, Vol. 95, No. 2, pp. 410–418, 2013.

77. Marr, A. G., "Growth Rate of Escherichia coli", *Microbiology and Molecular Biology Reviews*, Vol. 55, No. 2, pp. 316–333, 1991.

78. Takeuchi, S., W. R. Diluzio, D. B. Weibel and G. M. Whitesides, "Controlling the shape of filamentous cells of Escherichia coli", *Nano Letters*, Vol. 5, No. 9, pp. 1819–1823, 2005.

79. Julkowska, D., M. Obuchowski, I. B. Holland and S. J. Séror, "Branched swarming patterns on a synthetic medium formed by wild-type Bacillus subtilis strain 3610: Detection of different cellular morphologies and constellations of cells as the complex architecture develops", *Microbiology*, Vol. 150, No. 6, pp. 1839–1849, 2004.

80. Atsumi, T., S. Sugiyama, E. J. Cragoe and Y. Imae, "Specific inhibition of the Na+-driven flagellar motors of alkalophilic Bacillus strains by the amiloride analog phenamil", *Journal of Bacteriology*, Vol. 172, No. 3, pp. 1634–1639, 1990.

81. Ito, M., N. Terahara, S. Fujinami and T. A. Krulwich, "Properties of Motility in Bacillus subtilis Powered by the H+ - Coupled MotAB Flagellar Stator, Na+ - Coupled MotPS or Hybrid Stators MotAS or MotPB", *Journal of Molecular Biology*, Vol. 352, No. 2, pp. 396–408, 2005.

82. Imae, Y. and T. Atsumi, "Na + -Driven Bacterial Flagellar Motors", *Journal of Bioenergetics and Biomembranes*, Vol. 21, No. 6, pp. 705–716, 1989.

83. Denizci, A. A., D. Kazan and A. Erarslan, "Bacillus marmarensis sp. nov., an alkaliphilic, protease-producing bacterium isolated from mushroom compost", *International Journal of Systematic and Evolutionary Microbiology*, Vol. 60, pp. 1590–1594, 2010.

84. Özgören, T., O. Pinar, G. Bozdağ, A. A. Denizci, O. Gündüz, P. Çakır Hatır

and D. Kazan, “Assessment of poly(3-hydroxybutyrate) synthesis from a novel obligate alkaliphilic Bacillus marmarensis and generation of its composite scaffold via electrospinning”, *International Journal of Biological Macromolecules*, Vol. 119, pp. 982–991, 2018.